JOURNAL OF RESEARCH of the National Bureau of Standards
Vol. 86, No. 5, September–October 1981

Contents

page

Prediction of the Critical Line of a Binary Mixture: Evaluation of the Interaction Parameters. B.E. Eaton, J. Stecki, P. Wielopolski, and H.J.M. Hanley 419

Propagation of Density Fluctuations in Nonuniform Fluids: Simple Models. James C. Rainwater 429

A Transient Hot Wire Thermal Conductivity Apparatus for Fluids. Hans M. Roder 457

The Graphite Calorimeter as a Standard of Absorbed Dose for Cobalt-60 Gamma Radiation. John S. Pruitt, Steve R. Domen, and Robert Loevinger 495

Upper Limits for the Number of Bound States Associated with the Yukawa Potential. Herbert S. Bennett 503

A "Uniformity Principle" for Evacuation Route Allocation. Richard L. Francis. 509

Publications of the National Bureau of Standards 515

Library of Congress Catalog Card Number: 63–37059

For sale by the Superintendent of Documents, U.S. Government Printing Office.
Washington, D.C. 20402. Order by SD Catalog
No. C13.22/vol. 86(5). Single copy price $3.75 Domestic; $4.70 Foreign.
Subscription price: $16 a year; $4.00 additional for foreign mailing.

UNITED STATES GOVERNMENT PRINTING OFFICE, WASHINGTON: 1981

JOURNAL OF RESEARCH of the National Bureau of Standards
Vol. 86, No. 5, September–October 1981

Prediction of the Critical Line of a Binary Mixture: Evaluation of the Interaction Parameters

B. E. Eaton*

Department of Chemical Engineering, University of Colorado, Boulder, CO 80307

and

J. Stecki and P. Wielopolski****

Institute of Physical Chemistry, Polish Academy of Sciences, Warsaw, Poland

and

H. J. M. Hanley†

Department of Chemical Engineering, University of Colorado, Boulder, CO 80307

and

National Bureau of Standards,†† Boulder, CO 80307

March 23, 1981

The critical line of the binary mixture methane-ethane is calculated via the extended corresponding states Van der Waals one fluid theory. The Gibbs free energy criticality criteria are solved numerically. The numerical derivatives are compared with the exact analytical results derived previously for the special case of the shape factors of the extended corresponding states set equal to unity. Binary interaction parameters are adjusted to give a best fit of the critical line to experimental data. These interaction parameters are then used to evaluate vapor liquid equilibrium data away from the critical region. It appears that a fit of the critical line is not sufficient to obtain binary interaction parameters of general applicability. Optimization of the critical point predictions for the pure components is also discussed.

Key words: Binary interaction parameters; criticality criteria; extended corresponding states; gas-liquid critical line; one fluid theory; Van der Waals theory; VLE prediction.

1. Introduction

The prediction of phase equilibria is both a classical problem of the theory of liquids and a problem of engineering concern. Today the chemical and fuel industries have to increase productivity and conservation and transfer to new feedstocks; phase equilibria is a major factor. But it is well known that the prediction, even the correlation, of the properties of the appropriate systems can be exceptionally difficult if the results are required to any reasonable accuracy. Prediction techniques are needed especially because the number of possible systems makes measurement an overwhelming task. Prediction requires an understanding of theory but, unfortunately, theory cannot yet always handle adequately the complex systems encountered: the gap between a systematic practical theory and reality is large. One technique, however, has been applied successfully to simple systems and does show promise in that the assumptions can

*Supported by the National Science Foundation, Grant No. HES 7419548, SMI 7610647.

**Supported in part by the Maria Curie Sklodowska Fund, Grant No. NBS-196, established by contributions of the U.S. and Polish governments.

†Supported in part by the Office of Standard Reference Data, NBS.

††Thermophysical Properties Division, National Engineering Laboratory.

be identified clearly. This method is extended corresponding states. Here we apply it to a system of methane and ethane. A specific objective is to calculate the gas/liquid critical line and to observe the effect of the binary interaction parameters on the calculation. It is then interesting to see how these parameters, optimized for the critical line, represent vapor liquid equilibrium (VLE) data.

The critical line in a binary mixture may be calculated by solving the equations

$$\left(\frac{\partial^2 \widetilde{G}}{\partial x^2}\right)_{T,p} = 0 \,; \left(\frac{\partial^3 \widetilde{G}}{\partial x^3}\right)_{T,p} = 0$$

for a temperature (T) and pressure (p) with the mole fraction (x) specified. $\widetilde{G}$ is the molar configurational Gibbs free energy of the mixture. In this work these second and third order derivatives were evaluated numerically, but have been compared with the analytical results of Wielopolski [1][1] in the special case when the extended corresponding states shape factors are unity. The accuracy of the approach has thus been evaluated.

The system methane/ethane was selected for comparison with experiment since the VLE data have been evaluated for thermodynamic consistency by Hiza, et al. [2]. The procedure is quite general, however, and we have applied it to several mixtures. Variations have been reported extensively by Watson and Rowlinson [3], Gunning and Rowlinson [4], Teja and Rowlinson [5], Mollerup and Rowlinson [6], and Mollerup [7, 8]. The overall objective is to develop a general technique for calculating the critical line of a binary mixture and to see if the binary interaction parameters can be reliably evaluated by adjusting them to give the best least squares fit of the critical line data.

2. Corresponding states and equations

The basic postulate of the theory used here—the Van der Waals one fluid theory—is that if the components α ($\alpha = 1,n$ where n is the total number of species) of a mixture separately obey classical corresponding states, then their mixture will also obey corresponding states as if it were a single substance. The components can be represented by selected parameters, e.g., critical temperature (T_α^c) and critical molar volume (V_α^c), and the hypothetical equivalent substance, designed by subscript x, can be characterized by some suitable composition dependent averaged parameters T_x^c and V_x^c. The method then assumes that the properties of a pure substance at p and T, or V and T, can be evaluated with respect to those of a reference fluid, designated by subscript o, via

$$T_o = T/f_{\alpha\alpha,o} \text{ and } V_o = V/h_{\alpha\alpha,o} \tag{1}$$

where the scaling ratios h and f are defined respectively by

$$h_{\alpha\alpha,o} = V_\alpha^c / V_o^c \text{ and } f_{\alpha\alpha,o} = T_\alpha^c / T_o^c \tag{2}$$

For a mixture the most natural definition of h_x and f_x follows from the work of Henderson and Leonard [9] to give the Van der Waals one fluid mixing rules:

$$h_{x,o} f_{x,o} = \sum_\alpha \sum_\beta x_\alpha x_\beta f_{\alpha\beta,o} h_{\alpha\beta,o} \tag{3}$$

$$h_{x,o} = \sum_\alpha \sum_\beta x_\alpha x_\beta h_{\alpha\beta,o} \tag{4}$$

The cross coefficients $f_{\alpha\beta,o}$ and $h_{\alpha\beta,o}$ are left unspecified until further combination rules are defined, e.g.,

$$f_{\alpha\beta,o} = \xi_{\alpha\beta,o} (f_{\alpha\alpha,o} f_{\beta\beta,o})^{1/2} \tag{5}$$

$$h_{\alpha\beta,o} = \eta_{\alpha\beta,o} \left[\tfrac{1}{2} (h_{\alpha\alpha,o})^{1/3} + \tfrac{1}{2} (h_{\beta\beta,o})^{1/3}\right]^3 \tag{6}$$

where $\xi_{\alpha\beta,o}$ and $\eta_{\alpha\beta,o}$ are the binary interaction coefficients which, although formally close to unity, can play a major role in the calculation of phase equilibria.

One Fluid Mixture Equations:

The properties of a mixture can be evaluated in terms of the reference substance and the ratios of eq (2). The basic equations are:

Compressibility factor, Z

$$Z(T,V,x) \equiv Z_x(T,V,x) \tag{7}$$

$$= Z_o(T/f_{x,o},\ V/h_{x,o}) \tag{8}$$

Molar configurational Helmholtz free energy, $\widetilde{A}$

$$\widetilde{A}(V,T,x) \equiv \widetilde{A}_x(V,T,x) + RT \sum_\alpha x_\alpha \ln x_\alpha \tag{9}$$

where

$$\widetilde{A}_x(V,T,x) = f_{x,o}\, \widetilde{A}_o(V/h_{x,o},\ T/f_{x,o}) - RT \ln h_{x,o} \tag{10}$$

or the molar configurational Gibbs free energy, $\widetilde{G}$

$$\widetilde{G}(p,T,x) \equiv \widetilde{G}_x(p,T,x) + RT \sum_\alpha x_\alpha \ln x_\alpha \tag{11}$$

where

$$\widetilde{G}_x(p,T,x) = f_{x,o}\, \widetilde{G}_o(p h_{x,o}/f_{x,o},\ T/f_{x,o}) - RT \ln h_{x,o} \tag{12}$$

[1] Numbers in brackets refer to the literature references at the end of this paper.

The symbol ~ refers to the molar quantity. Equations (7)—(12) which define the properties of an n-component mixture, can also be used for pure component properties if all subscript x's are replaced with α's.

VLE Equations:

For pure component VLE, equating the molar Gibbs free energy of each phase results in the following expression:

$$\left[\tilde{A}_o^{Res}/RT_o - \ell n\, Z_o - 1 + Z_o\right]_{vap} = \left[\tilde{A}_o^{Res}/RT_o - \ell n\, Z_o - 1 + Z_o\right]_{liq} \quad (13)$$

$$\tilde{A}_o^{res} \equiv \tilde{A}(T/f_{\alpha\alpha,\rho}, V/h_{\alpha\alpha,\rho}) - \tilde{A}_{pg}(T/f_{\alpha\alpha,\rho}, V/h_{\alpha\alpha,\rho}) \quad (14)$$

In eq (13) superscript *Res* refers to the residual value defined by eq (14) with $\tilde{A}_{pg}$ the value of the equivalent perfect gas. Equation (13) is expressed in terms of the residual Helmholtz free energy rather than Gibbs since the reference equation of state has T and V (not T and p) as the independent variables.

For mixture VLE one can calculate the K-value for, say, species α at T and p:

$$K_\alpha = y_\alpha/x_\alpha \quad (15)$$

where one can derive

$$RT\, \ell n\, K_\alpha = (\mu_\alpha^{Res})_{Liq} - (\mu_\alpha^{Res})_{Vap} \quad (16)$$

with μ^{Res} the residual chemical potential. Further manipulations give μ^{Res} in terms of $\tilde{G}$ and, for a binary mixture,

$$\mu_\alpha^{Res} = \tilde{G}_x - RT\, x_\beta \left(\frac{\partial(\tilde{G}_x/RT)}{\partial x_\beta}\right)_{T,p} - RT\, \ell n\, \frac{p}{kT} \quad (17)$$

where

$$\frac{\tilde{G}_x}{RT} = \frac{\tilde{A}_o^{Res}}{RT_o} - \ell n\, Z_o - 1 + Z_o + \ell n\, \frac{p}{kT} \quad (18)$$

Critical Criteria:

The conditions for a critical point at T,p for a mixture are

$$(\partial^2 \tilde{G}/\partial x^2)_{T,p} = (\partial^3 \tilde{G}/\partial x^3)_{T,p} = 0. \quad (19)$$

Substitution of the one fluid equations gives

$$(\partial^2 (\tilde{G}_x/RT)/\partial x_\alpha^2)_{T,p} + \frac{1}{x_\alpha x_\beta} = 0 \quad (20)$$

and

$$(\partial^3 (\tilde{G}_x/RT)/\partial x_\alpha^3)_{T,p} + \frac{x_\alpha - x_\beta}{(x_\alpha x_\beta)^2} = 0 \quad (21)$$

which can thus be evaluated using eq (18).

The above equations and others have been discussed in full and derived by Rowlinson and Watson [3], by Eaton [10] and by other authors so it has been sufficient to be very brief. The equations form the basics of the evaluation of phase equilibria for a pure fluid or mixture, given the reference equation of state and the reference G_o or A_o.

Extended Corresponding States:

In general, since classical corresponding states is not obeyed, equations (8) and (10) or (8) and (12) are not satisfied with the scaling ratios of eq (2). It is possible, however, to *define* a corresponding states so that eqs (8) and (10) are satisfied *exactly*. To do this we define shape factors θ and ϕ so that (for a pure, for example)

$$T_o = T\left(\frac{T_o^c}{T_\alpha^c}\right)\frac{1}{\theta_{\alpha\alpha,\rho}} \quad ; \quad V_o = V\left(\frac{V_o^c}{V_\alpha^c}\right)\frac{1}{\phi_{\alpha\alpha,\rho}} \quad (22)$$

hence the ratios f and h become

$$f_{\alpha\alpha,\rho} = \left(\frac{T_\alpha^c}{T_o^c}\right)\theta_{\alpha\alpha,\rho} \quad ; \quad h_{\alpha\alpha,\rho} = \left(\frac{V_\alpha^c}{V_o^c}\right)\phi_{\alpha\alpha,\rho}. \quad (23)$$

The point about this redefinition, i.e., the basis of *extended* corresponding states theory, is that the corresponding states equations can be used formally with the provision that the scaling ratios are given by eq (23). It should be stressed that the ratios could be solved for either a pure or a mixture via eqs (8) and (10) but to do this would require a complete description of the fluids in question: essentially an impossibility. It is convenient to have some generalized analytical relation for θ and ϕ. Leach and Leland proposed the following [11]:

$$\theta_{\alpha\alpha,\rho}(T_\alpha^*, V_\alpha^*, \omega_\alpha) = 1 + (\omega_\alpha - \omega_o)\, F(T_\alpha^*, V_\alpha^*) \quad (24)$$

$$\phi_{\alpha\alpha,\rho}(T_\alpha^*, V_\alpha^*, \omega_\alpha) = [1 + (\omega_\alpha - \omega_o)\, G(T_\alpha^*, V_\alpha^*)]\frac{Z_\alpha^c}{Z_\alpha^c} \quad (25)$$

where

$$F(T_\alpha^*, V_\alpha^*) = a_1 + b_1\, \ell n\, T_\alpha^* + (c_1 + d_1/T_\alpha^*)(V_\alpha^* - 0.5) \quad (26)$$

and

$$G(T_\alpha^*, V_\alpha^*) = a_2 (V_\alpha^* + b_2) + c_2 (V_\alpha^* + d_2)\, \ell n\, T_\alpha^* \quad (27)$$

Here ω is the pitzer acentric factor or some chosen parameter and a, b, c, d are constants:

$$a_1 = 0.0892, \quad a_2 = 0.3903$$
$$b_1 = -0.8493, \quad b_2 = -1.0177$$
$$c_1 = 0.3063, \quad c_2 = -0.9462$$
$$d_1 = -0.4506, \quad d_2 = -0.7663$$

The asterisk denotes the value reduced by the critical value. The equations are constrained in that V_α^* is set equal to 2.0 for all $V_\alpha^* > 2.0$ and to 0.5 for $V_\alpha^* < 0.5$: T_α^* is set to 2.0 if $T_\alpha^* > 2.0$.

We [12] have recently tested the Leach-Leland equations for the hydrocarbons C_1–C_{20} over an extensive range of experimental conditions and revised coefficients are reported in the reference. We also verified that the original equations were satisfactory for reduced temperatures greater than 0.5.

3. Calculation and numerical methods

The objective is to solve the critical criteria eqs (20) and (21) for the methane/ethane system and in so doing, observe the effects of the interaction parameters ξ and η of eqs (5) and (6) on the results. Having these values, we then evaluate some K-values for selected temperatures using eqs (15)–(18). We chose methane as the reference fluid, the equation of state for which is the 32 term BWR of McCarty [13]. Critical parameters and Leach-Leland acentric factors for methane and ethane are given in table 1.

TABLE 1. *Parameters for Methane and Ethane*

	T^c (K)	$\bar{V}^c$ (cm³/mole)	p^c (Bar)	ω
CH_4	190.555	97.75	44.793	.005
C_2H_6	305.33	147.06	47.448	.105

Analytical and Numerical Evaluation of the Derivatives:

The numerical techniques used in this work are standard. We use the central difference formulas [14] for which the first two terms in the infinite power series expansions are given here. For the derivatives of a function f evaluated at a point x, one has

$$\left(\frac{df}{dx}\right)_x \approx \frac{f_1 - f_{-1}}{2h} - \frac{f_2 - 2f_1 + 2f_{-1} - f_{-2}}{12h} \tag{28}$$

$$\left(\frac{d^2f}{dx^2}\right)_x \approx \frac{f_1 - 2f_0 + f_{-1}}{h^2} - \frac{f_2 - 4f_1 + 6f_0 - 4f_{-1} + f_{-2}}{12h^2} \tag{29}$$

$$\left(\frac{\partial^3 f}{\partial x^3}\right)_x \approx \frac{f_2 - 2f_1 + 2f_{-1} - f_{-2}}{2h^3} - \frac{8h^3}{f_3 - 4f_2 + 5f_1 - 5f_{-1} + 4f_{-2} - f_{-3}} \tag{30}$$

where

$$f_o = f(x) \quad ; \quad f_n = f(x + nh) \tag{31}$$

The difficulty is to choose a value of h which is not too small (otherwise significant figures will be lost in evaluating the numerators of eqs (28)–(30)) but not too large (otherwise the truncation error, which can be estimated by the second term of eqs (28)–(30), will be large). One also has to consider the word length of the computer and the convenience of using single versus double precision. In this work we calculated on a CDC 6400 and a CDC 6600 machine with a 60 bit word length (13 significant figures).

We were able to observe definitely the effect of varying h for the special case $\theta = \phi = 1$, i.e., for classical corresponding states. Equations (19) and (20) have been solved *analytically* by Wielopolski (1980) and the lengthy expressions are reported in an NBS publication [1] and will not be repeated here. For example, table 2 lists the number of figures in the numerical results which were in agreement with the analytical results for the first, second, and third derivatives of $\bar{G}_x/RT$ for a particular test case. The number of figures in agreement for the function value of $\bar{G}_x/RT$ itself was 10–12.

TABLE 2. *Comparison of Numerical and Analytical Results for Derivative Calculations Using Single Precision Arithmetic. Subscripts refer to the derivation with respect to x.*

h	$(\bar{G}_x/RT)_x$	$(\bar{G}_x/RT)_{2x}$	$(\bar{G}_x/RT)_{3x}$
10^{-3}	6	5	4
10^{-3}	7	5	3
10^{-5}	7	3	0

Table 2 indicates that the first order derivative is truncation error controlled, since its value becomes more accurate as h is decreased. The second and third derivatives are, on the other hand, controlled by the loss of significant figures since as h is decreased, they lose accuracy. Since the third order derivative is the least accurate, we chose the value of h for which it is calculated most accurately.

We now consider what the smallest values of the second and third order derivatives are which can be calculated with $h = 10^{-3}$, since our eventual goal is to solve the equations for the critical point by driving the values of those derivatives to zero. The derivatives go to zero by a cancellation of the two terms in eqs (20) and (21), that is, the contribution from the hypothetical substance is cancelled by the ideal mixture contribution. For this reason, the values of the derivatives cannot be made arbitrarily small. The ideal mixture contribution (which can be computed with negligible error) can only cancel as many significant figures as appear in the hypothetical substance contribution. Consider the case in table 2 with $h = 10^{-3}$. For the second order derivative, the hypothetical substance contribution has five

significant figures, and its value is order unity (abbreviated 0(1)). If the ideal mixture contribution were to cancel all five of these figures, the result would be a number of $0(10^{-5})$ with no significant figures remaining. For the third order derivative, the hypothetical substance contribution contains four significant figures, and is 0(10). Cancelling all significant figures would leave a number of $0(10^{-3})$.

In our first attempt at calculating critical lines based on the numerical evaluation of the derivatives in eqs (20) and (21) using single precision arithmetic, we were unable to obtain convergence of the temperature and pressure to five significant figures. The problem appeared to be that there were not enough significant figures in the derivative calculations. While the truncation error is inherent to the formulas being used, the loss of significant figures can be compensated by adding more figures to the function values. This was done by the use of double precision arithmetic which gives us 26 significant figures on the CDC 6400. In table 3 below, the results for the numerical derivatives calculated using double precision arithmetic are compared with the results arrived at analytically. Again, reported in the table are the number of figures of agreement between the two results.

TABLE 3. *Comparison of Numerical and Analytical Results for Derivative Calculations Using Double Precision Arithmetic.*

h	$(\tilde{G}_x/RT)_x$	$(\tilde{G}_x/RT)_{2x}$	$(\tilde{G}_x/RT)_{3x}$
10^{-3}	6	5	4
10^{-4}	7	9	6
10^{-5}	7	8	7
10^{-6}	7	8	7
10^{-7}	7	8	7
10^{-8}	7	8	4
10^{-9}	7	8	1

For $h = 10^{-3}$, the single and double precision results are the same, which indicates that truncation error is controlling. Looking at the double precision results, the third derivative shows an increase in accuracy as h is decreased to 10^{-5}; clearly indicating that the truncation error is decreasing to this point. As h is decreased past 10^{-7}, accuracy is lost due to loss of significant figures.

Based on these results, a value of $h = 10^{-6}$ is chosen to compute the derivatives in double precision. Given this value for h, the smallest value of the second derivative which may be calculated (containing no significant figures) is $0(10^{-8})$, and that for the third derivative is $0(10^{-6})$. The calculations of the binary critical line were subsequently made to converge to five significant figures for both temperature and pressure.

4. Results

It must again be stressed that the general procedure for calculating the critical line or VLE is predictive and requires only the critical constants and an acentric factor for the fluid of interest, or of the components in a mixture. For a relatively simple system the results will be reasonable without optimization of any parameters. Since, however, we are concerned only with VLE and the critical point we considered two straightforward optimization procedures involving the factor ω. The first was to adjust ω to give the best representation of the pure component vapor pressure curve, the second was to force the critical temperature and pressure of the pure fluids to correspond exactly with those of the reference substance. This second variation is simply to set $\omega_\alpha = \omega_o$: hence by eqs (24) and (25) $\theta = 1$ and $\phi = Z_o^c/Z_\alpha^c$—a form of classical corresponding states. One should note that the two procedures are not the same because the Leach-Leland equations are not constrained at the critical point.

Ethane: Pure Component Results:

We first considered the ethane vapor pressure curve which was obtained using Leach's expression for the shape factors. The value of the acentric factor for the Leach equations was determined by optimizing agreement with the vapor pressure data by a trial and error procedure in which the sum of the average absolute deviations, for the vapor pressure, and saturated vapor and liquid densities, were minimized; temperature being chosen as the independent variable. The temperature range over which the results were optimized was 180 K to 300 K; 180 K being the lower limit for which Leach's equations were designed; 300 K corresponded to the maximum temperature for which the vapor pressure program would converge. Calculated and data values were compared at 10 K increments. The average deviations obtained for several values of acentric factor are given in table 4. The value chosen for acentric factor in this work ($\omega = 0.094$) is seen to give a substantial improvement over the Pitzer value ($\omega = 0.105$) which was used by Leach.

TABLE 4. *Variation of Ethane Vapor Pressure Curve With Acentric Factor (Leach θ, ϕ).*

Acentric Factor ω	Ave % $\frac{\lvert\Delta p\rvert}{p}$	Ave % $\frac{\lvert\Delta \varrho_{vap}\rvert}{\varrho_{vap}}$	Ave % $\frac{\lvert\Delta \varrho_{liq}\rvert}{\varrho_{liq}}$	Σ Ave %
0.105	2.080	3.148	0.6158	5.844
.100	1.259	2.215	.3706	3.845
.096	0.595	1.460	.3791	2.434
.095	.467	1.270	.3894	2.126
.094	.444	1.164	.4067	2.015
.093	.479	1.127	.4245	2.031
.092	.543	1.137	.4424	2.122
.090	.736	1.241	.4904	2.467
.005	60.579	61.633	4.746	126.958

The curves for vapor pressure and orthobaric densities ($\varrho = 1/V$), obtained using Leach's shape factors with the optimized acentric factor are compared with the correlations of Goodwin, et al. [15] to obtain the deviations plotted in figure 1.

Also in figure 1, deviations for the vapor pressure and orthobaric density curves predicted using classical corresponding states are presented. This figure emphasizes that the Leach shape factors make a significant difference. The vapor pressure deviations are positive, and become larger as the triple point is approached, since classical corresponding states predicts a slope of the vapor pressure curve (dP/dT) which is too small. The deviation of pressure goes to zero at the critical point because the two parameters are choosen to make the critical temperature and pressure correspond exactly.

The critical point results for ethane are in table 5. Notice that the results are better using classical corresponding states than with the Leach shape factors. This is because classical corresponding states forces either the critical temperature and density to correspond ($\theta = \phi = 1$), or it forces the critical temperature and pressure to correspond ($\theta = 1$, $\phi = Z_o^c/Z_o^c$).

TABLE 5. *Ethane Critical Point Predictions.*

	Data	Leach θ, $\phi(\omega=0.094)$	$\theta=\phi=1$	$\theta=1$, $\phi=Z_o^c/Z_1^c$
T_c (K)	305.33	307.01 (0.55)*	305.33	305.33
P_c (bar)	47.488	48.790 (2.83)	47.750 (0.55)	47.448
ϱ_c (mol/L)	6.80	6.98 (2.65)	6.80	6.76 (−.59)

* Percent deviation is in parentheses.

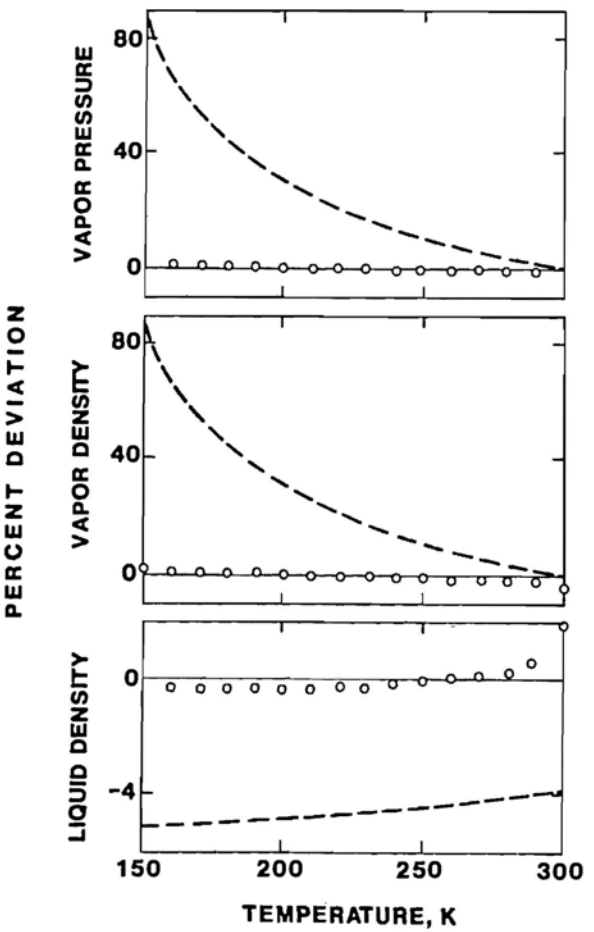

FIGURE 1. Percent deviations [(expt-calc) × 100/calc] for the vapor pressure, vapor density and liquid density for ethane at saturation. Data from Goodwin [15]. Calculations from the extended corresponding states method with the parameter ω_o optimized, circles. Also shown as the dashed line are the results with $\theta = 1$ and $\phi = Z_o^c/Z_o^c$, see equations (22)—(27).

The Critical Line:

We first calculate the critical line using the Leach shape factor equations with acentric factors of 0.005 and 0.094 for methane and ethane respectively. The results are plotted against the critical line data found in the review article of Hicks and Young [16], and identified in the caption to figure 2 (the symbols used in figure 2 are identical with those used in figures 3 through 7).

The results are presented in the form of T-x and p-x plots in figures 2–5 and show the general trends obtained by varying the binary interaction parameters, ξ and η. Holding ξ constant, figures 2 and 3 show that η has a small effect on the T-x curve, and a large effect on the p-x curve. In both cases, increasing η gives a better representation of the data.

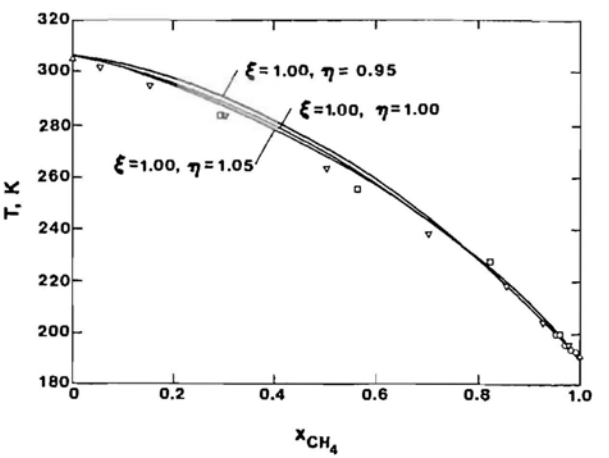

FIGURE 2. The methane-ethane T-x critical plot calculated via extended corresponding states showing the variation caused by the interaction parameter, η. Data [16]: ∇ Bloomer, Gani and Parent; □ Price and Kobayashi; ○ Wicheterle and Kobayashi. The values for the pures, △, are from Goodwin [15] and [19].

Holding η constant, figures 4 and 5 show that ξ has a much larger effect on the T-x curve than did η, and an equally large effect on the p-x curve. The important point to notice is that the maximum value in the p-x curve is shifted towards small mole fraction values (of CH_4) by decreasing ξ. The best representation of the P-x curve in figure 3 (i.e., $\xi = 1.00$, $\eta = 1.08$) indicates that the peak of the curve needs to be shifted towards the smaller mole fractions to improve the agreement, thus, ξ should be decreased.

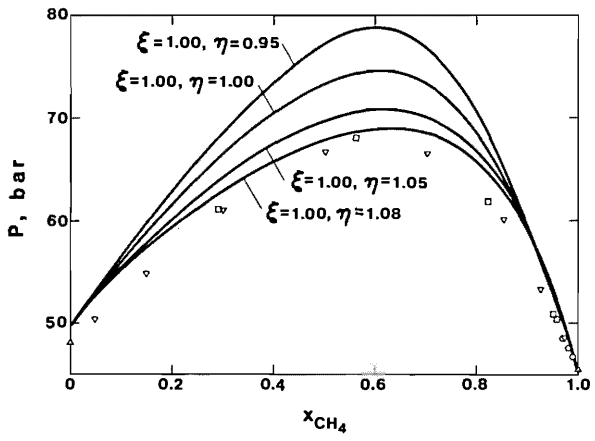

FIGURE 3. The p-plot corresponding to figure 2.

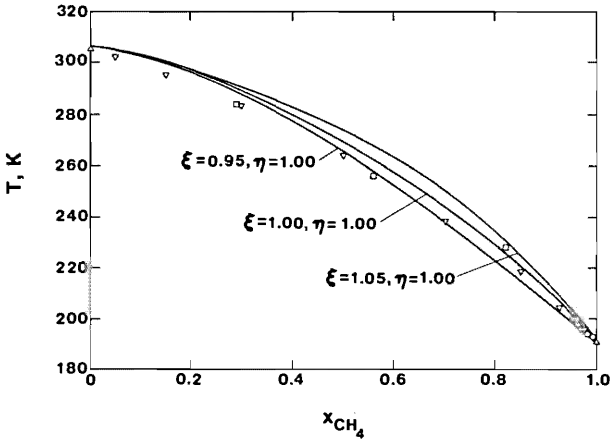

FIGURE 4. Variation of the parameter, ξ, for methane-ethane in the T-x plot.

To achieve the goal of obtaining the interaction parameters by fitting the critical line data, a manual search technique was initiated. The "best fit" was defined in the least squares sense. The results of this search were that $\xi = 0.97$, and $\eta = 1.13$ were chosen as the "best" values for the interaction parameters. The "best fit" T-x and p-x curves are presented in figures 6 and 7 respectively.

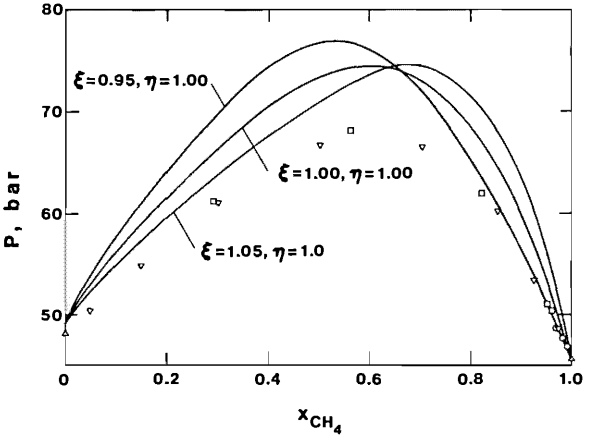

FIGURE 5. The p-x plot corresponding to figure 4.

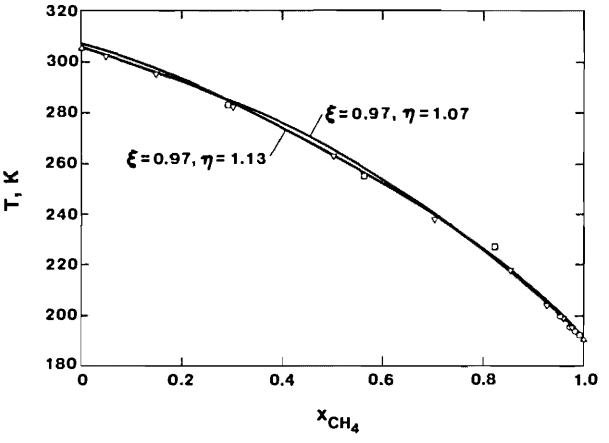

FIGURE 6. The T-x critical line of methane-ethane with optimized interaction parameters. The two curves correspond to extended corresponding states [$\xi = 0.97$, $\eta = 1.13$] and the classical corresponding states with $\omega_a = \omega_o$ [$\xi = 0.97$, $\eta = 1.07$].

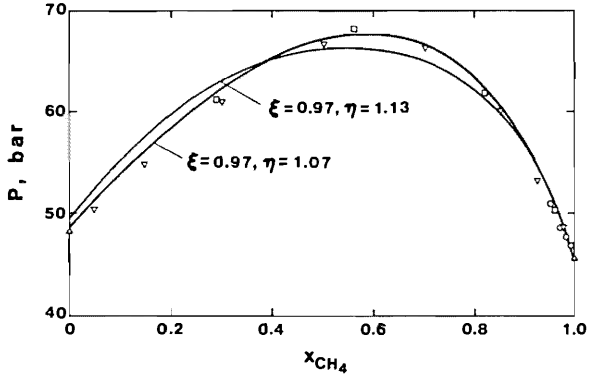

FIGURE 7. The p-x plot corresponding to figure 6.

The fit of the T-x curve is good, with only one data point which seems astray. The p-x curve, however, does not have the right shape to fit the data well. Part of the fitting problem is due to the bad prediction which is made for the critical point of pure ethane. This led us to try the second approach of setting $\omega_a = \omega_o$. Hence, the critical endpoints in the T-x, and p-x curves are exact. A new optimization led to the parameter values $\xi = 0.97$, $\eta = 1.07$. While the fit of the T-x curve was not significantly improved that for the p-x curve was. These results are shown in figures 6 and 7.

Vapor-Liquid Equilibria Results:

Of the VLE data judged to be thermodynamically consistent by Hiza, et al. [2], three representative isotherms were chosen to test the predictions made using the binary interaction parameters determined in the previous section. Two of the isotherms are supercritical (250 K and 199.92 K), and one is subcritical (144.26 K). The sources of the data are: 250 K isotherm, Davalos, et al. [17]; 199.92 K and 144.26 K isotherms, Wichterle and Kobayashi [18].

The VLE calculations used the Leach shape factors with the acentric factors 0.005 and 0.094 for methane and ethane respectively. The results are presented as K-value deviation plots for both the methane and the ethane K-value predictions. Figures 8, 9, and 10 contain these curves with the interaction parameters obtained from the critical line fit (i.e., $\xi = 0.97, \eta = 1.07$). These figures also show that setting the interaction parameters to unity gives much better VLE predictions than do the parameters obtained from the best fit of the critical line data.

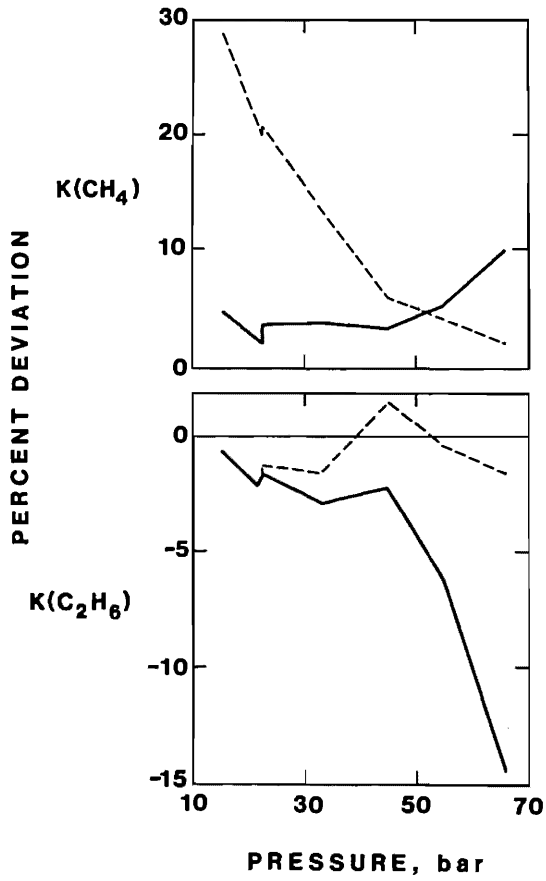

FIGURE 8. Methane-ethane K-value deviation plots at 250 K. Shown are the (dashed) curves with the interaction parameters from the critical line fit [$\xi = 0.97$, $\eta = 1.07$] and, for reference, with $\xi = \eta = 1.00$ as the solid curves.

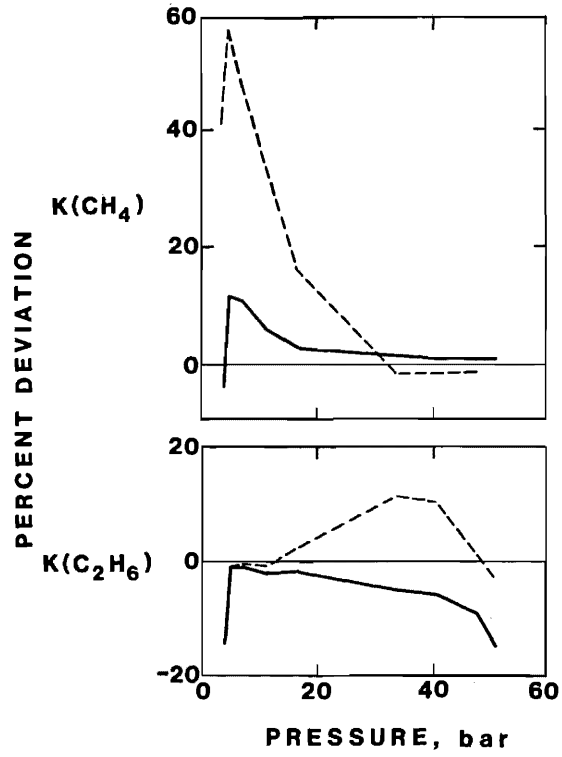

FIGURE 9. Methane-ethane K-values at 199.92 K.

5. Summary and Conclusions

The proposed technique of calculating binary critical lines by numerically evaluating the second and third order derivatives of the Gibbs free energy has been checked with an analytical solution for the special case of classical corresponding states, and has proven successful. The best least squares fit of the critical line data of the system methane-ethane was then shown to be poor (particularly the p-x curve) if the Leach shape factors are used with an acentric

factor optimized for pure component vapor pressure predictions. This is due to a bad prediction of the critical endpoint for ethane. To improve this fit, we use classical corresponding states to force correspondence of the temperature and pressure at the critical line endpoints. However we also show that the pure component vapor pressure predictions are not satisfactory if this is done. Finally, VLE predictions are made using Leach shape factors with the acentric factor optimized for vapor pressure predictions, and the binary interaction parameters obtained from the best fit of the critical line data (i.e., with $\theta = 1$, $\phi = Z_o^c/Z_d^c$). The results are not as good in general as those which are obtained by setting $\xi = \eta = 1$. Hence we conclude that a fit of the binary critical line does not yield binary interaction parameters of any general significance.

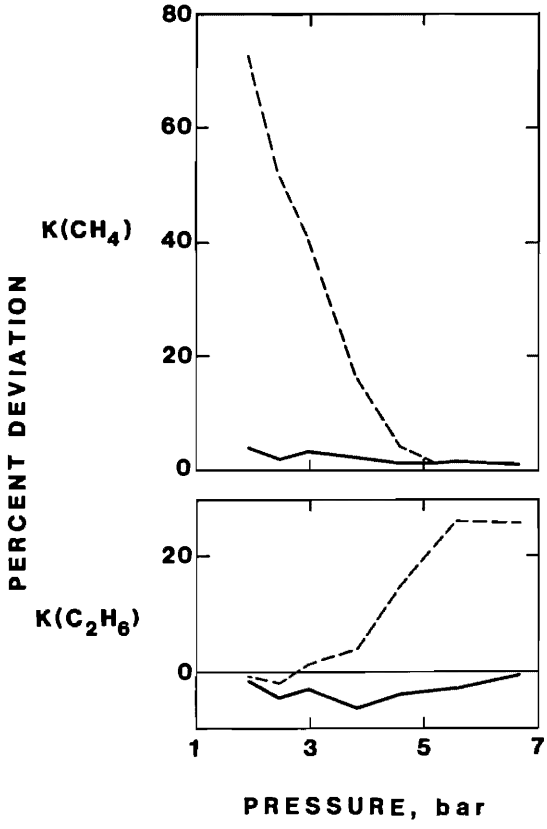

FIGURE 10. Methane-ethane K-values at 144.26 K.

6. References

[1] Wielopolski, P. On the calculation of critical liquid-vapor lines of binary mixtures. J. Res. Nat. Bur. Stand. (U.S.) **85**(6): 441-449; 1980 November-December.

[2] Hiza, M. J.; Miller, R. C.; Kidnay, A. J. A review, evaluation, and correlation of the phase equilibria, heat of mixing and change in volume on mixing for liquid mixtures of methane plus ethane. J. Phys. Chem. Ref. Data **8**(3): 799-816; 1979.

[3] Watson, I. D.; Rowlinson, J. S. The prediction of the thermodynamic properties of fluids and fluid mixtures. II. Liquid-vapor equilibrium in the system argon + nitrogen + oxygen. Chem. Eng. Sci. **24**: 1575-1580; 1969.

[4] Gunning, A. J.; Rowlinson, J. S. The prediction of the thermodynamic properties of fluids and fluid mixtures. III. Applications. Chem. Eng. Sci. **28**: 521-527; 1973.

[5] Teja, A. S.; Rowlinson, J. S. The prediction of the thermodynamic properties of fluids and fluid mixtures. IV. Critical and azeotropic states. Chem. Eng. Sci. **28**: 529-538; 1974.

[6] Mollerup, J.; Rowlinson, J. S. The prediction of the densities of liquefied natural gas and of lower molecular weight hydrocarbons. Chem. Eng. Sci. **29**: 1373-1381; 1974.

[7] Mollerup, J. Correlated and predicted thermodynamic properties of LNG and related mixtures in the normal and critical regions. Paper E-2 in Advances in Cryogenic Engineering, Vol. **20**. K. D. Timmerhaus, ed. New York, NY: Plenum Publishing Corp.; 1975. 172-194.

[8] Mollerup, J. Thermodynamic properties of natural gas, petroleum gas, and related mixtures: enthalpy predictions. Paper M-1 in Advances in Cryogenic Engineering, Vol. **23**. K. D. Timmerhaus, ed. New York, NY: Plenum Publishing Corp.; 1978. 550-560.

[9] Henderson, D.; Leonard, P. J. Physical Chemistry. Edit Eyning, H.; Henderson, D.; Jost, W.; (Academic Press, New York, 1971) Chapter 7, "Liquid Mixtures."

[10] Eaton, B. E. Prediction of the critical line of binary mixtures: Determination of binary interaction parameters. M.S. Thesis, University of Colorado, 1980. 151 p.

[11] Leach, J. W.; Chappelear, P. S.; Leland, T. W. Use of molecular shape factors in vapor-liquid equilibrium calculations with the corresponding states principle. A.I.Ch.E. J. **14**(4): 568-576; 1968.

[12] Ely, J. F.; Hanley, H. J. M. Ind. and Eng. Chem. Fund. (in press, 1981).

[13] McCarty, R. D. A modified Benedict-Webb-Rubin equation of state for methane using recent experimental data. Cryogenics **14**(5): 276-280; 1974.

[14] Hildebrand, F. B. *Introduction to Numerical Analysis*, 2nd ed. New York, NY: McGraw-Hill; 1974. 669 p.

[15] Goodwin, R. D.; Roder, H. M.; Straty, G. C. Thermophysical properties of ethane, from 90 to 600 K at pressures to 700 bar. Nat. Bur Stand. (U.S.) Tech. Note 684; 1976 August. 320 p.

[16] Hicks, C. P.; Young, C. L. The gas-liquid critical properties of binary mixtures. Chemical Reviews **75**(2): 139-175; 1975 April.

[17] Davalos, J.; Anderson, W. R.; Phelps, R. E.; Kidnay, A. J. Liquid-vapor equilibria at 250.00 K for systems containing methane, ethane, and carbon dioxide. J. Chem. Eng. Data **21**(1): 81-84; 1976.

[18] Wichterle, I.; Kobayashi, R. Vapor-liquid equilibrium of methane-ethane system at low temperatures and high pressures. J. Chem. Eng. Data **17**(1): 9-12; 1972.

[19] Goodwin, R. D. The thermophysical properties of methane, from 90 to 500 K at pressures to 700 bar. Nat. Bur. Stand. (U.S.) Tech. Note 653; 1974 April. 274 p.

JOURNAL OF RESEARCH of the National Bureau of Standards
Vol. 86, No. 5, September–October 1981

Propagation of Density Fluctuations in Nonuniform Fluids: Simple Models

James C. Rainwater*

National Bureau of Standards, Boulder, CO 80303

May 4, 1981

As a first step toward the understanding of Rayleigh-Brillouin scattering from a fluid with a temperature gradient, we analyze the initial value problem for certain prototype one-dimensional nonuniform systems. For sufficiently short times and localized initial pulses, it is not necessary to impose actual physical boundaries on the linearly nonuniform system. By a straightforward, though unconventional, application of Fourier and Laplace transform methods, explicit and physically reasonable solutions are constructed for the propagation of fluctuation pulses in space and time according to the nonuniform wave and diffusion equations and a special case of the nonuniform damped wave equation. The analog of the dynamic structure factor is also constructed for the latter two cases.

Key words: damped wave motion; density fluctuations; diffusion; dynamic structure factor; initial value problem; nonuniform systems; one-dimensonal models; Rayleigh-Brillouin scattering.

I. Introduction

There has been considerable recent interest in the problem of Rayleigh-Brillouin scattering in a fluid with a stationary temperature gradient. [1–10] [1] The problem, in essence, is to generalize Mountain's standard derivation of the equilibrium Rayleigh-Brillouin spectrum [11] to the nonequilibrium stationary state.

Laser light is scattered from a liquid because of random density (and therefore dielectric constant) fluctuations. [12, 13] In the hydrodynamic regime, a density fluctuation will propagate in time partly as a diffusion or "heat" mode, causing the Rayleigh line, and partly as a wave or "sound" mode, causing the two Brillouin lines. With a temperature gradient the spectrum is altered. For example, if more sound modes are generated at the hot side of the liquid than at the cold side, there will be a larger flux of sound modes from hot-to-cold than from cold-to-hot, thereby causing a size asymmetry in the Brillouin peaks. Some treatments of this problem, [1–4] in fact, predict no spectral changes other than an overall asymmetric scale factor in the Brillouin peaks. Such an asymmetry has recently been observed experimentally. [14]

Other authors [5–9] predict changes in the mathematical shape of the Brillouin lines from their equilibrium (Lorentzian) form. Such changes of shape, very difficult to measure experimentally, are interpreted here as the effect of propagation of modes through regions of changing sound speed, sound attenuation, and thermal diffusivity. Among the theories published to date, [1–10] there is significant disagreement as to the precise form of the nonequilibrium spectrum. Some discrepancies may arise from different assumptions about the nature of the nonequilibrium steady state, but it is not clear at this time if all do.

None of the theories published thus far appear to follow the procedure of ref. 11 explicitly, i.e., to solve the hydrodynamic equations for the time evolution of a density fluctuation and, subsequently, to perform a

*Continuous Process Technology Program, National Engineering Laboratory.

[1] Figures in brackets indicate literature references at the end of this paper.

stochastic and ensemble average to determine the dynamic structure factor and hence the spectrum of scattered light. Closest in spirit to such a procedure is the hydrodynamic approach of van der Zwan and Mazur, [7, 8] but they appear to bypass the calculation of the time development of an individual fluctuation.

An explicit calculation of the evolution in time and (both physical and Fourier) space of a spontaneous density fluctuation, in the presence of a temperature gradient, should shed considerable light on the presently confused predictions of Rayleigh-Brillouin scattering. The possibility of changes with temperature, and hence distance, of *all* physically relevant variables should be considered. Significantly, possible changes in the shape of the Rayleigh line have been substantially neglected thus far. [1–10]

This paper represents an initial step in the execution of the above program. Since the full three-dimensional problem of coupled equations in density and temperature fluctuations is very complex mathematically, it is illuminating to deal first with simplified models. Here we solve explicitly the one-dimensional wave, diffusion, and damped wave equations to first order in nonuniformity. Care is taken to select nonuniform equations which correspond as closely as possible to the physical nonequilibrium steady-state problem.

Our technique is a generalization of a method due to Brownell [15] to calculate the Green's function for a nonuniform wave equation. We show that the initial value problem for the nonuniform wave, diffusion, and damped wave equations can indeed be solved, to linear order in nonuniformity, in a manner which closely parallels Mountain's derivation. The methods are systematic, but the mathematics becomes rapidly more difficult with greater complexity of the underlying differential equations. Our eventual goal, yet to be attained, is the explicit solution of the coupled hydrodynamic equations and determination of the dynamic structure factor in one and, if possible, three dimensions. Since wave and diffusion equations are prevalent throughout physics, the techniques presented here may prove useful for a variety of other physical problems as well.

We begin in section 2 with a general discussion of some predictable mathematical difficulties. Section 2.1 examines the applicability of the initial value problem to Rayleigh-Brillouin scattering in a fluid with a temperature gradient. Section 2.2 describes the needed transformations of variable and examines the range of validity of a first-order nonuniformity calculation. Solutions to the various initial value problems in the uniform limit, mostly well-known, are outlined in Section 3. The subsequent three sections present explicit solutions, with intuitively oriented interpretations, to the initial value problem for the nonuniform wave, diffusion, and damped wave equations respectively. Results are summarized in Section 7.

2. Initial mathematical considerations

2.1. The initial value problem

The basic relationship between the measured spectrum of scattered light and the structure of a liquid sample is [12, 13]

$$I(\omega) = C\, S(\mathbf{k}, \omega) \quad . \tag{1}$$

where ω is the shift in frequency and $\mathbf{k}$ the shift in wave vector of the scattered light, I is the average measured intensity, and C is a constant, not important for our present interests. $S(\mathbf{k}, \omega)$, the dynamic structure factor, is the Fourier transform in time of the intermediate scattering function $F(\mathbf{k}, t)$

$$S(\mathbf{k}, \omega) = \int_{-\infty}^{\infty} e^{-i\omega t} F(\mathbf{k}, t)\, dt \tag{2}$$

where

$$F(\mathbf{k}, t) = \langle \bar{n}(-\mathbf{k}, 0)\, \bar{n}(\mathbf{k}, t) \rangle \, . \tag{3}$$

Here the brackets denote an ensemble average and $\bar{n}(\mathbf{k}, t)$ is the Fourier transform in space of $n(\mathbf{r}, t)$, the fluctuation of liquid density about equilibrium, i.e.,

$$\bar{n}(\mathbf{k}, t) = \int d\mathbf{r}\, e^{-i\mathbf{k}\cdot\mathbf{r}}\, n(\mathbf{r}, t)\,. \tag{4}$$

The hydrodynamic regime is defined by the inequality

$$k^{-1} >> \ell \tag{5}$$

where ℓ is the interparticle spacing, and

$$k = 2\, k_i \sin\frac{\theta}{2}\,, \tag{6}$$

where k_i is the wave vector of the incident light and θ is the angle by which the light is scattered. In a liquid ℓ is small and scattering experiments with visible light are always in the hydrodynamic regime. For dilute gases ℓ is large, but the hydrodynamic regime can be attained [16] with sufficiently small θ. Kirkpatrick, et al. [5] consider the nonuniform problem starting from the Boltzmann equation, which is strictly valid only for dilute gases. The initial experimental observation of changes in the scattered spectrum due to a temperature gradient has been made with liquid water at a very low scattering angle. [14].

Mountain's derivation [11] of Rayleigh-Brillouin scattering in equilibrium begins with the observation of Landau and Placzek [17] that, in the hydrodynamic regime, density fluctuations, $n(\mathbf{r}, t)$, and temperature fluctuations, $T(\mathbf{r}, t)$, satisfy a set of coupled second-order linear differential equations. After a Fourier transformation in space and a Laplace transformation in time, those equations become coupled algebraic equations which involve the initial ($t = 0$) values and time derivatives of the fluctuations. The derivation of ref. [11], in effect, makes the further simplifications

$$\dot{\bar{n}}(\mathbf{k}, 0) = 0 \tag{7}$$

$$\bar{T}(\mathbf{k}, 0) = 0 \tag{8}$$

where a dot denotes a time derivative. These simplifications are not literally correct, but are permissible because, at the end of the calculation when the autocorrelation function is evaluated, the above quantities are not correlated with the initial density fluctuations. In particular, because of time reversal invariance,

$$<\bar{n}(-\mathbf{k}, 0)\, \dot{\bar{n}}(\mathbf{k}, 0)> = 0 \tag{9}$$

and because of the thermodynamic independence of density and temperature,

$$<\bar{n}(-\mathbf{k}, 0)\ \bar{T}(\mathbf{k}, 0)> = 0. \tag{10}$$

The solution of the differential equations leads to a dynamic structure factor, eq. (2), in terms of the static structure factor

$$S(k) = <\bar{n}(-\mathbf{k}, 0)\, \bar{n}(\mathbf{k}, 0)> \tag{11}$$

which must be determined from separate (but well-known) thermodynamic considerations. [12, 18] An alternate method to the above initial value problem is to consider the response of the system to a random fluctuating force. [19]

In the presence of a stationary temperature gradient, time-reversal symmetry no longer holds, [1, 4] and eq (9) is no longer satisfied. Thus an initial value calculation, by itself, does not suffice to determine the altered Rayleigh-Brillouin spectrum. However, an initial value approach may suffice to determine "shape effects," as opposed to "size effects," in the altered spectrum.

More precisely, we define ϵ, which is proportional to $|\nabla T|$, as the appropriate dimensionless expansion parameter. The LHS of eq (9) will be $0(\epsilon)$ due to differences in the rate of generation of fluctuations at different positions in the fluid. These differences will lead to overall asymmetries in the Brillouin lines. A quite different effect is the change in the shape of the Rayleigh and Brillouin lines due to propagation of the unperturbed fluctuations through a nonuniform medium.

In the linearization of the problem about uniformity, it is reasonable to assume that the two effects are independent and additive. Further corrections due to the nonuniform propagation of fluctuations which are themselves generated by nonuniformity presumably lead to second order, $0(\epsilon^2)$ corrections.

Thus an initial value problem approach to Rayleigh-Brillouin scattering in a temperature gradient, while incomplete, may suffice to determine the shape changes of the lines, and hence will complement those approaches which appear to emphasize only size changes. [1, 4]

2.2. Transformations and nonuniformity expansions

In the presence of a temperature gradient, any relevant physical property A of a fluid may be expanded in a Taylor series about some convenient origin of position ($\mathbf{r} = 0$) in the fluid, i.e.,

$$A(\mathbf{r}) = A(0) + (\mathbf{r} \cdot \nabla T)\left(\frac{\partial A}{\partial T}\right)_{r=0} + \ldots . \tag{12}$$

For the linearized problem, only the above two terms are retained.

The coefficients of the hydrodynamic equations, in equilibrium eqs. (6)–(8) of ref. [11], will then be position-dependent according to eq (12). Since the differential operators do not commute with $\mathbf{r}$, it is important to return to the fundamental derivations of the differential equations governing the processes, to determine in what order differential operators and position-dependent coefficients should be placed.

In the prototype one-dimensional equations considered here, the coefficients will have the position dependence

$$a(x) = a_0 + a_1 x \tag{13}$$

where a_1 is assumed to be small.

We will examine for the various differential equations the initial value problem, i.e., the solution for $y(x,t)$ given $y(x,0)$ and zero initial time derivative,

$$\dot{y}(x,0) = 0 . \tag{14}$$

Equation (14) is not necessary for the diffusion equation, which is first order in time.

It is convenient at the outset to introduce a special notation for the several variable spaces which are required. Physical space or "P-space" denotes the variables $\{x,t\}$. Fourier space or "F-space" consists of the variables $\{k,t\}$, where

$$\bar{y}(k,t) = \int_{-\infty}^{\infty} dx\, e^{-ikx}\, y(x,t) . \tag{15}$$

Laplace space or "L-space" is formed by the variables $\{x,s\}$, where

$$\hat{y}(x,s) = \int_{-\infty}^{\infty} dt e^{-st}\, y(x,t) . \tag{16}$$

Finally, Fourier-Laplace space or "FL-space" consists of the variables $\{k,s\}$, where

$$\tilde{y}(k,s) = \int_{-\infty}^{\infty} dx\, e^{-ikx}\, \hat{y}(x,s) = \int_{-\infty}^{\infty} dt\, e^{-st}\, \bar{y}(k,t) . \tag{17}$$

Our convention for transformed functions is that a bar denotes F-space, a caret L-space, and a tilde FL-space.

The differential equations considered here require that certain coefficients be positive, which is, in general, in conflict with eq (13). For small but finite a_1, if

$$x < -a_0/a_1$$

then $a(x) < 0$, which could lead to physical nonsense, e.g., negative diffusion or imaginary wave speed. We must assume that such large negative values of position are irrelevant to the problem.

A possible escape from this difficulty is to impose explicit boundaries on the linearly nonuniform region of space with, for example, separate uniform regions outside those boundaries.

$$\begin{aligned} a(x) &= a^{(1)} && x \le -L \\ &= \frac{1}{2}[a^{(1)} + a^{(2)}] \\ &\qquad + \frac{1}{2}[a^{(2)} - a^{(1)}]\frac{x}{L} && -L \le x \le L \\ &= a^{(2)} && x \ge L \end{aligned}$$

We elect, however, not to proceed in this manner because a new parameter L is introduced into the problem, and the exact solution for a general L is likely to be mathematically cumbersome. Furthermore, for the conditions we seek to impose, there should exist a unique linearized solution

$$y(x, t) = y^{(o)}(x, t) + a_1 y^{(1)}(x, t) + O(\epsilon^2), \tag{18}$$

where $y^{(o)}$ is the uniform solution, which is independent of L. These conditions are that the initial value packet be localized and that the time be small compared to the time required for the packet to propagate (in significant measure) to the region of negative a. We consider initial value packets of finite width w_o, i.e.,

$$y(x, 0) = 0 \qquad |x| > \frac{w_o}{2} \tag{19}$$

and the "smallness" of a_1 is made precise in dimensionless form by

$$\frac{a_1 w_o}{a_o} << 1 . \tag{20}$$

Additionally, we require a constraint on the time t of propagation. For example, the solution to the uniform wave equation moves with constant velocity c, so we require times short enough that

$$\frac{a_1 ct}{a_o} << 1 \tag{21}$$

or, for the diffusion equation, since the mean-square width of an initial delta-function pulse is (in one dimension)

$$\langle x^2 \rangle = 2Dt \tag{22}$$

the appropriate condition on the time is

$$a_1 (2Dt)^{1/2}/a_o << 1 . \tag{23}$$

Calculation of the dynamic structure factor, in principle, requires an integral from $t = 0$ to $t = \infty$. Nevertheless, we expect the linear nonuniformity theory to give a meaningful structure factor if the fluctuation has substantially decayed away in a time such that the inequalities (21) and (23) are valid. The phrase "decay away" is imprecise; a *norm* of the fluctuation needs to be defined and must be shown to be negligible after some particular time interval.

One possible norm is

$$\|y\| = \int_{-\infty}^{\infty} dx\, y(x, t)\,, \tag{24}$$

but, for the equations considered here, eq (24) happens to be a constant of the motion, and does not decay in time at all.

What do decay in time however, are Fourier components of the fluctuation for finite k. The $k = 0$ componenet is $\|y\|$ itself. For diffusion, $\bar{y}(k, t)$ decays as e^{-Dk^2t}, and for the damped wave equation considered here, it decays as $e^{-\Gamma k^2 t}$, where Γ is the attenuation coefficient. In the Rayleigh-Brillouin experiment, a particular value of k is monitored by virtue of the fixed laser light frequency and scattering angle. If we are similarly interested in monitoring a particular value $k = k_o$, then for the times

$$t_D = (D\, k_o^2)^{-1} \tag{25}$$

and

$$t_\Gamma = (\Gamma\, k_o^2)^{-1} \tag{26}$$

we require that inequalities (21) and (23) hold. The various inequalities for our particular applications in terms of variables defined in later sections are listed in table I.

TABLE 1.

Differential Equation	Conditions for Validity of $y(x,t)$	Conditions for Validity of $S(k,\omega)$
Undamped wave	$\frac{bw_0}{a} << 1$	Never valid
	$\frac{bct}{a} << 1$	
Diffusion	$\frac{bw_0}{a} << 1$	$\frac{b}{ak} << 1$
	$\frac{b}{a}(D_0 t)^{1/2} << 1$	
Damped wave	$\frac{bw_0}{a} << 1$	
		$\frac{bc}{a\Gamma k^2} << 1$
$(\frac{\Gamma k}{c} << 1)$	$\frac{bct}{a} << 1$	

The standard method of solution to the initial value problem for a partial differential equation in P-space is to transform to FL-space. In the uniform cases, the equation is an algebraic one and is easily solved. The solution is completed upon inverse transformation to P-space. In ref. [11] only the inverse transformation to F-space is required to obtain the intermediate scattering function, eq (3), and the dynamic structure factor, eq (2).

Since, under Fourier transformation

$$x \rightarrow i \frac{\partial}{\partial k}$$

a partial differential equation in P-space with linearly nonuniform coefficients becomes, in *FL*-space, a linear differential equation in k. It is always possible to solve a linear differential equation by the integrating factor technique. [20] However, a unique solution requires a boundary value on k, and the problem appears at first not to specify any particular boundary value. We shall see that this apparent new degree of freedom is bogus and that the physics imposes a particular boundary value on k.

A more cumbersome problem is the inverse transformation. As stated previously, in *P*-space the solution is nonzero only within a width w about the origin such that (20) holds. In *F*-space, according to Heisenberg's inequality, [21] the solution $\bar{y}(k, t)$ has a width w_o^{-1}. Only the values of x such that

$$\frac{a_1 |x|}{a_o} << 1 \tag{27}$$

are significant; however, in *F*-space there is no analogous inequality. For example,

$$\frac{a_1}{a_o |k|} << 1 \tag{28}$$

does not hold for all significant values of $|k|$, since such values of $|k|$ can range from *zero* to w_o^{-1}.

We conclude that there is no natural means, in *FL*-space or *F*-space, to take advantage of the smallness of the nonuniformity parameter. Therefore, after solving the linear differential equation in *FL*-space, we must first inverse transform to *L*-space (and expand in nonuniformity where convenient), then inverse transform to *P*-space (and further expand in nonuniformity), and lastly transform to *F*-space. This circuitous but required route is shown schematically in figure 1.

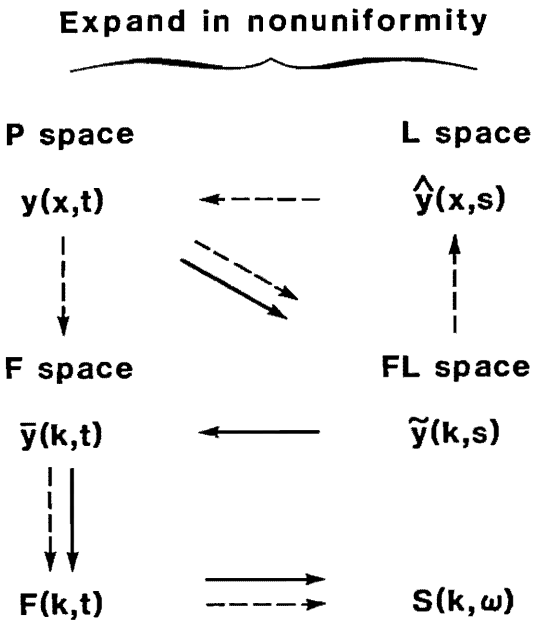

FIGURE 1. Sequence of transformations for the uniform problem (solid arrows) and for the nonuniform problem (dashed arrows).

In the following sections we carry out the above procedure explicitly for three nonuniform differential equations, after first reviewing their respective uniform solutions.

3. Uniform differential equations

In this section, for reference purposes, we briefly outline the soluions to the initial value problem for the one-dimensional *uniform* wave, diffusion, and damped wave equations. These results are well-known.

3.1. Wave equation

The wave equation in P-space is

$$\frac{\partial^2 y}{\partial x^2} - \frac{1}{c^2}\frac{\partial^2 y}{\partial t^2} = 0\,. \tag{29}$$

We assume a given initial wave packet $y(x, 0)$ with zero initial time derivative. The equation is FL-space is

$$-k^2\,\bar{y}(k, s) - \frac{s^2}{c^2}\,\bar{y}(k, s) + \frac{s}{c^2}\,\bar{y}(k, 0) = 0 \tag{30}$$

with the solution

$$\bar{y}(k, s) = \frac{s\bar{y}(k, 0)}{s^2 + c^2k^2}\,. \tag{31}$$

The solution in F-space is

$$\bar{y}(k, t) = \frac{1}{2}\,\bar{y}(k, 0)\,[e^{ickt} + e^{-ickt}]\,, \tag{32}$$

the solution in L-space is

$$\hat{y}(x, s) = \frac{1}{2c}\int_{-\infty}^{\infty} du\; e^{-s|u|/c}\, y(x - u, 0) \tag{33}$$

and the solution in P-space is d'Alembert's solution,

$$y(x, t) = \frac{1}{2}\,[y(x - ct, 0) + y(x + ct, 0)], \tag{34}$$

i.e., the pulse divides in half and each half moves, without change of shape, at speed c. For an ensemble of packets, the analog of the intermediate scattering function is

$$\langle \bar{y}(-k, 0)\,\bar{y}(k, t)\rangle = \frac{1}{2}\,\langle \bar{y}(-k, 0)\,\bar{y}(k, 0)\rangle\,[e^{ickt} + e^{-ickt}] \tag{35}$$

and its Fourier transform in time, the analog of the dynamic structure factor, is

$$S(k, \omega) = \pi\,\langle \bar{y}(-k, 0)\,\bar{y}(k, 0)\rangle\,[\delta(\omega - ck) + \delta(\omega + ck)], \tag{36}$$

i.e., two "Brillouin lines" of infinitely small width, since there is no damping.

3.2. Diffusion equation

The diffusion equation in P-space is

$$\frac{\partial y}{\partial t} - D\frac{\partial^2 y}{\partial x^2} = 0. \tag{37}$$

An initial wave packet $y(x, 0)$ is given. Since the equation is first-order in time, no initial time derivative is specified. The equation in FL-space is

$$s\tilde{y}(k, s) - \bar{y}(k, 0) + Dk^2\,\tilde{y}(k, s) = 0 \tag{38}$$

with solution

$$\tilde{y}(k, s) = \frac{\bar{y}(k, 0)}{s + Dk^2}\,. \tag{39}$$

The solution in F-space is

$$\bar{y}(k, t) = \bar{y}(k, 0)\, e^{-Dk^2 t}\,, \tag{40}$$

the solution in L-space is

$$\hat{y}(x, s) = \frac{1}{2}(s\,D)^{-1/2} \int_{-\infty}^{\infty} dv\, y(v, 0)\, e^{-(s/D)^{1/2}|x-v|}, \tag{41}$$

and the solution in P-space is

$$y(x, t) = \frac{1}{2(\pi\, Dt)^{1/2}} \int_{-\infty}^{\infty} dv\, y(v, 0)\, e^{-(x\,-\,v)^2/4Dt}\,. \tag{42}$$

For a δ-function initial condition, $y(x, 0) = \delta(x)$, the solution takes the familiar form

$$y(x, t) = \frac{1}{2(\pi\, Dt)^{1/2}}\, e^{-x^2/4Dt}\,. \tag{43}$$

The analog of the intermediate scattering function is

$$< \bar{y}(-k, 0)\, \bar{y}(k, t) > \;=\; < \bar{y}(-k, 0)\, \bar{y}(k, 0) > e^{-Dk^2 t} \tag{44}$$

and the analog of the dynamic structure factor is

$$S(k, \omega) = < \bar{y}(-k, 0)\, \bar{y}(k, 0) > \frac{2D\,k^2}{\omega^2 + (D\,k^2)^2}\,, \tag{45}$$

i.e., a Lorentzian "Rayleigh line" with width Dk^2.

3.3. Damped wave equation

There are several possible choices for a wave equation with damping. We choose the case that corresponds most closely to the Rayleigh-Brillouin problem, i.e., an equation with "k^2-damping." In P-space this is

$$\frac{\partial^2 y}{\partial x^2} + \frac{2\Gamma}{c^2}\,\frac{\partial^2}{\partial x^2}\,\frac{\partial y}{\partial t} - \frac{1}{c^2}\,\frac{\partial^2 y}{\partial t^2} = 0\,. \tag{46}$$

We again begin with an initial wave packet $y(x, 0)$ with zero initial time derivative. The equation in F-space is

$$k^2\,\bar{y}(k, t) + \frac{2\Gamma k^2}{c^2}\,\frac{\partial}{\partial t}\,\bar{y}(k, t) + \frac{1}{c^2}\,\frac{\partial^2}{\partial t^2}\,\bar{y}(k, t) = 0 \tag{47}$$

which is the equation for a damped harmonic oscillator. The condition that the oscillation be underdamped, which we impose here, is

$$\frac{\Gamma k}{c} < 1\,. \tag{48}$$

The equation in FL-space is

$$k^2\,\tilde{y}(k,\,s) + \frac{2\Gamma s\,k^2}{c^2}\,\tilde{y}(k,\,s) - \frac{2\Gamma\,k^2}{c^2}\,\bar{y}(k,\,0) + \frac{s^2}{c^2}\,\tilde{y}(k,\,s) - \frac{s}{c^2}\,\bar{y}(k,\,0) = 0 \tag{49}$$

with the solution

$$\tilde{y}(k,\,s) = \bar{y}(k,\,0)\,\frac{s + 2\Gamma k^2}{s^2 + 2\Gamma s k^2 + c^2 k^2}\,. \tag{50}$$

The solution in F-space is

$$\bar{y}(k,\,t) = \frac{1}{2}\,\bar{y}(k,\,0)\left\{e^{-\Gamma k^2 t}\left[e^{i(c^2-\Gamma^2k^2)^{1/2}kt} + e^{-i(c^2-\Gamma^2k^2)^{1/2}kt}\right] + \frac{\Gamma k}{i(c^2-\Gamma^2k^2)^{1/2}}\,e^{-\Gamma k^2 t}\left[e^{i(c^2-\Gamma^2k^2)^{1/2}kt} - e^{-i(c^2-\Gamma^2k^2)^{1/2}kt}\right]\right\} \tag{51}$$

and the solution in L-space is

$$\hat{y}(x,\,s) = \frac{1}{2(c^2+2\Gamma s)^{1/2}}\int_{-\infty}^{\infty} dv\,\left[y(v,\,0) - \frac{2\Gamma}{s}\,\frac{\partial^2}{\partial v^2}\,y(v,0)\right] \times e^{-s|x-v|\,/\,(c^2+2\Gamma s)^{1/2}}\,. \tag{52}$$

However, to the best of our knowledge, there is no representation of the solution in P-space in terms of elementary functions. But a convenient approximate solution in P-space may be obtained by means of a dispersion expansion. First, the concept of a k-dependent wave speed is introduced, i.e.,

$$c(k) = c\left(1 - \frac{\Gamma^2k^2}{c^2}\right)^{1/2}. \tag{53}$$

If $\frac{\Gamma k}{c} << 1$ (extreme underdamping) we may expand in this small "dispersion parameter." Then eq (44), to leading order, is

$$\bar{y}(k,\,t) = \frac{1}{2}\bar{y}(k,\,0)\left\{e^{-\Gamma k^2 t}\left[e^{ickt} + e^{-ickt}\right]\right\} \tag{54}$$

with a corresponding solution in P-space

$$y(x,\,t) = \frac{1}{4(\pi\Gamma t)^{1/2}}\int_{-\infty}^{\infty} dv\,y(v,\,0)\left[e^{-(x-v+ct)^2/4\Gamma t} + e^{-(x-v-ct)^2/4\Gamma t}\right], \tag{55}$$

which corresponds to two wave pulses travelling in opposite directions and spreading with time in a diffusionlike manner. In the nonuniform case there will be expansions in both dispersion and nonuniformity; however it is reasonable to assume that the two expansions are independent of each other.

From the lowest-order solution, eq (54), the analog of the intermediate scattering function is

$$\langle\bar{y}(-\,k,\,0)\,\bar{y}(k,\,t)\rangle = \frac{1}{2}\,\langle\bar{y}(-\,k,\,0)\,\bar{y}(k,\,0)\rangle\,e^{-\Gamma k^2 t}\left[e^{ickt} + e^{-ickt}\right] \tag{56}$$

and the analog of the dynamic structure factor is

$$S(k,\,\omega) = \langle\bar{y}(-\,k,\,0)\,\bar{y}(k,\,0)\rangle \times \left[\frac{\Gamma k^2}{(\omega-ck)^2+(\Gamma k^2)^2} + \frac{\Gamma k^2}{(\omega+ck)^2+(\Gamma k^2)^2}\right], \tag{57}$$

i.e., two Lorentzian "Brillouin lines" each with width Γk^2.

4. Nonuniform wave equation

Having reviewed the initial value problem for the three uniform differential equations, we next derive solutions to their nonuniform counterparts. The solutions must have the form of the uniform solution plus a small correction linear in nonuniformity. In all cases the nonuniformity parameter will be denoted by the variable b. The solutions are subject to the constraints on time, distance, and wavenumber described in section 2.2.

In the following three sections we first present the exact form of the nonuniform differential equation which we take to be (in one dimension) closely analogous to the three-dimensional Rayleigh-Brillouin experimental situation described earlier. Thereafter we present a detailed mathematical derivation of the solution. Each selection then ends with a physical interpretation of the solution thus derived.

4.1. The differential equation

Following Brownell, [15] we write the nonuniform wave equation as

$$\varrho(x)\frac{\partial^2 y}{\partial t^2} - T\frac{\partial^2 y}{\partial x^2} = 0 \tag{58}$$

where

$$\varrho(x) = a + bx\,. \tag{59}$$

Physically, this corresponds to a stretched string with a variable mass per unit length $\varrho(x)$ at a constant tension T. This is analogous to the fluid with a stationary temperature gradient, where the pressure is constant throughout but the density varies (to first order linearly) with distance due to the gradient in temperature. Again we consider a given initial pulse $y(x, 0)$ with zero initial time derivative.

4.2. Solution

The equation in *FL*-space is

$$\frac{\partial}{\partial k}\bar{y}(k, s) - \left[\frac{ia}{b} + \frac{Tk^2 i}{bs^2}\right]\bar{y}(k, s) = \frac{1}{s}\frac{\partial}{\partial k}\bar{y}(k, 0) - \frac{ai}{bs}\bar{y}(k, 0)\,. \tag{60}$$

The first-order differential equation in k is solved by standard methods [20] as

$$\bar{y}(k, s) = \int_{k_1}^{k} dk'\left[\frac{ai}{bs}\bar{y}(k', 0) - \frac{1}{s}\frac{\partial}{\partial k'}\bar{y}(k', 0)\right] \times exp\left[-\frac{ia(k'-k)}{b} - \frac{Ti(k'^3 - k^3)}{3bs^2}\right]. \tag{61}$$

Formally, the integration constant k_1 appears to give a new and unwanted degree of freedom to the problem. However, as pointed out by Brownell [15], the existence of an inverse transformation requires certain analyticity properties in the complex s-plane. In our formulation, the requirement is that $\bar{y}(k, s)$ be analytic in the right half of the complex s-plane, which in turn requires that $(k'^3 - k^3)$ be the same sign for all k. This requires that $k_1 = \infty$. We also henceforth assume, without loss of generality, that b is positive.

Changing variables to $u = k' - k$ yields

$$\bar{y}(k, s) = \int_0^{\infty} du\left[\frac{ai}{bs}\bar{y}(u + k, 0) - \frac{1}{s}\frac{\partial}{\partial k}\bar{y}(u + k, 0)\right] \times exp\left[-\frac{iau}{b} - \frac{Ti}{3bs^2}u(u^2 + 3ku + 3k^2)\right]. \tag{62}$$

As explained in section 2.2, we must now transform to L-space. Let $\mathcal{F}^{-1}$ denote the inverse Fourier transform operator, i.e.,

$$\mathcal{F}^{-1}\{f(k)\} = \frac{1}{2\pi}\int_{-\infty}^{\infty} dk\, e^{ikx} f(k)\,. \tag{63}$$

Now,

$$\mathcal{F}^{-1}\left[\frac{ai}{bs}\bar{y}(u+k,0) - \frac{1}{s}\frac{\partial}{\partial k}\bar{y}(u+k,0)\right]$$

$$= \frac{ai}{bs}y(x,0)\,e^{-iux}\left(1+\frac{bx}{a}\right). \tag{64}$$

Next we require the inverse Fourier transform of the second term in eq (62). The relation

$$\int_{-\infty}^{\infty} dk\, e^{-\alpha k^2-\beta k} = \left(\frac{\pi}{\alpha}\right)^{1/2} e^{\beta^2/4\alpha} \tag{65}$$

holds for complex α and β providing $Re\alpha > 0$. To apply eq (65), we must assign a small negative imaginary component to T, i.e.,

$$T \to T - i\epsilon \tag{66}$$

with the limit $\epsilon \to 0$ taken at the end of the calculation. It then follows that

$$\mathcal{F}^{-1}\left\{exp\left[-\frac{iau}{b} - \frac{Ti}{3bs^2}u(u^2+3ku+3k^2)\right]\right\}$$

$$= \frac{1}{2}s(b/\pi uiT)^{1/2}\,exp\left[\frac{i}{4}\left(\frac{Tu^3}{bs^2} - 2ux + \frac{bs^2x^2}{Tu}\right)\right] \tag{67}$$

$$\times\, exp\left[-\frac{iau}{b} - \frac{Tiu^3}{3bs^2}\right].$$

The assignment of a small imaginary part to the coefficient T appears arbitrary. It may be justified mathematically by an extension of Brownell's method, [15] which uses the complex Laplace transform with real coeffients and appropriate contours off the real axis in the complex s-plane. Here we employ the operationally simpler, and presumably equivalent, method of complex coefficients and a real Laplace transform variable.

From eqs (62), (64), and (67), and the convolution theorem for Fourier transforms, we obtain

$$\hat{y}(x,s) = \frac{1}{2}ai\,(\pi iT)^{-1/2}\int_0^{\infty} dw\, w^{-1/2} exp\left(-iaw - \frac{Ti\,b^2w^3}{3s^2}\right)$$

$$\times \int_{-\infty}^{\infty} dv\, y(v,0)\, exp(-ibvw)\left(1+\frac{bv}{a}\right) \tag{68}$$

$$\times\, exp\left\{\frac{i}{4}\left[\frac{Tb^2w^3}{s^2} - 2bw(x-v) + \frac{s^2(x-v)^2}{Tw}\right]\right\}$$

where $w = bv$. At this point we may discard terms which are explicity $O(b^2)$ and rearrange, with the result that

$$\hat{y}(x,s) = \frac{1}{2}ai\,(\pi iT)^{-1/2}\int_{-\infty}^{\infty} dv\, y(v,0)\left(1+\frac{bv}{a}\right)$$

$$\times \int_0^{\infty} dw\, w^{-1/2}\, exp[-iaw - \frac{i}{2}bw(x+v) + is^2(x-v)^2/4Tw]. \tag{69}$$

To evaluate the w-integral, we make the substitution $w = z^2$. The relation [22]

$$\int_0^\infty e^{-\alpha z^2 - \beta/z^2}\, dz = \frac{1}{2}\left(\frac{\pi}{\alpha}\right)^{1/2} e^{-2(\alpha\beta)^{1/2}} \tag{70}$$

holds for all α, β such that $Re(\alpha) > 0$ and $Re(\beta) > 0$. To apply this relation to eq (69), in addition to the small negative imaginary term added to T, a small positive imaginary term must be added to a. Then eq (69) reduces to

$$\hat{y}(x, s) = \frac{1}{2}(a/T)^{1/2} \int_{-\infty}^{\infty} dv\, y(v, 0)\left(1 + \frac{bv}{a}\right)\left[1 + \frac{b}{2a}(x + v)\right]^{-1/2}$$

$$\times \exp\left\{-s\,|x - v|\,[(a + \frac{1}{2}b\,[x + v])/T]^{1/2}\right\}. \tag{71}$$

At this point it is evident, by inspection, that the uniform limit $b \to 0+$ recovers the uniform solution, eq (33), where $c = (T/a)^{1/2}$.

To find the P-space solution, we use the relation

$$\mathcal{L}^{-1}\{e^{-\alpha s}\} = \delta(t - \alpha) \tag{72}$$

where $\mathcal{L}$ is the Laplace transform operator. This holds for real positive α, and hence is applicable provided that

$$(x + v) > -\frac{2a}{b}. \tag{73}$$

Thus we see that the concerns raised in section 2.2 about the absence of explicit boundaries are built into the mathematics of the solution; an inverse Laplace transform cannot be performed for large negative x, where the differential equation becomes physical nonsense.

With this proviso, the P-space solution is

$$y(x, t) = \frac{1}{2}(a/T)^{1/2} \int_{-\infty}^{\infty} dv\, y(v, 0)\left(1 + \frac{bv}{a}\right)\left[1 + \frac{b}{2a}(x + v)\right]^{-1/2}$$

$$\delta(t - |x - v|\,[a + \frac{1}{2}b\,(x + v)]^{1/2}/T) \tag{74}$$

which, to leading order in nonuniformity, may be reduced to the more suggestive form,

$$y(x, t) = \frac{1}{2}\left(1 - \frac{bct}{4a}\right) y(x - ct\,[1 - \frac{b}{4a}(2x - ct)],0)$$

$$+ \frac{1}{2}\left(1 + \frac{bct}{4a}\right) y(x + ct\,[1 - \frac{b}{4a}(2x + ct)],0) \tag{75}$$

where $c = (T/a)^{1/2}$, i.e., two moving pulses. It is easy to show that, through terms linear in b, the pulses separately satisfy the original differential equation, eqs (58) and (59).

The F-space solution may be derived from eq (75) and, to leading order in nonuniformity, can be represented in a similarly suggestive form,

$$\bar{y}(k, t) = \frac{1}{2}\left(1 - \frac{3bct}{4a}\right) \bar{y}(k\,[1 - \frac{bct}{2a}], 0)\, exp[-ic\left(1 - \frac{bct}{4a}\right) kt]$$

$$+ \frac{1}{2}\left(1 + \frac{3bct}{4a}\right) \bar{y}(k\,[1 + \frac{bct}{2a}], 0)\, exp[\,ic\left(1 + \frac{bct}{4a}\right) kt], \tag{76}$$

cf. eq (32).

Since eq (76) holds only for small times (cf. table 1), and there is no damping for the unperturbed solution, it is not meaningful to construct a dynamic structure factor for this case.

4.3. Interpretation

It is at this point easily seen that the solution has the proper physical behavior expected on intuitive grounds. The first term of eq (75) is the rightward moving pulse. Since b is positive, the wave speed decreases to the right, and, as it should, the pulse moves more slowly as time progresses. The factor $(1 - \frac{bct}{4a})$ indicates that the pulse size decreases with time, as it should since it moves into a region of greater inertia. In addition, the width of the pulse gets smaller in time by a factor $(1 + \frac{bct}{2a})^{-1}$, because the front end of the pulse moves more slowly than the back end. Conversely, the leftward moving pulse, or second term of eq (75), gets larger and wider and moves faster with time.

The F-space solution, eq (76), may be interpreted similarly. The rightward pulse, the first term, propagates with a decreasing time-dependent effective speed of $c(1 - \frac{bct}{4a})$. Due to Heisenberg's inequality, [21] the rightward pulse in F-space gets wider in time. To compensate, so that Parseval's theorem is satisfied, the factor in front must decrease more rapidly with time than the corresponding P-space factor. The converse observations apply to the leftward pulse.

We reiterate that it is apparently not possible to go directly from the FL-space solution, eq (62), to the leading-order F-space solution, eq (76), by means of an inverse Laplace transform. The concept of a nonuniformity expansion, as discussed in section 2.1, appears to be meaningful only in P-space and L-space, not in F-space or FL-space. Hence we must follow the circuitous route shown in figure 1.

5. Nonuniform diffusion equation

5.1. The differential equation

In the study of the nonuniform diffusion equation, we must at the outset distinguish material diffusion from diffusion of a thermal pulse. The equation for material diffusion in one dimension is [23]

$$\frac{\partial}{\partial t} y(x, t) - \frac{\partial}{\partial x} [D(x) \frac{\partial}{\partial x} y(x, t)] = 0 \tag{77}$$

and the case of interest to us is

$$D(x) = D_0 + D_1 x \tag{78}$$

where D_1 is small.

Diffusion of a thermal pulse in one dimension, [24] which corresponds more closely to the Rayleigh-Brillouin problem, is characterized by a thermal conductivity $\lambda(x)$ and a heat capacity per unit length $\sigma(x)$. The differential equation is [24]

$$\frac{\partial}{\partial t} y(x, t) - \frac{1}{\sigma(x)} \frac{\partial}{\partial x} [\lambda(x) \frac{\partial}{\partial x} y(x, t)] = 0 \tag{79}$$

and the cases of interest are

$$\begin{aligned} \lambda &= \lambda_0 + \lambda_1 x \\ \sigma &= \sigma_0 + \sigma_1 x \end{aligned} \tag{80}$$

where λ_1 and σ_1 are small.

To linear order in nonuniformity, we may represent both equations by the convenient form

$$(a - bx) \frac{\partial y}{\partial t} - c \frac{\partial^2 y}{\partial x^2} + \gamma b \frac{\partial y}{\partial x} = 0 \tag{81}$$

where, for material diffusion,

$$\frac{c}{a} = D_o$$

$$\frac{b}{a} = D_1/D_o \tag{82}$$

$$\gamma = -D_o$$

and for diffusion of a thermal pulse,

$$a = \sigma_o\lambda_o$$

$$b = \sigma_o\lambda_1 - \lambda_o\sigma_1 \tag{83}$$

$$c = \lambda_o^2$$

$$\gamma = \lambda_o\lambda_1/b.$$

The equation thus is characterized by two nonuniformity parameters b and γ, and a single small parameter b.

5.2. Properties of the solution

Before embarking on a derivation of the solution to eq (81), it is of interest to examine certain properties of the solution which follow directly from the differential equation itself. We multiply both sides of eq (81) by $(1 + bx/a)$, discard terms quadratic in b, and integrate over x from $-\infty$ to ∞. The result is

$$\frac{\partial}{\partial t} \int_{-\infty}^{\infty} y(x, t)\, dx = 0 \tag{84}$$

so that the norm $\|y\|$ considered previously, eq (24), is a constant of the motion. For material diffusion, eq (77), the norm is constant for any possible $D(x)$, a consequence of the conservation of diffusing material. For thermal diffusion, eq (79), the above norm is not constant in general, but is so to first order in nonuniformity.

If we consider pulses with unit norm, the central position is given by

$$\langle x \rangle = \int_{-\infty}^{\infty} x\, y(x, t)\, dx\,. \tag{85}$$

Multiplying the differential equation by x and integrating yields

$$\frac{\partial}{\partial t}\langle x \rangle = \frac{2cb}{a^2} + \frac{\gamma b}{a}\,. \tag{86}$$

Physically, for positive λ_1 and negative σ_1 the diffusion coefficient effectively increases with x. Here b and γ are positive, so the average position of the pulse drifts to the right. In the converse situation, the pulse drifts to the left.

A similar calculation yields the time derivative of the mean-square displacement,

$$\frac{\partial}{\partial t}\langle x^2 \rangle = 2\frac{c}{a} + \left(\frac{2\gamma b}{a} + \frac{6bc}{a^2}\right)\langle x \rangle\,, \tag{87}$$

and the mean-square width,

$$\frac{\partial}{\partial t}\langle \Delta x^2 \rangle = \frac{\partial}{\partial t}[\langle x^2 \rangle - \langle x \rangle^2] = \frac{2c}{a} + \frac{2cb}{a^2}\langle x \rangle \tag{88}$$

so that the increase in width with time is independent of γ.

5.3. Solution

The solution of the nonuniform diffusion equation closely parallels that of the nonuniform wave equation. The differential equation in *FL*-space is

$$\frac{\partial}{\partial k}\,\bar{y}(k,\,s) + \left[\frac{ai}{bs} + \frac{ck^2 i}{bs} - \frac{\gamma k}{s}\right]\bar{y}(k,\,s) = \frac{1}{s}\,\frac{\partial}{\partial k}\,\bar{y}(k,\,0) + \frac{ai}{bs}\,\bar{y}(k,\,0)\,. \tag{89}$$

Again, this linear differential equation in k is solved by the integrating factor technique, with the boundary condition $k_1 = \infty$. The result is

$$\bar{y}(k,\,s) = -\int_0^\infty du\left[\frac{ai}{bs}\,\bar{y}(u + k,\,0) + \frac{1}{s}\,\frac{\partial}{\partial k}\,\bar{y}(u + k,\,0)\right] \times exp\left[\frac{aiu}{b} + \frac{ci}{3bs}\,u(u^2 + 3uk + 3k^2) - \frac{\gamma}{2s}\,u(u + 2k)\right]. \tag{90}$$

Without loss of generality we consider only positive b. The convolution theorem is used to transform the solution to L-space. We are required to add a small positive imaginary part to c. The result is

$$\hat{y}(x,\,s) = \frac{1}{2}\,a(bsic\pi)^{-1/2}\int_0^\infty u^{-1/2}\,du\,exp\left[\frac{aiu}{b} + \frac{ciu^3}{3bs} - \frac{\gamma u^2}{2s}\right] \times \int_{-\infty}^{\infty} dv\,y(v,\,0)\left[1 - \frac{bv}{a}\right]exp[-iuv] \times exp\left[-\frac{cu^3 i}{4bs} - \frac{ibs}{4cu}\,(x - v)^2 - \frac{iu}{2}\,(x - v) + \frac{b\gamma^2 ui}{4cs^2} + \frac{\gamma b}{2c}\,(x - v) + \frac{\gamma u^2}{2s}\right]. \tag{91}$$

Again we make the substitution $u = bw$ and then discard all $O(b^2)$ terms. We next explicitly perform the w-integral by means of the substitution $w = z^2$ and eq (70). It is necessary to assign a small positive imaginary element to a. The result of these operations is

$$\hat{y}(x,\,s) = \frac{1}{2}\,(a/cs)^{1/2}\int_{-\infty}^{\infty} dv\,y(v,\,0)\left[1 - \frac{bv}{a}\right]\left[1 - \frac{b}{2a}\,(x + v)\right]^{-1/2} \times exp\left[\frac{\gamma b}{2c}\,(x - v)\right] exp\,-\left\{(sa/c)^{1/2}\,|x - v|\,\left[1 - \frac{b}{2a}\,(x + v)\right]^{1/2}\right\}. \tag{92}$$

At this point it is easily seen that the uniform limit, $b \to 0+$, recovers the uniform solution, eq (41) with $D = c/a$.

To determine the *P*-space solution, we use the relation

$$\mathcal{L}^{-1}\left\{s^{-1/2}\,e^{-\alpha s^{1/2}}\right\} = (\pi t)^{-1/2}\,e^{-\alpha^2/4t}\,. \tag{93}$$

This equation is applicable for real positive α, which requires that

$$x + v < \frac{2a}{b}\,. \tag{94}$$

Once again, it is built into the mathematics that a solution does not exist for large displacements where the original differential equation becomes unphysical.

The P-space solution initially is most conveniently represented in kernel form,

$$y(x, t) = \int_{-\infty}^{\infty} y(v, 0)\, K(x, v; t)\, dv \tag{95}$$

where, to linear order in b,

$$K(x,v;t) = \frac{1}{2}(\pi D_o t)^{-1/2}\left[1 + \frac{b}{4a}(x - 3v) + \frac{\gamma b}{2c}(x - v)\right] \times exp\left\{-(x - v)^2\left[1 - \frac{b}{2a}(x + v)\right]/4D_o t\right\} \tag{96}$$

and $D_o = c/a$ is the coefficient of diffusion in the uniform limit.

However, there is a severe mathematical difficulty with eqs (95) and (96) in their present form; namely, the integral of eq (95) does not exist as written. There is an essential difference between the solutions of the undamped wave equation and the diffusion equation. For the undamped wave equation, if the initial pulse is *strictly* localized around the origin, i.e., $y(x, 0) = 0$ identically for $|x| > w_o/2$, then, for any large distance L, $y(L, t)$ remains strictly zero until some finite time of the order L/c. However, as governed by the diffusion equation, a similar localized pulse causes a finite displacement at L after *any* time interval, however small, as an infinite tail is instantaneously created of the form $exp(-x^2)$ at large x. Then, since the kernel of eq (96) goes as $exp(+v^3)$ for large v, the integral of eq (95) is formally infinite after any two successive finite time steps.

Physically, however, it is not possible for a pulse to diffuse over large distances instantaneously; this phenomenon should be interpreted as a mathematical artifact. We believe the proper way to interpret eqs (95) and (96) physically is to remove this artifact in the following manner. The kernel of the integrand is a distorted Gaussian function integrated over an undistorted measure. A transformation is made so that the kernel becomes an undistorted Gaussian integrated over a distorted measure. Specifically, we define the new measure

$$u^2 = (x - v)^2\left[1 - \frac{b}{2a}(x + v)\right] \tag{97}$$

and

$$u = (v - x)\left[1 - \frac{b}{4a}(x + v)\right] + 0(b^2)\,. \tag{98}$$

Then, if terms higher than linear order in b are discarded, eq (95) becomes

$$y(x, t) = \frac{1}{2}(\pi D_o t)^{-1/2} \int_{-\infty}^{\infty} du\, y(x + u[1 + \frac{b}{4a}(2x + u)], 0) \left[1 - \frac{bu}{4a} - \frac{\gamma bu}{2c}\right] e^{-u^2/4D_o t}. \tag{99}$$

The major formal change between eq (95) and eq (99) is the upper limit of infinity on the u integration, whereas, from eq (97), as $v \to +\infty$, u becomes, formally, infinite and *imaginary*. The objective of the transformation is to suppress the unphysical behavior for $x > a/b$ where the diffusion is mathematically negative. Equation (99) is a well-behaved solution to linear order in nonuniformity which connects smoothly to the uniform case.

To check the solution, we first verify that $K(x,v;t)$ satisfies the boundary condition

$$K(x,v;0) = \delta(x - v) \tag{100}$$

which is equivalent to

$$K(x,v;0) = 0 \quad [x \neq v] \tag{101}$$

and

$$\int_{-\infty}^{\infty} K(x,v;0)\, dv = 1. \tag{102}$$

Equation (101) is verified by inspection, and eq (102) is seen to be valid in the sense of the transformation from eq (96) to eq (99). Finally, it is straightforward to show that the kernel should and does satisfy the differential equation

$$c\frac{\partial^2}{\partial x^2}K(x,v;t) - (a - bx)\frac{\partial}{\partial t}K(x,v;t) - \gamma b\frac{\partial}{\partial x}K(x,v;t) = 0 \tag{103}$$

through linear order in b.

The F-space solution may be derived by expanding y in the integrand of eq (99) through linear order in b, rearranging the integrand into sums of terms of the form $f(u)g(x-u)$, and applying the convolution theorem. The result is

$$\begin{aligned}\bar{y}(k,t) = \bar{y}(k,0)\, e^{-D_o k^2 t}\left[1 - i\left(\frac{2b}{a} + \frac{\gamma b}{c}\right) D_o k t + i\frac{b}{a} D_o^2 k^3 t^2\right] \\ -\left[\frac{\partial}{\partial k}\bar{y}(k,0)\right] e^{-D_o k^2 t}\, i\frac{b}{a} D_o k^2 t\end{aligned} \tag{104}$$

This solution satisfies the initial condition by inspection. It is also straightforward to check that it satifies the differential equation, eq (81) transformed to F-space, through linear order in b.

We proceed to calculate the dynamic structure factor, the time Fourier transform of the intermediate scattering function $F(k,t)$ (cf. eqs (2-3)). The solution of the initial value problem in principle yields $F(k,t)$ only for positive times. We employ the usual convention for a time correlation function that for negative times [25] the function is defined to be

$$F(\mathrm{k,t}) = F^*(k,-t) \tag{105}$$

where the asterisk denotes a complex conjugate, in which case

$$S(k,\omega) = 2\,Re\int_0^\infty e^{-i\omega t} F(k,t)\, dt \tag{106}$$

Applying eq (106) to our solution yields the result

$$\begin{aligned}S(k,\omega) = \langle\bar{y}(-k,0)\,\bar{y}(k,0)\rangle\left\{\frac{2D_o k^2}{\omega^2 + (D_o k^2)^2} - \left(\frac{2b}{a} + \frac{\gamma b}{c}\right)\frac{4D_o^2\,\omega k^3}{\left[\omega^2 + (D_o k^2)^2\right]^2}\right. \\ \left. + 2\frac{b}{a} D_o^2 k^3 \frac{\omega^3 - 3\omega(D_o k^2)^2}{\left[\omega^2 + (D_o k^2)^2\right]^3}\right\} - \langle y(-k,0)\frac{d}{dk}\bar{y}(k,0)\rangle\frac{4b}{a}\frac{D_o^2\omega k^4}{\left[\omega^2 + (D_o k^2)^2\right]^2}.\end{aligned} \tag{107}$$

5.4. Interpretation

The most important physical features of the solution to the nonuniform diffusion equation may be given a simple interpretation as a "Doppler shift" similar to that of the uniform damped wave equation. In particular, eq (86) shows that the diffusion pulse, on the average, drifts in the direction of increasing diffusion with a velocity c_D given by

$$c_D = \frac{2cb}{a^2} + \frac{\gamma b}{a} \tag{108}$$

The uniform damped wave pulse undergoes a similar motion with the wave speed c and an "effective diffusion rate" of Γ. By a naive analogy we would expect that the F-space nonuniform solution is

$$\bar{y}(k,t) = \bar{y}(k,0)\, e^{-D_o k^2 t}\, e^{-ic_D k t} \tag{109}$$

which, through first order in c_D, yields the first two terms of eq (104). By similar reasoning we would obtain the dynamic structure factor

$$S(k,\omega) = < -\bar{y}(-k, 0)\, \bar{y}(k, 0) > \frac{2\, D_o k^2}{(\omega + c_D k)^2 + (D_o k^2)^2} \tag{110}$$

which similarly accounts for the first two terms of eq (107) through 0 (c_D).

The third term of eq (107) gives a rather complicated change of shape of the "Rayleigh line" not predicted by the above heuristic arguments. The term oscillates several times and is qualitatively akin to the third frequency derivative of the primary Lorentzian function, so it alters, in leading order, neither the mean frequency nor the width.

The ensemble average of the fourth term in eq (107) vanishes for a uniform system because of invariance under a parity transformation. This term is somewhat difficult to interpret, but, when averaged over an appropriate ensemble, is presumably no more than first order in nonuniformity. Hence the entire term presumably yields a contribution second order in nonuniformity and may be neglected.

6. Nonuniform damped wave equation

6.1. The differential equation

We first seek the appropriate one-dimensional nonuniform analog to the equation, first derived by Stokes, for the propagation of a plane sound wave in an isotropic viscous medium, [26]

$$\varrho \frac{\partial^2 \zeta}{\partial t^2} - \varkappa \frac{\partial^2 \zeta}{\partial x^2} - \frac{4}{3} \mu \frac{\partial^2}{\partial x^2} \frac{\partial \zeta}{\partial t} = 0 , \tag{111}$$

cf. eq (46), where ϱ is the density, ζ the displacement, $\varkappa$ the effective bulk modulus, and μ the viscosity. This corresponds to the neglect of coupling between density and temperature fluctuations in the Rayleigh-Brillouin scattering problem. [11]

The following model, though somewhat contrived, appears to be the one-dimensional analog to the above with the appropriate properties. The viscous term corresponds in three dimensions to an off-diagonal term in the pressure tensor, which, crudely speaking, represents a torque per unit volume. In one dimension, this would be a torque per unit length.

We consider a stretched string with position-dependent mass per unit length $\varrho(x)$. We imagine that, as the string vibrates transversely, it traverses a viscous medium which exerts a torque ΔL on a length element Δx. On each element Δx there is a force $F(x)$, perpendicular to the string, acting at one end and an equal and opposite force acting on the other end. Thus

$$\Delta L = [F(x) + F[x + \Delta x)]\, \Delta x . \tag{112}$$

We further assume that the force is proportional to the spatial derivative of the velocity of the segment, the analog of the three-dimensional velocity gradient

$$F(x) = 2\mu(x) \frac{\partial}{\partial x} \frac{\partial y}{\partial t} \tag{113}$$

where $\mu(x)$ is analogous to viscosity and may be position-dependent.

Next we generalize the standard derivation [27] of the wave equation for a stretched string under tension T by the inclusion of this new force. As usual it is assumed that the angle between a vibrating segment of the string and the equilibrium direction is sufficiently small that its sine and tangent are equivalent. Applying Newton's second law to the segment of the string from x_1 to x_2 yields

$$\int_{x_1}^{x_2} \varrho(x) \frac{\partial^2 \gamma}{\partial t^2}\, dx = \int_{x_1}^{x_2} \frac{\partial}{\partial x}\left[T \frac{\partial \gamma}{\partial x}\right] dx + 2 \int_{x_1}^{x_2} \frac{\partial}{\partial x}\left[\mu(x) \frac{\partial}{\partial x} \frac{\partial \gamma}{\partial t}\right] \tag{114}$$

or, since x_1 and x_2 are arbitrary,

$$\varrho(x) \frac{\partial^2 \gamma}{\partial t^2} - T \frac{\partial^2 \gamma}{\partial x^2} - 2 \frac{\partial}{\partial x} \mu(x) \frac{\partial}{\partial x} \frac{\partial \gamma}{\partial t} = 0 . \tag{115}$$

This is the particular nonuniform damped wave equation to be analyzed here. We are interested in the special case

$$\varrho(x) = a + bx \tag{116}$$

$$\mu(x) = \mu + \beta x \tag{117}$$

where b and β are small.

6.2. Solution

The solution of the nonuniform damped wave equation closely parallels those of the undamped wave and diffusion equations. The equation in FL-space is

$$as^2 \tilde{y} + ibs^2 \frac{\partial \tilde{y}}{\partial k} + Tk^2 \tilde{y} + 2\mu s k^2 \tilde{y} + 2\beta i k s \tilde{y} + 2\beta i k^2 s \frac{\partial \tilde{y}}{\partial k} = as\, \bar{y}(k, 0) + ibs \frac{\partial}{\partial k} \bar{y}(k, 0) + 2\mu k^2\, \bar{y}(k, 0) + 2\beta i k\, \bar{y}(k, 0) + 2\beta i k^2 \frac{\partial}{\partial k} \bar{y}(k, 0) . \tag{118}$$

As before, this linear differential equation may be solved by the integrating factor technique. [20] However, at this point we anticipate a mathematical difficulty. In previous examples, where the linear differential equation had the form

$$\frac{\partial \tilde{y}}{\partial k} + f(k)\, \tilde{y} = g(k) \tag{119}$$

the variable $f(k)$ had the form of a quadratic polynomial in k. This property made possible the subsequent inverse Fourier transformation (from FL-space to L-space) by means of eq (65). Upon examination of eq (118), we note that $f(k)$ is quadratic if and only if $\beta = 0$. We shall therefore set $\beta = 0$ in the remainder of this section. This corresponds to uniform "viscosity" with nonuniform density, or a particular correlated case of nonuniform wave speed and wave damping.

Again we use the boundary condition $k_1 = \infty$, and make the substitution $k' = u + k$ [cf. eqs (61)–(62)]. The FL-space solution is

$$\tilde{y}(k, s) = \int_0^\infty du \left[\frac{ai}{bs} \bar{y}(u + k, 0) + \frac{2i\mu(u+k)^2}{bs^2} \bar{y}(u + k, 0) - \frac{1}{s} \frac{\partial}{\partial k} \bar{y}(u + k, 0)\right] exp\left[-\frac{iau}{b} - \frac{(T+2\mu s)i}{3bs^2} u(u^2 + 3ku + 3k^2)\right]. \tag{120}$$

Without loss of generality, we consider only positive b. The convolution theorem is then used to derive the L-space solution. Once again, it is necessary to assign a small negative imaginary component to T. The result is

$$\hat{y}(x, s) = \frac{ai}{2}[\pi bi(T + 2\mu s)]^{-1/2} \int_o^\infty du\, u^{-1/2} exp\left[-\frac{iau}{b}\right.$$

$$\left. - \frac{(T+2\mu s)iu^3}{3bs^2}\right] \int_{-\infty}^{\infty} dv \left[y(v, 0)(1 + \frac{bv}{a}) - \frac{2\mu}{as}\frac{\partial^2}{\partial v^2} y(v, 0)\right] \tag{121}$$

$$\times exp(-iuv)\, exp\left\{\frac{i}{4}\left[\frac{(T+2\mu s)u^3}{bs^2} - 2u(x - v) + \frac{bs^2(x-v)^2}{(T+2\mu s)u}\right]\right\}.$$

As in the undamped wave solution, we make the substition u = bw and discard terms explicitly $0(b^2)$. We then let $w = z^2$ and apply eq (70), after assigning a small positive imaginary part to a. The result is

$$\hat{y}(x,s) = \tfrac{1}{2}a^{1/2}(T+2\mu s)^{-1/2} \int_{-\infty}^{\infty} dv \left[y(v, 0)[1 + \frac{bv}{a}] - \frac{?\mu}{as}\frac{\partial^2}{\partial v^2} y(v, 0)\right]$$

$$\left[1 + \frac{b}{2a}(x + v)\right]^{-1/2} exp\left\{-s|x - v|\,[1 + \frac{b}{2a}(x + v)]^{1/2}[a/(T + 2\mu s)]^{1/2}\right\}. \tag{122}$$

In the uniform limit, $b \to 0+$, we recover eq (52), with $\Gamma = \mu/a$ and $c = (T/a)^{1/2}$.

At this point we encounter the problem of dispersion discussed in section 2.3. Since there is no general *P*-space solution to the uniform damped wave equation in terms of elementary functions, we cannot expect to find an explicit *P*-space solution to the nonuniform equation either (to all orders in dispersion). A formal expression may be written,

$$y(x,t) = \tfrac{1}{2}\int_{-\infty}^{\infty} dv\,[1 + \frac{b}{2a}(x + v)]^{-1/2}\left[y(v, 0)(1 + \frac{bv}{a})\mathcal{L}^{-1}\left\{(c^2 + 2\Gamma s)^{-1/2}\right.\right.$$

$$exp\left[-s|x - v|\,[1 + \frac{b}{2a}(x + v)]^{1/2}(c^2 + 2\Gamma s)^{-1/2}\right]\Big\} - 2\Gamma\frac{\partial^2}{\partial v^2} y(v, 0)\mathcal{L}^{-1}\left\{s^{-1}\right. \tag{123}$$

$$\left.\left.(c^2 + 2\Gamma s)^{-1/2}\, exp\left[-s|x - v|\,[1 + \frac{b}{2a}(x + v)]^{1/2}(c^2 + 2\Gamma s)^{-1/2}\right]\right\}\right]$$

where $\mathcal{L}^{-1}$ is the inverse Laplace transform operator. However, this form is not particularly illuminating physically.

To display a more transparent solution, we assume that there exists an operator $\tilde{\mathcal{L}}^{-1}$ which simultaneously performs an inverse Laplace transformation and projects out the leading term in a dispersion expansion. For example, on comparing eqs (52) and (55), we see that such an operator should effect the transformation

$$\tilde{\mathcal{L}}^{-1}\left\{(c^2 + 2\Gamma s)^{-1/2}\, exp[-s|x - v|\,(c^2 + 2\Gamma s)^{-1/2}]\right\}$$

$$= \tfrac{1}{2}(\pi\Gamma t)^{-1/2}\left[e^{-(x-v+ct)^2/4\Gamma t} + e^{-(x-v-ct)^2/4\Gamma t}\right]. \tag{124}$$

We further assume that $\tilde{\mathcal{L}}^{-1}$ obeys the change of scale property of Laplace transforms, namely, if

$$\tilde{\mathcal{L}}^{-1}\left\{f(s)\right\} = F(t) \tag{125}$$

then

$$\tilde{\mathcal{L}}^{-1}\left\{f(\alpha s)\right\} = \frac{1}{\alpha}F\left(\frac{t}{\alpha}\right), \tag{126}$$

at least providing α depends only on position and nonuniformity parameters. The above is, in essence, a statement of the independence of nonuniformity and dispersion expansions.

The second term of eq (116) is of higher order in dispersion than the first term and may be neglected. On replacing $\mathcal{L}^{-1}$ by $\tilde{\mathcal{L}}^{-1}$ in eq (123) and using eqs (124)—(126), we obtain the solution

$$y(x,\, t) = \tfrac{1}{4}(\pi\Gamma t)^{-1/2} \int_{-\infty}^{\infty} dv\, y(v,\, 0)[1 + \frac{bv}{a}][1 + \frac{b}{2a}(x+v)]^{-1/2}$$

$$\left[exp\left\{-[ct - (1 + \frac{b}{2a}[x + v])^{1/2}(x - v)]^2/4\Gamma t\right\}\right. \tag{127}$$

$$\left. + exp\left\{-[ct + (1 + \frac{b}{2a}[x + v])^{1/2}(x - v)]^2/4\Gamma t\right\}\right]$$

which bears a strong similarity to the nonuniform diffusion solution, eqs (95)—(96), for $\gamma = 0$.

As in the case of diffusion, we encounter problems with divergences in the integrals due to mathematically instantaneous propagation of the pulse to points at large distances from the origin, where the original differential equation makes no physical sense. We again surmount the difficulty by transforming to a distorted measure in which the Gaussians of the kernel are undistorted. The new measure is

$$u = (x - v)[1 + \frac{b}{2a}(x + v)]^{1/2}. \tag{128}$$

Then a calculation, discarding terms higher than linear order in b, analogous to that of diffusion yields

$$y(x,\, t) = \tfrac{1}{4}(\pi\Gamma t)^{-1/2} \int_{-\infty}^{\infty} du\, y[x - u(1 - \frac{b}{4a}[2x - u]),\, 0]$$

$$(1 - \frac{bu}{4a})[e^{-(u-ct)^2/4\Gamma t} + e^{-(u+ct)^2/4\Gamma t}]. \tag{129}$$

Since

$$\lim_{\Gamma \to 0} \tfrac{1}{2}(\pi\Gamma t)^{-1/2} e^{-(u \pm ct)^2/4\Gamma t} = \delta(u \pm ct) \tag{130}$$

it is easily checked that, in the limit of zero damping, the nonuniform undamped wave equation solution, eq (75), is recovered.

We recall that in the present problem there are two small expansion parameters, namely, nonuniformity and dispersion. Since the latter is defined in terms of F-space variables, there is no natural means of checking that the P-space solution satisfies the differential equation.

The F-space solution may be derived by expanding y in the integrand of eq (129) through linear order in b, rearranging the integrand into sums of terms of the form $f(u + ct)\, g(x - u)$, and repeatedly applying the convolution theorem. The end result is rather lengthy and is best expressed as the sum of a rightward and a leftward pulse.

$$\bar{y}(k,\, t) = \bar{y}_r(k,t) + \bar{y}_l(k,t) \tag{131}$$

where

$$\bar{y}_r(k,t) = \bar{y}(k,\, 0)\, e^{-\Gamma k^2 t} e^{-ickt}$$

$$[\frac{1}{2} + \frac{b}{a} i\Gamma kt - \frac{3b}{8a} ct - \frac{b}{2a} i\Gamma^2 k^3 t^2 + \frac{b}{2a} \Gamma c k^2 t^2 + \frac{b}{8a} ic^2 k t^2] \tag{132}$$

$$+ [\frac{\partial}{\partial k} \bar{y}(k,\, 0)]\, e^{-\Gamma k^2 t} e^{-ickt} [\frac{b}{2a} i\Gamma k^2 t - \frac{b}{4a} ckt]$$

and $\bar{y}_l$ is obtained from $\bar{y}_r$ by replacing c by $-c$ throughout. Since we only desire the solution through linear order in dispersion, the term above containing Γ^2 may be discarded.

The F-space transformation of the original differential equation, eqs (115–117) with $\beta = 0$, is

$$\frac{\partial^2 \bar{y}}{\partial t^2} + \frac{b}{a} \mathrm{i} \frac{\partial}{\partial k} \frac{\partial^2 \bar{y}}{\partial t^2} + k^2 c^2 \bar{y} + 2\Gamma k^2 \frac{\partial \bar{y}}{\partial t} = 0 \tag{133}$$

At this point it can be checked that the solution, eq (132), satisfies the differential equation, eq (133), if terms $0(b^2)$, second order in nonuniformity, and $0(\Gamma^2)$, second order in dispersion, are neglected.

The solution satisfies the initial value condition by inspection, but does not satisfy the condition on the initial time derivative. The latter, however, is not a failing of the nonuniformity analysis but, rather, a feature of the truncation of the dispersion expansion of the *uniform* damped wave solution. In particular, eq (51) is the correct solution to all orders in dispersion, whereas eq (54) satisfies the differential equation and initial value condition through first order in dispersion, but *not* the initial time derivative condition. A fully consistent first-order truncation of the dispersion expansion which includes the time derivative condition would retain the second term of eq (51) and replace $(c^2 - \Gamma^2 k^2)^{1/2}$ by c throughout.

A similar difficulty appears in the standard treatment of Rayleigh-Brillouin scattering; compare, for example, eq (27) of ref. [11] with eq (97) of ref. [28]. Although the extra term required to make the initial time derivative vanish is in practice often neglected, for the sake of a fully consistent solution through first order in both dispersion and nonuniformity we shall find and include such terms here.

We note that eq (131) remains a solution through the required order if terms are added which are proportional to either Γ times the solution with $\Gamma \to 0$ in the brackets of eq (132), or b times the solution with $b \to 0$ in the same brackets. It is straightforward to set up a trial solution with variable coefficients for the required additional terms, and solve for the coefficients subject to the constraints that the initial value vanish and the initial time derivative be equal and opposite to that of eqs (131)–(132). To obtain the desired result, a term

$$\begin{aligned} \Delta\bar{y}_r(k,t) = \bar{y}(k,0)\, e^{-\Gamma k^2 t} e^{-ickt} & \left[\frac{i\Gamma k}{c}\left(\frac{1}{2} - \frac{3b}{8a}\, ct + \frac{b}{8a}\, ic^2 k t^2\right) + \frac{5\Gamma b}{8ca}\right] \\ + \left[\frac{\partial}{\partial k}\, \bar{y}(k,0)\right] e^{-\Gamma k^2 t} e^{-ickt} & \left[\frac{\Gamma k b}{4ca} - \frac{i\Gamma b k^2 t}{4a}\right] \end{aligned} \tag{134}$$

must be added to $\bar{y}_r(k,t)$, and a term $\Delta\bar{y}_i(k,t)$, eq (134) with c replaced by $-c$ throughout, must be added to $\bar{y}_i(k,t)$. We could, in a similar manner, impose a nonzero initial time derivative proportional to b and determined from external considerations, but will not do so here.

In the construction of the dynamic structure factor we will, for reasons decribed in section 5.4, neglect terms involving $\left(\frac{d}{dk}\, \bar{y}(k,0).\right)$ The resulting dynamic structure factor may be written as

$$S(k,\omega) = S_r(k,\omega) + S_i(k,\omega) \tag{135}$$

where

$$\begin{aligned} S_r(k,\omega) = \langle \bar{y}(-k,0)\, \bar{y}(k,0) \rangle \times & \left[\left(1 + \frac{5\Gamma b}{8ca}\right) \frac{\Gamma k^2}{(\omega + ck)^2 + (\Gamma k^2)^2}\right. \\ + \frac{\Gamma k}{c} & \frac{\omega + ck}{(\omega + ck)^2 + (\Gamma k^2)^2} + \frac{5b}{2a}\, \Gamma^2 k^3 \frac{\omega + ck}{[(\omega + ck)^2 + (\Gamma k^2)^2]^2} \\ - \frac{3bc}{4a} & \frac{(\Gamma k^2)^2 - (\omega + ck)^2}{[(\omega + ck)^2 + (\Gamma k^2)^2]^2} + \frac{3bc}{2a}\, (\Gamma k^2)^2 \frac{(\Gamma k^2)^2 - 3(\omega + ck)^2}{[(\omega + ck)^2 + (\Gamma k^2)^2]^3} \\ + \frac{bc^2 k}{2a} & \left.\frac{3(\omega + ck)(\Gamma k^2)^2 - (\omega + ck)^3}{[(\omega + ck)^2 + (\Gamma k^2)^2]^3}\right] \end{aligned} \tag{136}$$

and $S_i(k,\omega)$ is given by eq (136) with c replaced by $-c$ throughout.

6.3. Interpretation

In order to develop a physical understanding of the nonuniform damped wave equation solution, we first note that the effects of nonuniform speed and nonuniform damping are not independent and, in the special case considered here, tend to cancel each other. According to eqs. (115–117) with $b > 0$ and $\beta = 0$, both the wave speed and attenuation decrease to the right and increase to the left. Hence we expect the rightward pulse to undergo less damping, effectively, than in the uniform case. However, as has been seen explicitly with the nonuniform undamped wave solution, the decreasing wave speed attenuates the rightward pulse in a different sense by lowering its time-dependent integrated norm [eq (24)].

We have been careful to retain all terms linear in the nonuniformity and/or dispersion parameters. However, some terms in the end give much smaller contributions to $S(k,\omega)$ than others. For example, the conditions from table I on the validity of $S(k,\omega)$ together with the smallness of the dispersion parameter imply the inequalities

$$\frac{b}{ak} << \frac{\Gamma k}{c} << 1 . \tag{137}$$

The rightward pulse (with our sign conventions) corresponds to the Brillouin line (Stokes line) centered at $\omega = -ck$. The additional factor $5\Gamma b/8ca$ multiplying the primary Brillouin line [first term in eq (136)] is by (137) at least three orders of magnitude less than unity, and thus utterly negligible.

The remaining terms in eq (136) are conveniently classified quantitatively, to leading order, in terms of the shift in mean frequency or change in width they cause in the Brillouin line. Since the more commonly used definitions of mean position or width of a peak involve integrals which diverge for the Lorentzian function, we employ the following alternate definitions, for mean frequency,

$$\bar{\omega} = \int_{-\infty}^{\infty} \omega\,[f(\omega)]^2\,d\omega \Big/ \int_{-\infty}^{\infty} [f(\omega)]^2\,d\omega \tag{138}$$

and for width of the line,

$$(\Delta\omega)^2 = \int_{-\infty}^{\infty} (\omega - \bar{\omega})^2\,[f(\omega)]^2\,d\omega \Big/ \int_{-\infty}^{\infty} [f(\omega)]^2\,d\omega . \tag{139}$$

For the primary Brillouin line eq (139) gives, as usually defined, $\Delta\omega = \Gamma k^2$. The precise definitions are not important but the above ones serve as convenient measures of changes in the spectrum for purposes of discussion.

The second term of eq (136) is antisymmetric about $\omega = -ck$ and corresponds to the well-known first-order dispersion term in the Rayleigh-Brillouin spectrum [28] in the limit that the specific heat ratio approaches unity. To leading order in dispersion this term causes a shift of $(2\Gamma^2k^3/c)$ to the right in the mean frequency of the line.

The third term of eq (136) is also antisymmetric about $\omega = -ck$. It has the effect of shifting the mean frequency to the right by $(5b\Gamma k/a)$. This represents a very small shift, which by (137) is less than that of the previous dispersion term which is itself usually neglected in practical applications.

Upon comparison with the undamped wave solution, the fourth term of eq (136) is seen to originate from the decreasing wave speed or increasing inertia in the rightward direction. This term is symmetric about $\omega = -ck$ and, to leading order, increases the width of the line by $3bc/4a$. An increase in width corresponds physically to a larger effective attenuation coefficient.

The fifth term of eq (136) is symmetric about $\omega = -ck$ and, by the definition (139), results in a *decrease* in width of $3bc/4a$. Thus the fourth and fifth terms effectively, if not identically, cancel each other. One possible physical interpretation of the latter term is as follows. The Fourier component of wavenumber k of the rightward pulse has a lifetime of $(\Gamma k^2)^{-1}$, and therefore a mean path length $c/\Gamma k^2$. Equations (115–117) imply a distance-dependent attenuation factor

$$\Gamma(x) = \Gamma\left(1 - \frac{bx}{a}\right) \tag{140}$$

from which we infer that the effective attenuation coefficient of the kth Fourier component of the rightward pulse is

$$\Gamma_{eff} = \Gamma - f_1 \frac{bc}{ak^2} \tag{141}$$

where f_1 is a positive number of order unity, and the resulting width of the Brillouin line is $\Gamma_{eff}k^2$. The full analysis then gives $f_1 = 3/4$.

Hence the near-cancellation of the previous two terms may be an artifact of setting $\beta = 0$ in eq (117). For a more general solution where, for example, wave speed and damping increase in *opposite* directions, the corresponding new terms might reinforce each other. In any case, measurement of such a width change would be difficult as it would require a fractional precision in the width measurement equal to the fractional change in attenuation over the path length of the monitored Fourier component.

Finally, the last term in eq (136) is highly oscillatory and qualitatively similar to the third derivative of the Lorentzian. Like its counterpart in the diffusion solution, it would be very difficult to detect and may be neglected.

Similar observations, with appropriate changes of sign in some cases, apply to $S_t(k,\omega)$, the anti-Stokes line centered at $\omega = ck$ resulting from the leftward pulse.

7. Summary

As an initial step toward the understanding of Rayleigh-Brillouin scattering in a temperature gradient, which involves nonuniform, three-dimensional coupled damped wave and diffusion equations, we have analyzed in detail the initial value problem for a set of prototype one-dimensional differential equations with linearly nonuniform coefficients, to first order in nonuniformity.

A question which first arose was whether explicit boundaries were necessary for the system, since at large distances the differential equations become unphysical. For the models studied, it is possible to derive meaningful solutions of the initial value problem without such boundaries for sufficiently narrow initial pulses and sufficiently short times. Also, if the equation has a damping mechanism, it is possible to construct a meaningful dynamic structure factor for values of k whose Fourier components are damped sufficiently rapidly. Conditions for the validity of solutions are listed in table 1.

Our procedure has been first to Fourier transform in space and Laplace transform in time. The resulting equations, algebraic in the uniform case, become first-order differential equations in k for the linear nonuniform case. An expansion through quadratic order in nonuniformity would lead to a second-order differential equation in k, for which there is no general method of solution.

We have seen that the condition of small nonuniformity cannot be represented by any dimensionless parameter in F-space or FL-space. Therefore, to construct the time evolution of the pulse and, ultimately, the dynamic structure factor, we must follow the circuitous path indicated in figure 1. The ability to perform the initial inverse Fourier transform restricts the range of solvability of the linear differential equation in k. One of our initial goals, the solution of the nonuniform damped wave equation with arbitrary, independent variation of the nonuniformity in both wave speed and damping, for this reason has not been realized.

We have derived explicit solutions to the initial value problem for the nonuniform undamped wave, diffusion, and (for a special case) damped wave equations. These solutions display properties expected on intuitive grounds, and reduce properly to their respective uniform solutions.

Throughout the derivations, certain mathematical liberties have been taken. We have assigned small imaginary parts to intrinsically real coefficients, although these imaginary components go to zero at the end of the calculation. For the diffusion and damped wave equations, we have altered the measure of integration

in the final solution to suppress singularities at large distance. In the damped wave equation, we have introduced and postulated properties of an operator which simultaneously performs an inverse Laplace transformation and projects out the leading term in a dispersion expansion. Attempts to justify these liberties have been based on pragmatism and physical intuition rather than mathematical rigor, although we conjecture that such steps could (probably) be justified mathematically. Of course, an *a posteriori* justification is that our solutions explicitly satisfy the differential equations through linear order in nonuniformity, and that our initial conditions specify a unique solution.

Since the present formalism neglects coupling between wave and diffusion modes, three-dimensional effects, finite initial time derivatives and position-dependent rates of generation of fluctuations, one should be cautious in drawing conclusions from these results about experimental Rayleigh-Brillouin scattering from a fluid in a temperature gradient. However, the results suggest that further studies of possible changes in the Rayleigh line could be fruitful. Kirkpatrick, et al. [6] have noted that certain modifications of the Brillouin spectrum vanish when an average over a finite volume of the fluid is taken. But according to the simple and intuitive arguments of section 5.2, all heat modes within a given volume should experience a drift velocity in the direction of increasing thermal diffusivity. Our one-dimensional results suggest that the Rayleigh line is thus Doppler shifted. Detection of such a shift, if it persists in the coupled three-dimensional problem, depends on precision calibration of the incoming laser frequency and precision measurement of the mean frequency of the Rayleigh line. The shift would be most pronounced for systems whose thermal conductivity changes rapidly with temperature and for large values of k. By contrast, the asymmetry in the size of the Brillouin peaks predicted by previous authors, [1–10] and not considered here, is generally agreed to be inversely proportional to k^2, and experiments to detect such an effect [14] have thus been performed at very small values of k.

The author thanks R. D. Mountain for elucidating many aspects of light scattering theory and for guidance and encouragement. He thanks H. J. Raveche and the staff of the Thermophysics Division, National Bureau of Standards, Washington, DC for their hospitality during the author's visit in 1979, when much of this work was completed. He also thanks S. W. Haan, R. J. Rubin and J. R. Dorfman for valuable suggestions.

8. References

According to conversations with J. R. Dorfman and G. van der Zwan, the authors of refs. [1–10] have now formed a consensus that the correct leading-order spectrum is that given in refs. [6, 9, and 10].

[1] Procaccia, I.; Ronis, D.; Oppenheim, I. Light scattering from nonequilibrium states: the implication of broken time-reversal symmetry. Phys. Rev. Lett. **42**(5): 287–291, 1979 January 29.

[2] Procaccia, I.; Ronis, D.; Collins, M. A.; Ross, J.; Oppenheim, I. Statistical mechanics of stationary states. I. Formal theory. Phys. Rev. A **19**(3): 1290–1306; 1979 March.

[3] Ronis, D.; Procaccia, I.; Oppenheim, I. Statistical mechanics of stationary states. II. Application to low-density systems. Phys. Rev. A **19**(3): 1307–1323; 1979 March.

[4] Ronis, D.; Procaccia, I.; Oppenheim, I. Statistical mechanics of stationary states. III. Fluctuations in dense fluids with applications to light scattering. Phys. Rev. A **19**(3): 1324–1339; 1979 March.

[5] Kirkpatrick, T.; Cohen, E. G. D.; Dorfman, J. R. Kinetic theory of light scattering from a fluid not in equilibrium. Phys. Rev. Lett. **42**(14): 862–865; 1979 April 2.

[6] Kirkpatrick, T.; Cohen, E. G. D.; Dorfman, J. R. Hydrodynamic theory of light scattering from a fluid in a nonequilibrium steady state. Phys. Rev. Lett. **44**(7): 472–475; 1980 February 18.

[7] Van der Zwan, G.; Mazur, P. Light scattering from a fluid with a stationary temperature gradient. Phys. Lett. **75A**(5): 370–371; 1980 February 4.

[8] Van der Zwan, G. On some aspects of fluctuating hydrodynamics. Thesis. Ryksuniversiteit te Leiden; 1980.

[9] Tremblay, A.-M. S.; Siggia, E. D.; Arai, M. R. Fluctuations about hydrodynamic nonequilibrium steady states. Phys. Lett. **76A**(1): 57–60; 1980 March 3.

[10] Ronis, D.; Putterman, S. Simplified hydrodynamic therory of nonlocal stationary state fluctuations. Phys. Rev. A **22**: 773–777; 1980 August.

[11] Mountain, R. D. Spectral distribution of scattered light in a simple fluid. Rev. Mod. Phys. **38**(1): 205–214; 1966 January.

[12] Komarov, L. I.; Fisher, I. Z. Theory of Rayleigh scattering of light in liquids. Soviet Phys. J.E.T.P. **16**(5): 1358–1361; 1963 May.

[13] Pecora, R. Doppler shifts in light scattering from pure liquids and polymer solutions. J. Chem. Phys. **40**(6): 1604–1614; 1964 March 15.

[14] Beysens, D.; Garrabos, Y.; Zalczer, G. Experimental evidence for Brillouin asymmetry induced by a temperature gradient. Phys. Rev. Lett. **45**(6): 403-406; 1980 August 11.
[15] Brownell, J. H. Wave number space analysis of propagation in nonuniform media. Am. J. Phys. **41**(2): 207-212; 1973 February.
[16] Clark, N. A. Inelastic light scattering from density fluctuations in dilute gases. The kinetic-hydrodynamic transition in a monatomic gas. Phys. Rev. A **12**(1): 232-244; 1975 July.
[17] Landau, L.; Placzek, G. Structure of the undisplaced scattering line. Physik Z. Sowjetunion **5**: 172; 1934.
[18] Reif, F. *Statistical and thermal physics.* New York: McGraw-Hill; 1965; p. 301.
[19] Mountain, R. D. Generalized hydrodynamics. Adv. Mol. Relax. Proc. **9**: 225-291; 1976.
[20] Mathews, J.; Walker, R. L. *Mathematical methods of physics.* New York: Benjamin; 1965; p. 3.
[21] Dym, H.; McKean, H. P. *Fourier series and integrals.* New York: Academic Press; 1972; p. 116.
[22] Gradshteyn, I. S.; Ryzhik, I. M. *Tables of integrals, series and products.* New York: Academic Press; 1965; p. 307.
[23] Richardson, L. F. Atmospheric diffusion shown on a distance-neighbour graph, Proc. Roy. Soc. London Series A **110**(756): 709-737; 1926 April.
[24] Berg, P. W.; McGregor, J. L. chapter 3 in *Elementary partial differential equations.* San Francisco: Holden-Day; 1966; 29-33.
[25] McQuarrie, D. A. *Statistical mechanics.* New York: Harper and Row; 1976; p. 563.
[26] Crandall, I. B. *Theory of vibrating systems and sound.* New York: Van Nostrand; 1926; p. 110.
[27] Berg, P. W.; McGregor, J. L. chapter 8 in *Elementary partial differential equations.* San Francisco: Holden-Day; 1966; p. 181-187.
[28] Mountain, R. D. Liquids: dynamics of liquid structure. Chem. Rubber Co. Crit. Revs. Solid State **1**(1): 5-46; 1970.

JOURNAL OF RESEARCH of the National Bureau of Standards
Vol. 86, No. 5, September–October 1981

A Transient Hot Wire Thermal Conductivity Apparatus for Fluids*

Hans M. Roder†

National Bureau of Standards, Boulder, CO 80303

May 26, 1981

A new apparatus for measuring the thermal conductivity of fluids is described. This is an absolute method utilizing a transient hot wire. Measurements are made with a 12.7 μm diameter platinum wire at real times of up to 1 second. The data acquisition system includes a minicomputer and a digital voltmeter. The experimental core of the system incorporates a compensating hot wire in a Wheatstone bridge circuit. The cell containing the core of the apparatus is designed to accommodate pressures from 0 to 70 MPa and temperatures from 70 to 320 K. Oxygen was measured over a wide range of physical states including the dilute gas, the moderately dense gas, the near critical region, the compressed liquid states, and the vapor at temperatures below the critical temperature. Performance checks of the apparatus were conducted with nitrogen, helium and argon. Measurement of rare gases allows a direct comparison to the kinetic theory of gases through the viscosity. A second check looks at the variation of the measured thermal conductivity as a function of the applied power. The precision (2 σ) of the new system is between 0.5 and 0.8 percent for wire temperature transients of 4 to 5 K, while the accuracy is estimated at around 1.5 percent.

Key words: Helium; hot wire; nitrogen; pressure; temperature; thermal conductivity; transient.

1. Introduction

Thermal conductivity values are necessary whenever a heat transfer problem is to be evaluated. In addition, thermal conductivity is a property of fundamental interest in developing the theory of fluids. Accurate measurements of thermal conductivity are of considerable difficulty. Methods and geometries abound each with its adherents and its inherent drawbacks. The steady state hot wire experiment is one of the older, well established methods. The transient hot wire method, however, has come into its own only with recent advances in digital electronics. The evolution of the modern transient hot wire experiment can be traced from the early experiments of Pittman [1][1], Haarman [2], and Mani [3]. However, the major exposition of both theory and application of this method was accomplished by Kestin and his coworkers during the last decade [4–9] for the gas phase. Similar instruments have been used by Wakeham and his coworkers for both gas and liquid measurements [10, 11] and by de Castro and his coworkers for liquid measurements [12–13].

*This work was carried out at the National Bureau of Standards under the sponsorship of the National Aeronautics and Space Administration (C-32369-C).

†Thermophysical Properties Division, National Engineering Laboratory.

[1] Figures in brackets indicate literature references at the end of this paper.

2. Method

A hot wire system normally involves a vertical, cylindrical symmetry where the wire serves both as heating element and as thermometer. Almost without exception platinum is the wire of choice. The mathematical model that one attempts to approximate is that of an infinite line source of heat suspended vertically in an infinite medium. The method is labeled transient because the power is applied abruptly and the measurement is of short duration. The working equation is based on a specific solution of Fourier's law and can be found in standard texts (see for example reference [14], page 261).

$$T(t) - T_{ref} = \Delta T = \frac{q}{4\pi\lambda} \ln\left(\frac{4K}{a^2 C}\, t\right) \qquad (1)$$

Where $T(t)$ is the temperature of the wire at time t;

T_{ref} is the reference temperature, the temperature of the cell;

q is the applied power;

λ is the thermal conductivity of the fluid, a function of both temperature and density;

K is the thermal diffusivity of the fluid, i.e., $K = \lambda/\varrho C_p$. K is normally taken at the temperature T_{ref} and is nearly constant since the fluid properties do

not change drastically with a small increase in temperature;

a is the radius of the wire; and

$\ell n\ C = \gamma$ where γ is Euler's constant.

The relation given by eq (1) implies a straight line for a plot of ΔT versus $\ell n(t)$. In practice systematic deviations occur at both short and long times. However, for each experimental measurement there exists a range of times over which eq (1) is valid, that is the relation between ΔT and $\ell n(t)$ is linear. This range of validity is determined from 250 measured ΔT-t pairs by selecting a beginning time t_1 and an ending time t_2. The slope of the ΔT versus $\ell n(t)$ relation is obtained over the valid range, i.e., between times t_1 and t_2, and using the applied power the thermal conductivity is calculated from eq (1). The temperature assigned to the measurement of λ is given by

$$T = T_{ref} + \frac{1}{2}[\Delta T(t_1) + \Delta T(t_2)] \qquad (2)$$

The density assigned to the measurement of λ is taken from an equation of state using an experimentally measured pressure and the temperature assigned above. The equations of state used for nitrogen and helium are given in subsequent sections. The experimentally determined temperature rise of the wire is ΔT_w. A number of corrections account for the departure of the real instrument from the ideal model:

$$\Delta T = \Delta T_w - \Sigma\, \delta T_i \qquad (3)$$

These corrections δT_i have been fully described elsewhere [5]; the most important at lower times is δT_1, the effect of the finite heat capacity of the wire.

3. Apparatus

The various elements of the apparatus, the hot wires, the high pressure cell and wire supports, the Wheatstone bridge, the cryostat, the measuring and control circuitry, the sample handling system, and the minicomputer are described here and in figures 1-6.

3.1. The Hot Wires

Platinum wire is the normal choice because the resistance-temperature relation of platinum is well known [15]. In the resistance thermometer grade of the wire the smallest sizes available commercially are 7 μm, 12.7 μm, and 25.4 μm in diameter. The smallest of these was considered to be too fragile for the present application, the largest would not provide a sufficiently large resistance for the cell size under consideration. Therefore, the 12.7 μm diameter wire was chosen for both primary and compensating hot wire. The long or primary hot wire is approximately 10 cm in length. Its resistance varies from about 20 Ω at 76 K to 90 Ω at 298 K. The short or compensating wire is approximately 5 cm in length and its resistance varies from 10 to 45 Ω. To allow for thermal expansion over the range of operating temperatures the wires are mounted with a small weight attached at the bottom. The wires are mounted in the hard drawn (as received) state, because in the annealed state platinum has a rather low tensile strength [16].

3.2. High Pressure Cell and Wire Supports

The cell has been designed to withstand pressures of up to 70 MPa. In addition, if the cell is to be isothermal, its thermal conductivity should be high. Accordingly, the cell is made from beryllium copper, a material which meets these contradictory requirements best. Cell sizing, cell closure, and wire support are shown in figure 1. The cell is quite similar to those used in other experiments in this laboratory [17-20]. It is mounted with the closure facing down. Three solid steel pins serve as electrical leads. They pass through the high pressure closure (stainless steel) and are insulated

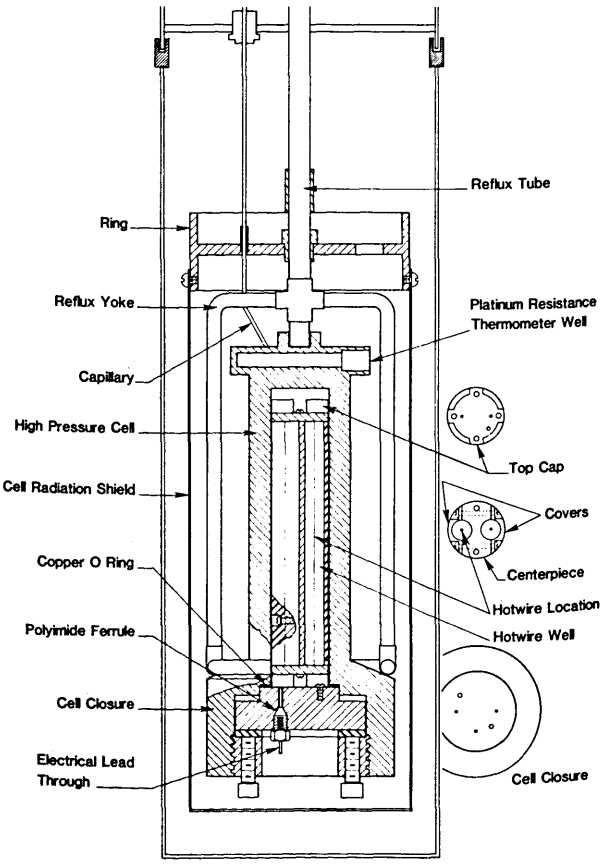

FIGURE 1. The high pressure cell and wire support unit.

from it using polymide ferrules [21]. The capillary which admits the sample is soldered into the top of the cell. Much of the interior of the cell is filled by the wire support unit which is made from copper and includes a centerpiece, two covers, a top and a bottom cap. The wire support unit is mounted on the high pressure closure. When assembled the wire support unit provides two cylindrical wells 9 mm in diameter and 11 cm long to accomodate the hot wires. Mounted in the top cap with friction fit are two 5 mm sections of a small coaxial cable. The hot wires are soft soldered to the center leads of these coaxial sections. To the bottom of the long hot wire is soldered a short section of teflon covered wire which terminates in a 4–80 brass nut, the weight. The teflon covered section provides isulation between bottom cap and the extension of the long hot wire as well as centering for it. The long hot wire section is connected to one of the steel pins by a small loop of 12.7 μm copper wire. The short hot wire is soft soldered to the other coaxial section in the top cap. To its bottom end a short length of copper wire centered in a second 4–80 brass nut is soldered. The leads on the short hot wire side are completed by a loop of 12.7 μm copper wire which connects to a 5 cm length of coaxial cable. This section of coax is friction fit into the bottom cap and is sufficiently rigid to stand alone. A second loop of copper connects this coax to the second steel pin. Long and short hot wire sections are connected together above the top cap with the center tap soldered in the middle of this connection. The center tap is a 11 cm long section of the coax which at the bottom end is connected to the third steel pin.

Liquid oxygen safety is one of the additional design considerations for the cell since the interior of the cell will be exposed to very high pressure 70 MPa (10,000 psi) liquid. The materials directly exposed to liquid oxygen have been limited to beryllium copper, copper, stainless steel, silver, teflon, and a polyimide (kapton) all of which have been found to be "oxygen compatible" [22]. Cleaning procedures for cell, wire supports, capillary and sample handling system were extensive [23].

3.3. The Wheatstone Bridge

Precision measurements of resistance can be made by using a four lead technique or by using a Wheatstone bridge. In the present apparatus we follow the general development of the hot wire instrument pioneered by Haarman [2], de Groot, et al. [4], Assael, et al. [10] and de Castro, et al. [12] and use a Wheatstone bridge to measure resistances. End effect compensation is provided by placing the long hot wire in one working arm of the bridge and a shorter, compensating wire on the other. In contrast to other instruments where values of time are measured in the present instrument the voltage developed across the bridge is measured directly as a function of time with a fast response digital voltmeter (DVM). The DVM is controlled by a minicomputer which also handles the switching of the power and the logging of the data. The automation of the voltage measurement follows the work of Mani [3] who used a similar arrangement with a transient hot wire cell to measure resistance by the four lead technique rather than using a bridge.

Figure 2 shows the Wheatstone bridge circuit. Each arm of the bridge is designed to be 100 Ω, two arms R_1 and R_2 are standard resistors. The resistance in each of the other arms R_3 and R_4 is a composite of the hot wire, the leads into the cryostat and an adjustable ballast resistor. The leads are roughly 6 Ω at room temperature and 2 Ω when the cell is at 76 K. The ballast resistors allow each working arm to be adjusted to a value of 100 Ω.

The measurement of thermal conductivity for a single point is accomplished in two phases. In the first phase the bridge is balanced as close to null as is practical. To start with, switch 1 is turned from dummy to the bridge while switch 2 is open. With a very small applied voltage, 0.1 Volts normally, and the cell essentially at constant temperature, the voltages are read on channels 0 through 7. The lead, hot wire, and ballast resistances are calculated from the ratios of the appropriate channel voltgage to the voltage across the standard 100 Ω resistor on channel zero. The ballasts are adjusted until each leg is approximately 100 Ω. Finally, with switch 2 closed, the bridge null is checked on channel 6. The second phase incorporates the actual thermal conductivity measurement. The power supply is set to the applied power desired, switch 2 is closed, and switch 1 is switched from dummy to bridge. The voltage developed across the bridge as a function of time is read on channel 6 and stored. The basic data is a set of 250 readings taken at 3 ms intervals. Finally the voltage on channel 0 is read to determine the exact applied power, and the power is switched back to the dummy resistor.

3.4. The Cryostat

The cryostat for the apparatus, shown in figure 3, is adapted from a general design first used in a PVT apparatus at this laboratory [24]. The cell is connected by the reflux tube to the inner refrigerant tank. The reflux tube is filled with gas which sometimes corresponds to the liquid used as the refrigerant. Varying the gas pressure changes the amount of refrigeration applied to the cell. A cooling yoke and ring insure that the refrigeration is applied primarily at the bottom of the cell. In this way a slight gradient can be maintained between cell top and cell bottom. To avoid convection inside the cell we normally maintain the cell bottom slightly colder than the cell top. The cell and its radiation shield is located in a vacuum environment. A

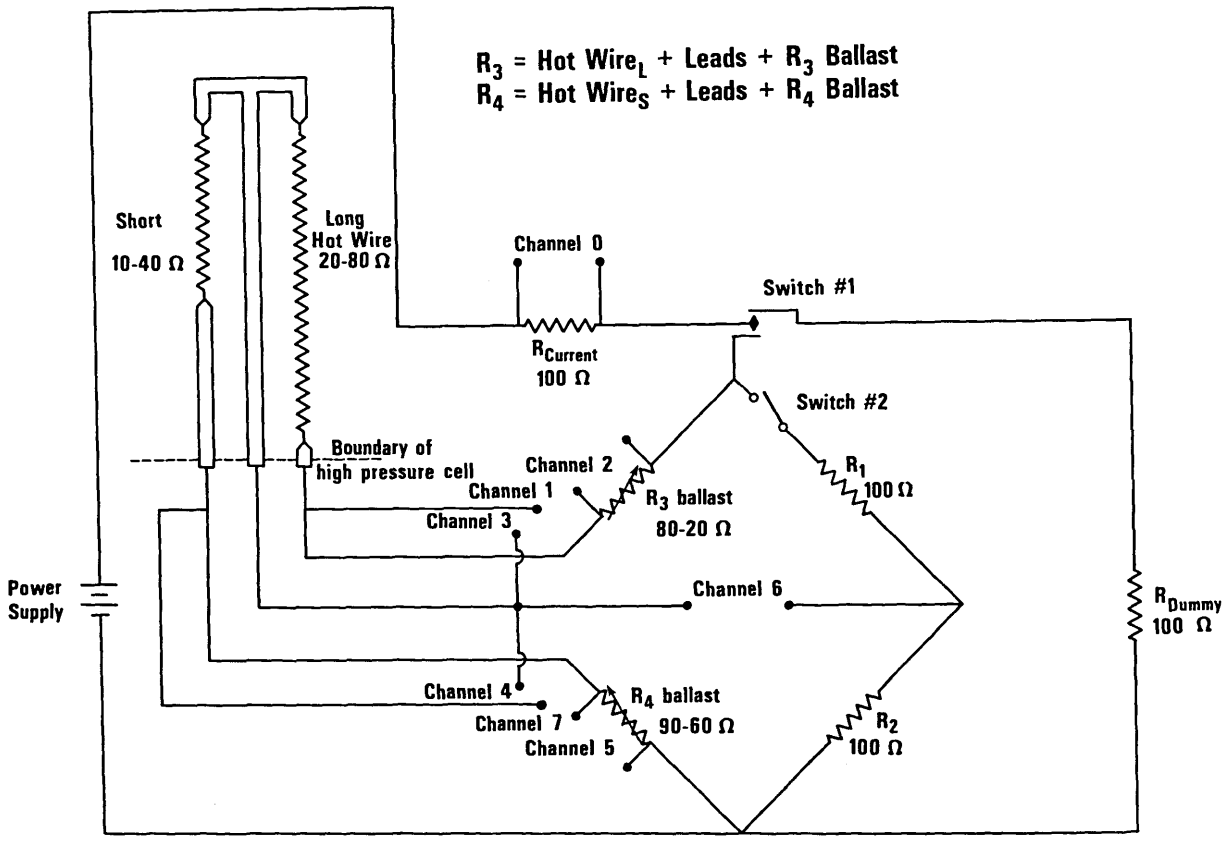

FIGURE 2. The Wheatstone bridge circuit.

tube which serves as the inner vacuum line also admits lead wires and the capillary into the inner vacuum space surrounding the cell. The leads are tempered on two rings, one is attached directly to the inner refrigeration tank, the other is the guard ring which is attached to the reflux tube. The cell radiation shield in turn is attached to the guard ring. The inner refrigerant tank is insulated by the outer vacuum system, which in turn is protected by the outer refrigerant, usually liquid nitrogen, in a dewar. All of the various access tubes, fill and vent lines, and vacuum lines pass through the mounting plate which rests on the mounting bracket attached to the wall. Cell alinement is achieved by adjustment of three set screws.

3.5. Cryostat Temperature Control

A diagram of this circuitry is shown in figure 4. The cell temperature is monitored with the platinum resistance thermometer which is mounted in the cell. The PRT resistance is measured by the four lead method as a ratio against a 10 Ω standard using a microvolt potentiometer, a stable current supply, and a high gain dc null detector. The amplified output of the detector is used in a feedback loop to provide power to the cell heater [25]. The ratio of power applied to cell top and cell bottom is monitored with a thermocouple and adjusted by hand. The temperature of the guard ring and cell radiation shield are maintained close to the cell temperature by the use of a second feedback loop. This loop includes a differential thermocouple and a low level dc voltage detector whose amplified output is routed to a power supply which in turn feeds the ring and shield heater. A separate, manual heater is mounted on the capillary. This heater is operated intermittently as needed. Its function is to ensure that the sample does not freeze in the capillary should by chance some unusual temperature conditions prevail at some spot in the capillary.

3.6. Sample Handling and Vacuum Systems

Block diagrams for both systems are shown in figure 5. The vacuum system is conventional except for an automatic back pressure control with alarm and solenoid valve. These

items were installed as a safety precaution should the silver plated copper O-ring in the cell closure spring a leak and discharge oxygen into the vacuum space.

The sample handling system was also designed with oxygen in mind. It consists of the sample from a gas bottle, a molecular sieve to capture moisture, and a small diaphragm compressor as pressure intensifier. The compressor uses an oxygen compatible oil and has specially hardened check valves and seals. A pressure relief valve was provided in the cell pump-out line to protect against the possibility of an accidental oxygen overpressure, even though the forepump is charged with an oxygen compatible pump oil. With a few changes the sample system was able to handle a liquid sample, propane. Ordinarily the compressor requires an input pressure of about 5 MPa (700 psi). However, if liquid is provided at the intake and sufficient time between strokes is allowed, then the compressor handles a liquid sample quite well. For propane, removing the molecular sieve and turning the supply bottle upside down ensured a direct flow of liquid.

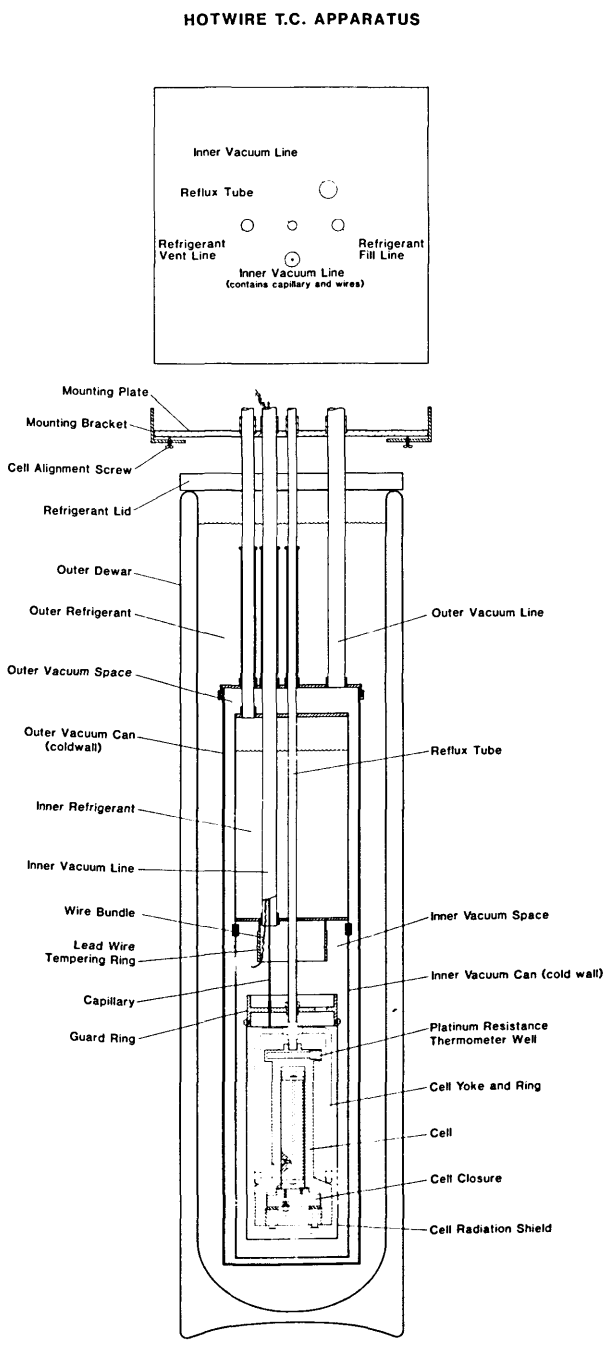

FIGURE 3. The cryostat.

3.7. The Minicomputer

A simplified block diagram of the minicomputer and its peripherals is shown in figure 6. The CPU uses 18 bits per word with BASIC as the operational language. Program storage is on floppy disks, program input on the CRT, program listings are handled on the printer. Data can be displayed on the CRT and on the printer, and can be stored on floppy disk or magnetic tape. Input voltages, i.e., voltages to be read are routed from the 50 input channels by the multiplexer to the DVM where the analog to digital (A/D) conversion is effected. Output voltages, i.e., voltages to be used for experimental control are processed by the logic control unit where the digital to analog conversion takes place. These voltages are available at any of six output channels.

4. Data Measured

In the course of making a single thermal conductivity measurement a large number of variables are measured and recorded. The minicomputer program which controls the measurement is shown in appendix I. An example of a data file as assembled in the minicomputer and then transferred to magnetic tape is shown in appendix II. The first two lines of the data file are keyed in through the CRT. These lines contain the date, run and point number, the PRT reading from the microvolt potentiometer with the last digit repeated, the reading of the pressure gage, the barometer reading, the wire resistance for both long and short hot wire, the sums of lead and ballast resistance for both long and short hot wire sections, the time increment at which the voltage readings were taken, and lastly the voltage applied to the bridge. The remainder of the file contains the set of 250 voltage readings across the Wheatstone bridge.

4.1. Cell Temperature

The PRT is a standard capsule thermometer. It has been calibrated by the NBS temperature section. The voltage

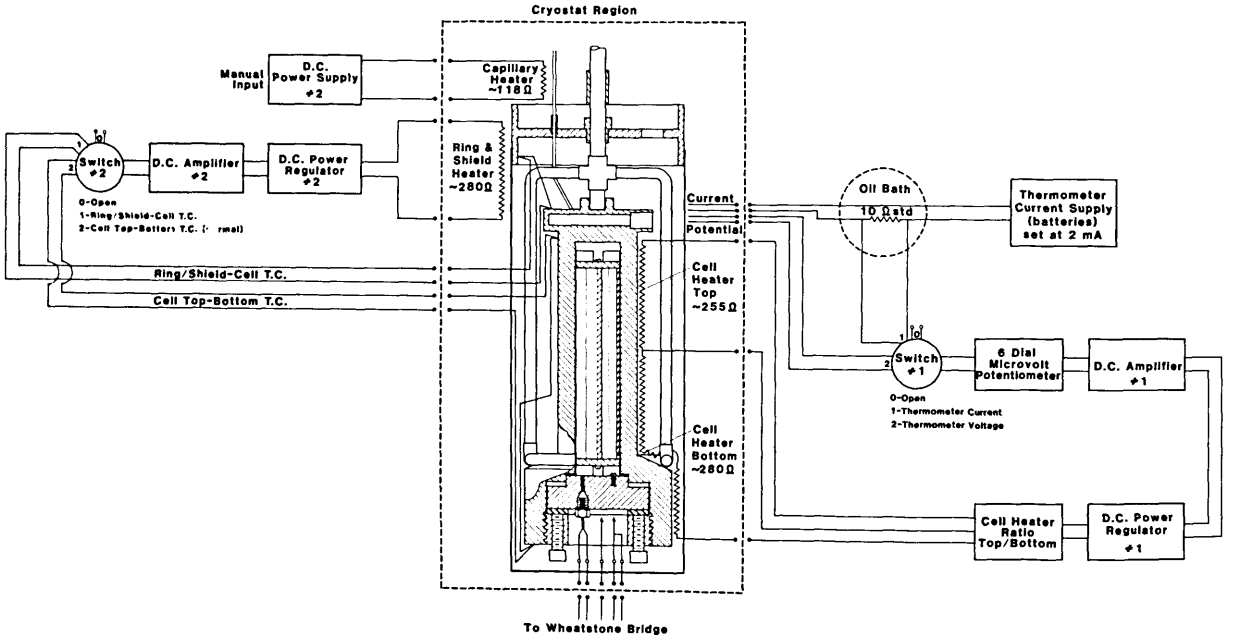

FIGURE 4. Block diagram of temperature measurement and cryostat control circuits.

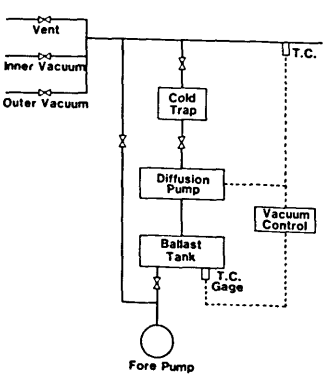

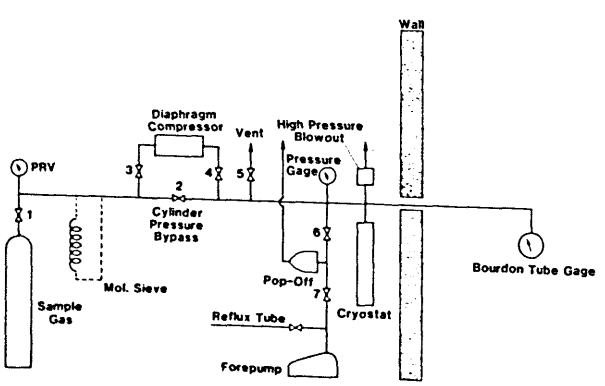

FIGURE 5. Vacuum and sample handling systems.

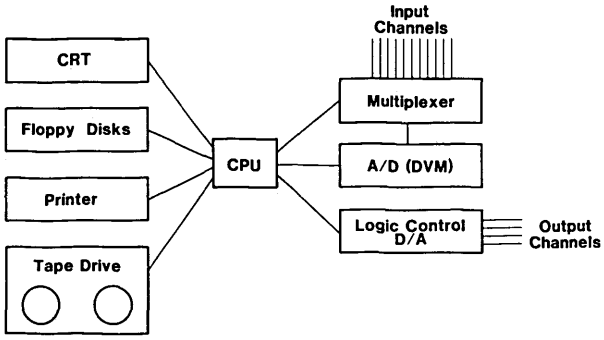

FIGURE 6. The minicomputer.

read across the 10 Ω standard resistor is used to adjust the thermometer current so that a current of 1 ma is flowing in the PRT circuit. A second voltage reading across the PRT proper allows its resistance to be calculated. The second voltage reading is the only value that is keyed into the CRT. The error in the cell temperature as established from a calibration of the microvolt potentiometer used is 0.001 K at 80 K increasing to 0.007 K at 292 K.

4.2. Cell Pressure

The cell pressure is read with a commercial high precision steel bourdon tube. The unit was selected because it is "compatible" with high pressure oxygen. The unit is calibrated by the vendor with the calibration traceable to NBS. A digital readout is provided through an optical sensor, with the units of the readout in "counts." At the maximum pressure 96000 counts correspond to approximately 68 MPa. At the higher pressures the bourdon tube displays hysteresis under loading as a function of time. It is this hysteresis that gives rise to the stated uncertainty of ± 0.03 MPa. The pressure gage calibration was represented by a low order polynomial for use in the data reduction program. The error attributable to this curve fit is well within the stated error of the gage. Vapor pressure checks of the gage at approximately 1 MPa with both oxygen [26] and propane [27] confirm the calibration at the lower end of the pressure scale.

4.3. Resistances

Direct resistance measurements are made while balancing the Wheatstone bridge. The resistances of the hot wires, of the leads, and of the ballast resistors are measured with the DVM set at the optimum gain. The resistance measurements are made using the four terminal method; the voltage across a standard 100 Ω resistor defines the current in the circuit and the voltage reading across the unknown defines the resistance in question. In actual practice each voltage reading is the average of 100 individual readings. Each hot wire section measurement must be corrected for leads inside the high pressure cell which are short pieces of copper and steel wire. The corrections were calculated from wire dimensions and tabulated resistivities [28]. They are estimated to be 0.22 Ω for the long hot wire section and 0.65 Ω for the short hot wire section at room temperature. The corrections are handled in the data reduction program and are further adjusted for changes in bath temperature.

In order to obtain the temperature increase of the platinum wires from the corresponding resistance increase, we need to know the variation of resistance with temperature for both wires. It has been shown in the past [8, 12, 13, 29] that an in situ calibration of the wires is desirable and also that the resistances per unit length of both wires should be the same to within about 2 percent.

The wire resistances measured at essentially zero applied power in the balancing of the bridge together with the cell temperatures as determined from the platinum resistance thermometer are taken as the in situ calibration of the wires. During measurements on oxygen [26] some 1800 values were collected for each wire in the temperature range 76–320 K with pressures from atmospheric to about 70 MPa. The resistance relation for each wire is represented by an analytical function of the type

$$R(t) = A + B\,T + C\,T^2 + D\,P \qquad (4)$$

where T is the temperature in kelvin and P the pressure gage reading. The pressure dependence is small but statistically significant and reflects the fact that the calibration measurements are made with a small applied voltage of 0.1 volts. Coefficients for eq (4) were determined in two ranges of temperature with some overlap in the range of the fits as shown in table 1. The standard deviation of the resistance measurements as well as the equivalent temperature errors are shown in table 1. The long wire has a length of 10.453 cm at room temperature, the short wire one of 5.143 cm. Both wires have a nominal diameter of 0.001270 ± 0.000001 cm, thus the radius a in eq (1) is 0.000625 cm. If we use these values and the measured resistances we can calculate a resistivity of 10.07×10^{-6} Ω-cm at 273.15 K compared to a best value of 9.60×10^{-6} Ω-cm for an annealed high purity specimen [28]. The difference is ascribed to the hard drawn condition of our wires. The α of these wires, defined as $(R(373.15)-R(273.15)/(100.\ R(273.15))$ is 0.0037944 which is lower than the value 0.003925 required for use in an annealed platinum resistance thermometer [26]. Finally, we evaluate

$$\sigma_L = \frac{R_L(T)}{\ell_L(T)} \quad \text{and} \quad \sigma_S = \frac{R_S(T)}{\ell_S(T)} \qquad (5)$$

Table 1. Calibration Constants of Wires.

	Temperature Range of L.S. Fit	Number of Points In Fit	Applicable Temperature Range	Coefficients A(Ω)	B(Ω K^{-1})	C(Ω K^{-2})	D(Ω $(MPa)^{-1}$)	Standard Deviation of Fit, One Sigma	Equivalent Error in T
Long wire	76 - 158 K	707	77 - 150 K	-10.231206	0.3670809	$-0.9903371 \times 10^{-4}$	-7.796325×10^{-4}	0.01 Ω	0.023 K
	142 - 305 K	1684	150 - 315 K	- 9.065472	0.3534445	$-0.5923443 \times 10^{-4}$	-1.401463×10^{-3}	0.019 Ω	0.054 K
Short wire	76 - 158 K	707	77 - 150 K	- 5.057558	0.1823527	$-0.5257280 \times 10^{-4}$	-4.144377×10^{-4}	0.01 Ω	0.059 K
	142 - 305 K	1684	150 - 315 K	- 4.346459	0.1740251	$-0.2831553 \times 10^{-4}$	-6.565822×10^{-4}	0.011 Ω	0.065 K

Table 2. Wire Resistances as a Function of Temperature

Pressure MPa	Temperature K	Wire Resistances long, Ω	short, Ω	Wire Lengths long, cm	short, cm	Resistances/Unit Length long, Ω/m	short, Ω/m	Percent difference
.1013	75.00	16.7427	8.3231	10.434	5.134	160.5	162.1	-1.03
.1013	100.00	25.4865	12.6519	10.436	5.135	244.2	246.4	- .89
.1013	125.00	34.1064	16.9150	10.438	5.136	326.8	329.4	- .79
.1013	150.00	42.6026	21.1124	10.440	5.137	408.1	411.0	- .72
.1013	175.00	50.9731	25.2407	10.442	5.138	488.1	491.3	- .64
.1013	200.00	59.2539	29.3259	10.444	5.139	567.3	570.7	- .59
.1013	225.00	67.4606	33.3756	10.447	5.140	645.8	649.3	- .55
.1013	250.00	75.5934	37.3900	10.449	5.141	723.5	727.3	- .53
.1013	273.15	83.0582	41.0758	10.451	5.142	794.7	798.8	- .51
.1013	275.00	83.6520	41.3690	10.451	5.142	800.4	804.5	- .51
.1013	300.00	91.6366	45.3126	10.454	5.143	876.6	881.0	- .50
.1013	325.00	99.5472	49.2208	10.456	5.144	952.1	956.8	- .49

and compare σ_L and σ_S in the experimental range. Table 2 shows the percent difference between σ_L and σ_S as a function of T. It is apparent that for the lower temperatures the correction proposed by Kestin and Wakeham [8] would apply except that in this apparatus independent calibrations for both long and short hot wire are used.

4.4. Time Increment

The timing of the experiment is based on the internal clock of the minicomputer, a temperature stabilized quartz crystal oscillator that divides a second into roughly 20,000 parts. Available to the programmer is a real time clock which is incremented in milliseconds. During a run this clock is first zeroed, line 620 in appendix I, next 250 voltage readings are taken across the bridge, and finally the clock is read, line 670 in appendix I. The gain of the DVM is set before starting the voltage readings. There are 250 steps in the program loop, where each step includes reading the DVM, storing the result, and time for the computer to execute the step. The time required to execute the program loop is 755 ms, which means that the DVM is read every 3.02 milliseconds. Separate timing runs establish the time necessary to read the clock as about 1 ms. This means the time increment could be as small as 3.012 ms. Actual calculations using the data reduction program show that for this variation in time increment the thermal conductivity results are affected by less than 1 part in 20,000.

The time increment between readings of the DVM can be varied by inserting a delay of several ms into the program loop. Increments of 5, 10, and 15 ms were tried. In general, the use of larger time increments simply reduces the number of useful points for the thermal conductivity analysis since for nearly all fluid conditions the onset of convection occurs at around one second in this apparatus.

4.5. Power Level

The ideal analysis stipulates that the heat flux q, applied to the wire remains constant during a given run. Under experimental conditions q is nearly ideal at room temperature, i.e., it varies by about two parts in 10000. However, at the very lowest temperatures the q will vary from beginning to end of a run by values up to several percent. To see why this is so, and to find the correction that has to be applied consider the following.

The power supply used provides a constant voltage at its terminals to a circuit which consists of a 100 Ω standard resistor in series with the Wheatstone bridge. The effective bridge resistance is nominally 100 Ω but changes as the run progresses. The voltage of the power supply is preset, it is known to an accuracy of ± 200 μV. The set value is entered

through the key board, just prior to switching the power to the bridge. After the run is completed, but before the power is switched back to the dummy resistor, the voltage across the standard resistor, channel 0 in figure 2, is read. The difference between this voltage and the preset one is the voltage applied to the bridge a short time after completion of the run. The difference is one of the items placed on magnetic tape, and it is used in the data reduction program to calculate the power applied to the bridge. The instantaneous heat flux is determined from the equation.

$$q(t) = I^2R/\ell = [V(t)/(R_3(t) + R_4(t))]^2 (R_L(t) + R_S(t))/(\ell_L + \ell_S) \quad (6)$$

where $V(t)$ is the voltage applied to the bridge, and R_3 and R_4 are defined in figure 2. The voltage $V(t)$, both hot wire legs of the bridge R_3 and R_4, and the hot wire resistances themselves change as a function of time. At room temperature the drop in the current is almost exactly offset by the rise in the hot wire resistances. At low temperatures the fractional change in the hot wire resistances predominates. As an extreme example consider a run in liquid propane at say 110 K. For a 3 K rise in wire temperature the long hot wire rises by 1 Ω from an initial value of 30 Ω, or 3.3 percent. This rise is only partially offset by the 0.7 percent drop in the hot wire current leaving a net rise in q of 2.6 percent from $t = 0$ to t = 755 ms. The range of valid times for a run is generally $t_1 = 150$ ms, $t_2 = 755$ ms. Over this range of times the variation in q is less than the extreme case because a large part, 70 percent or so, of the resistance change of the hot wires occurs during the times not valid for the experiment. Nevertheless, the remaining variation in q is significant and we apply a correction to account for it. We select a time in the middle of the valid time interval $t_a = (t_1 + t_2)/2$ and correct the experimental ΔT's by the ratio of the instantaneous q to the q at the median time

$$\Delta T(t)_{corr} = \Delta T(t)_{raw} * q(t_i)/q(t_a) \ldots . \quad (7)$$

$V(t)$ varies by about one part in 1000 over a run, and some calculation verified that $V(t)$ varies as the $\ell n(t)$, and further that the value measured was actually achieved at the requisite time after the end of the run.

4.6. Bridge Voltages

The voltages measured across the bridge, actually a measure of the bridge unbalance, are the basic data in this experiment. A typical set of 250 of these voltages for point No. 9044 is shown in appendix II and is plotted in figure 7. The general shape of this curve is logarithmic, as expected.

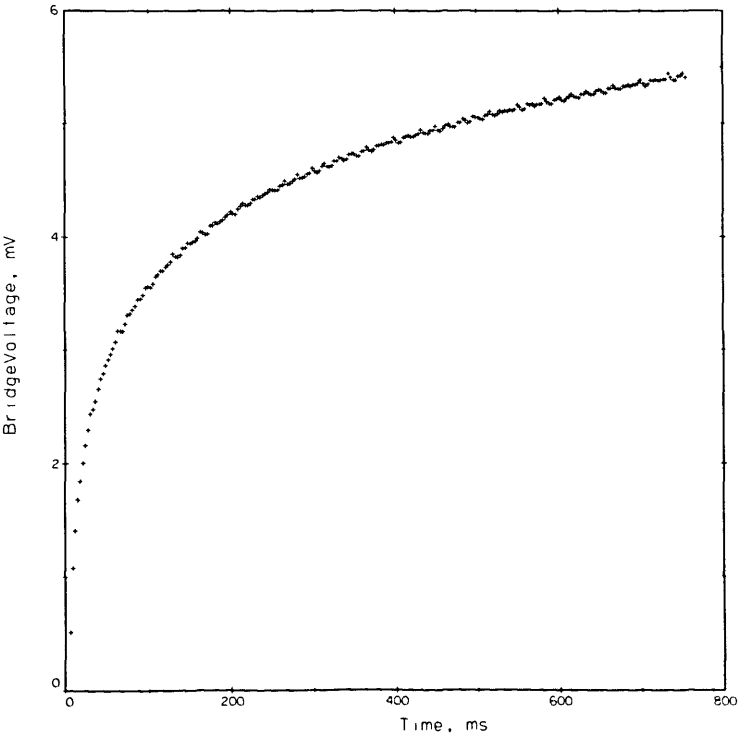

FIGURE 7. Typical bridge voltages versus time, point 9044, helium gas.

Noise levels in these readings are evident. Considerable effort went into reducing the noise level, and also into tracing the source. The DVM, when shorted, exhibits an error band of $\pm$ 6 μV. When a 100 Ω resistor is placed across the DVM, no applied power yet, the band increases to $\pm$ 17 μV. With the experimental system connected to the DVM the error band becomes $\pm$ 28 μV which is roughly equivalent to $\pm$ .026 K in the ΔT. Only a small part, some 20 or 30 percent, is due to AC pickup. Use of integrating or averaging DVM's will reduce the noise level at the expense, however, of a smaller number of measurements.

5. Data Reduction

A listing of the data reduction program used for helium is given in appendix III. Experimental values are read from the magnetic tape. Initial calculations and corrections include corrections for the bias of the DVM, corrections for the leads inside the high pressure cell, and an estimation of the instantaneous voltage applied to the bridge. The ΔT_w values are calculated from the voltages applied to the bridge, the offset or measured voltages across the bridge and the two hot wire calibrations. The bridge equation is solved repeatedly until the increases in the hot wire resistances together with the voltage applied to the bridge yield an offset voltage equal to the measured one. The various corrections to the ΔT_w are applied to obtain the ΔT, and then the ΔT's and $\ell n(t)$'s are passed to a least squares regression routine. Microfilm plots of both ΔT and the deviation of each measured point from the regression line versus $\ell n(t)$ are set up. Typical examples again for point No. 9044 are shown in figures 8a and 8b. In the final steps of the data reduction program an equation of state is used to find the applicable density, the experimental thermal conductivity is compared to any previous correlation that might exist, and the results are printed.

A certain amount of judgement enters into the data reduction process particularly in the selection of t_1 and t_2, the range of times over which the least squares straight line regression is to be evaluated. The criterion for a valid result is that the ΔT values as plotted in the example, figure 8a, shall form a straight line versus the $\ell n(t)$. The deviation plot as shown in figure 8b is used to help determine the valid range of the least squares fit. For most experimental conditions t_1 = 150 ms and t_2 = 755 ms. In both figures, 8a and 8b, the points plotted begin at index 11 or t = 33 ms. The first 30 or so points are seen to fall somewhat below the straight line. By inspection the fit for point 9044 could have included an index as low as 41 or t_1 = 124 ms. In figure 8b the standard deviation for the regression fit of point 9044 is roughly 0.2 percent, or at the 3σ level 0.65 percent.

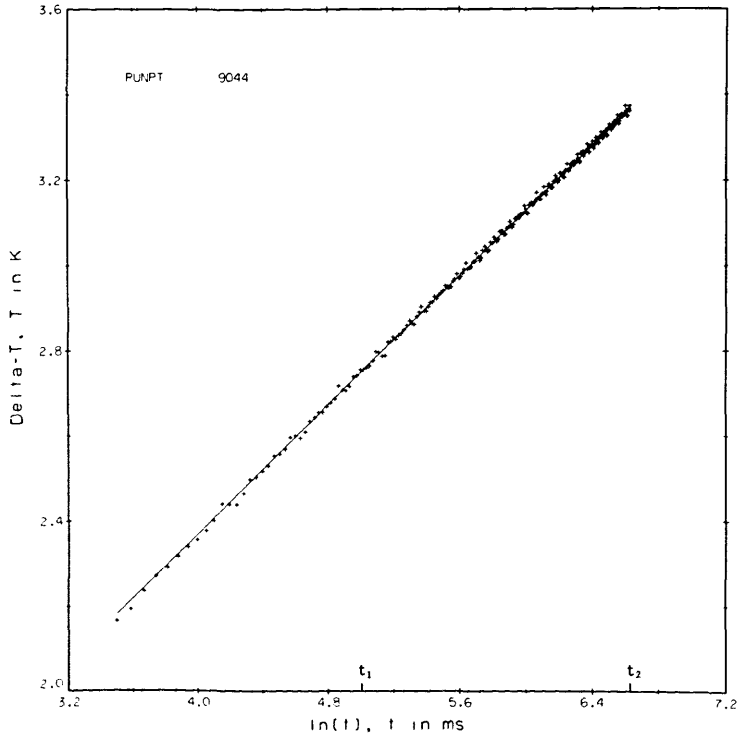

FIGURE 8a. Typical temperature rises versus the logarithm of time, point 9044, helium gas.

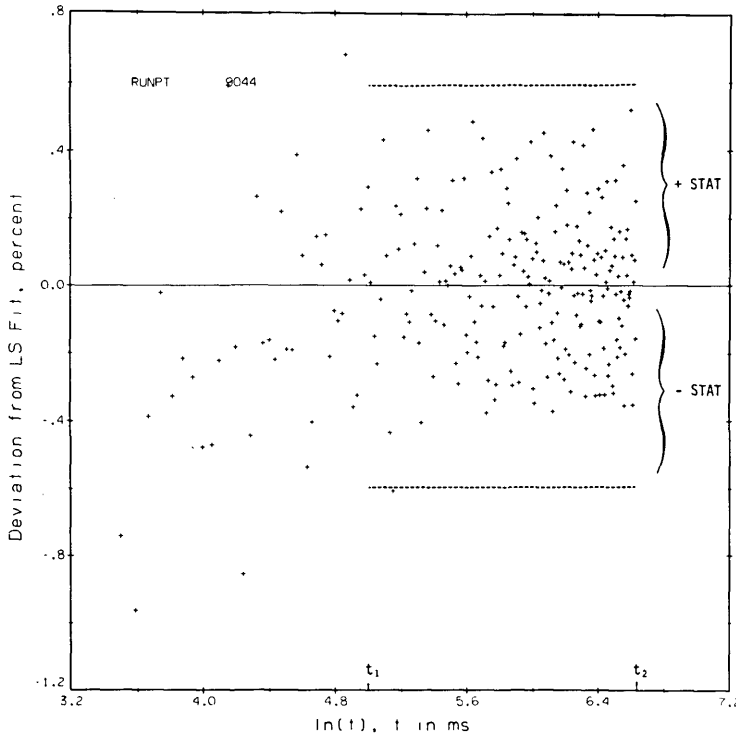

FIGURE 8b. Typical deviations of experimental temperature rises from the calculated straight line versus the logarithm of time, point 9044, helium gas.

By implication, it is equally important to recognize and interpret nonstandard results obtained, so that invalid results can be identified and rejected. A description of several of the more interesting malfunctions follows. In figure 9a we see that the ΔT values are nearly constant toward the end of the run. This state of affairs depending on the state of the fluid sample is interpreted as (a) the apparatus is operating in the steady state mode, or (b) as the onset of convection in the run.

If a similar run at higher fluid densities is taken to much longer experimental times the plot is as shown in figure 9b. Here the effect of convection is clearly seen as a rapid cooling of the hot wires after the maximum ΔT is passed. In principle we could get a valid result for the transient hot wire by selecting $t_1 = 690$ ms and $t_2 = 1353$ ms. However, the number of ΔT values useful for the straight line regression has now dropped to 50. In practice it turns out that the applied power level, as seen in the resulting ΔT's of 10 to 12 K, was simply too large to be useful. The plot of figure 9c shows the effect of gas circulation within the cell. The precise cause is not known. Convection combined with thermal oscillations when the capillary cools are suspected reasons. From the plot it is clear that the wires experience a non-uniform temperature field and are subject to abrupt segments of convection cooling. Measurements with a plot of this type are rejected.

In figure 9d the DVM saturated toward the end of the run. By excluding the points for which the voltage readings are constant, and provided there are sufficient measurements to extract a straight line fit, a measurement of this type can be used. At the very lowest pressures (densities) in the vapor phase at temperatures much below the critical temperature some plots look like the one shown in figure 9e. The physical interpretation of this run is that we see a Knudsen effect at short times and an outer boundary effect at the longer times. No valid range for the hot wire instrument exists and these results are rejected. In the region near the critical point the onset of convection occurs much more rapidly. Measurements in this fluid region have to be made at lower power levels and at shorter times. For the measurements on oxygen experimental times of $t_1 \cong 33$ ms and $t_2 \cong 500$ ms were found to be appropriate.

A second criterion which is used in accepting or rejecting experimental measurements is by considering the change in the measured thermal conductivity as the applied power, q, is varied. Examples are given in the sections on nitrogen and helium. In a general way this criterion suggests that measurements in which the final ΔT's are larger than about 5 K are suspect. This includes most of the critical region where the results have to be evaluated quite carefully, almost on an individual point by point basis.

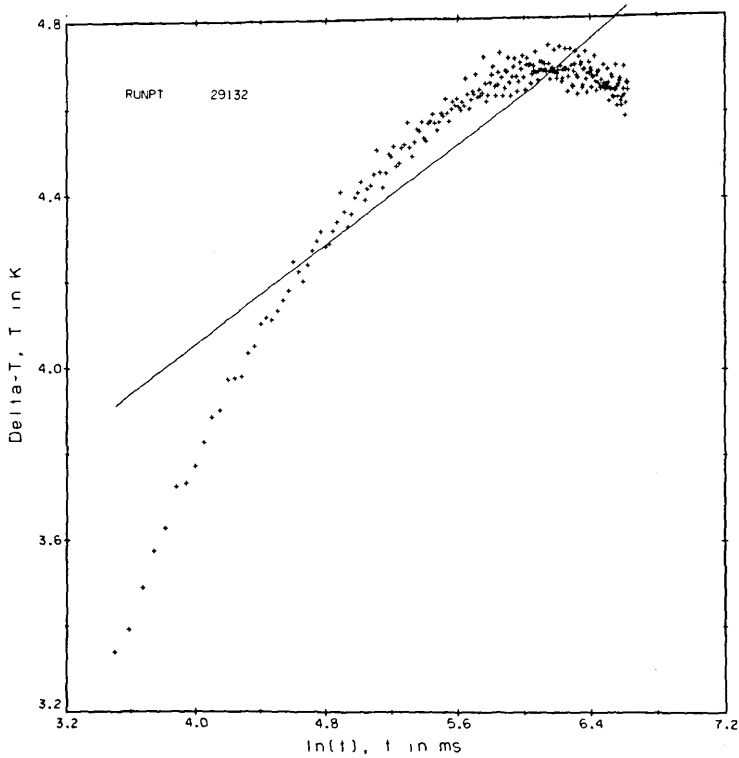

FIGURE 9a. Plots of experimental malfunctions. Point 29132, argon gas.

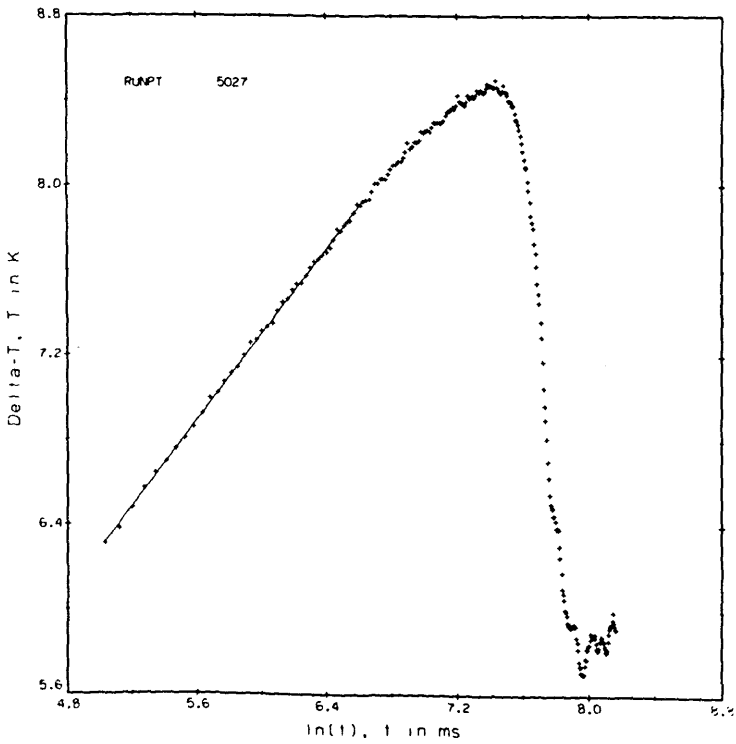

FIGURE 9b. Point 5027, nitrogen gas.

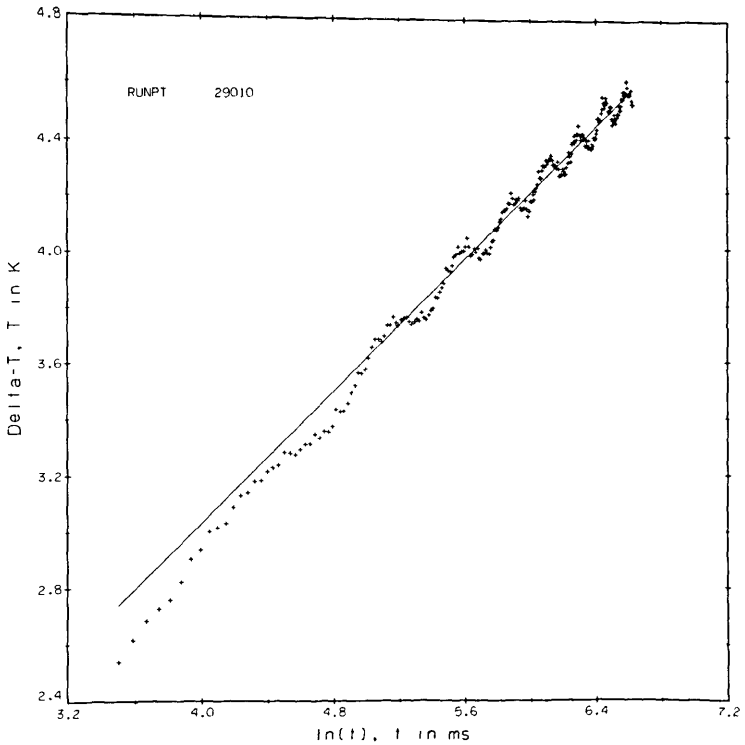

FIGURE 9c. Point 29010, argon gas.

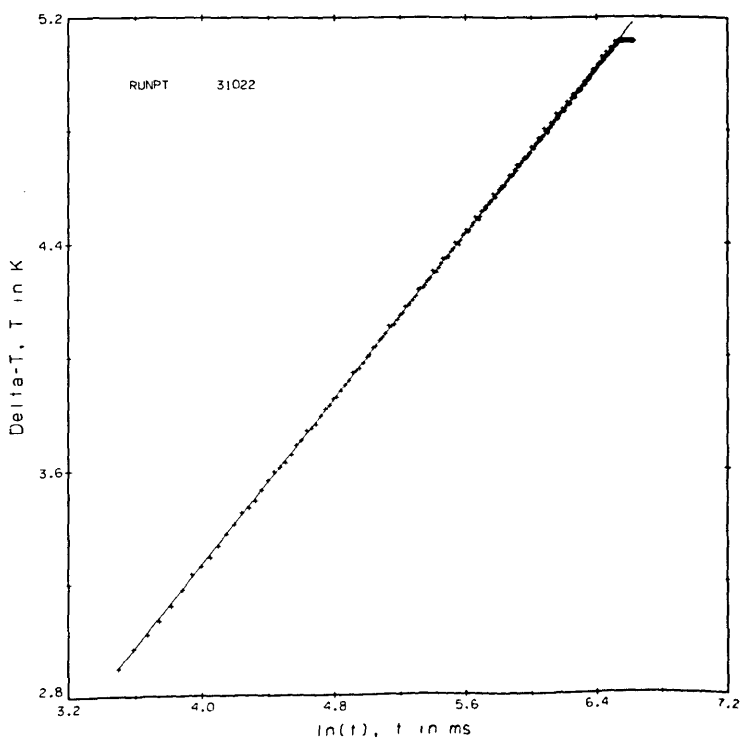

FIGURE 9d. Point 31022, propane liquid.

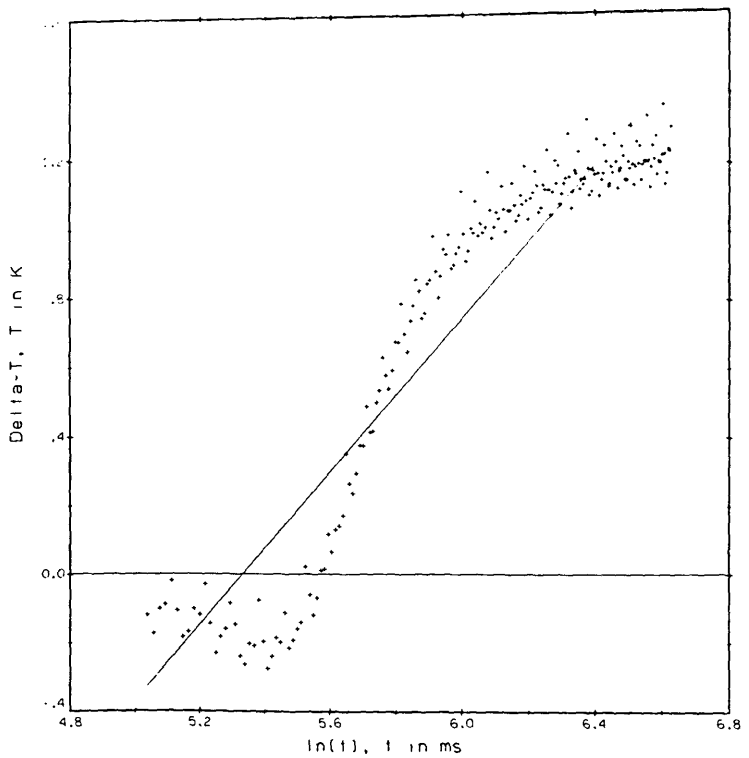

FIGURE 9e. Point 28003, oxygen vapor.

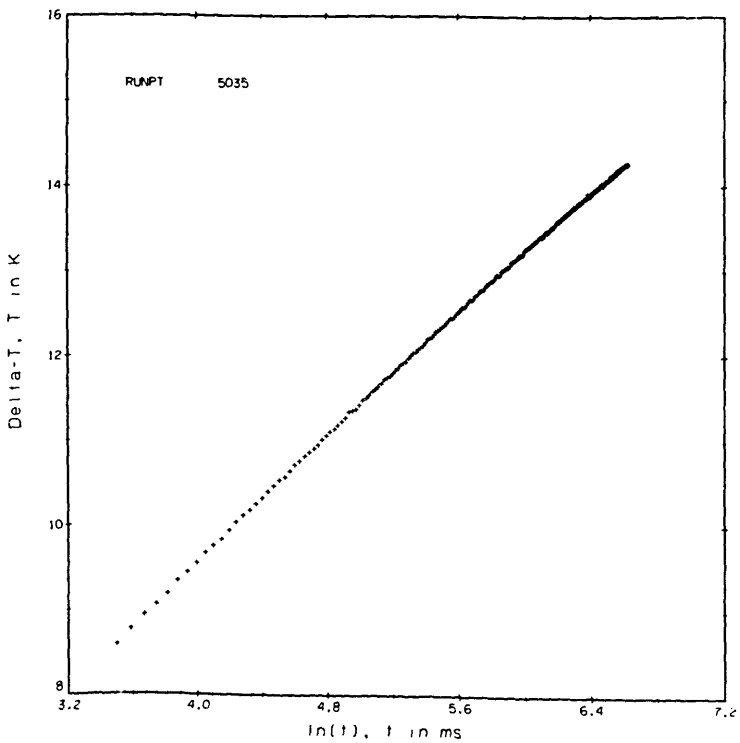

FIGURE 9f. Point 5035, nitrogen gas.

6. Performance Verification

6.1. Nitrogen Results

One of the gases selected for apparatus testing was nitrogen. Typical measurements on nitrogen are presented in table 3. There are two different sets of measurements. Run 4 is an abbreviated isotherm to check the functioning of the system as the pressure is varied. In contrast, all measurements of run 5 are taken at a single density while several of the pertinent apparatus parameters are varied.

Run 4, the pseudo-isotherm, was measured at temperatures between 297 and 301 K with pressures up to 68 MPa. At each pressure (density) level a minimum of four different power settings were used. The results, a total of 50 points at varying temperatures are shown in table 3. For easy comparison with the results of others and using a fixed $d\lambda/dT$ of 0.00063 W/m•K² the results were shifted at the experimental densities to an even temperature of 300.65 K as shown in the next to last column of table 3. The results so adjusted are represented with a curve fit of the type used by Clifford, et al. [31]

$$\lambda = A + B\varrho + C\varrho^2 + D\varrho^3 \qquad (8)$$

The coefficients were determined as $A = 0.02550$, $B = 0.000112$, $C = 0.310567 \times 10^{-4}$, and $D = 0.261641 \times 10^{-5}$ with λ in W/m•K and ϱ in mol/L. The standard deviation for the fit is 0.00022 W/m•K which translates to roughly 0.5 percent in the middle of the density range. The experimental measurements as adjusted to 300.65 K and the curve fit are shown in figure 10. Taking the curve fit of eq (8) as the base, the present results and those of others [31,32,33] are compared in figure 11. When all results are considered together they span a range of 3 percent. The differences between the present results and those of Clifford, et al. [31] who use a transient hot wire system range between 1.3 and 2.3 percent, the differences to the more recent measurements of Assael, et al. [32] range from 1.1 to 1.7 percent. Differences between the present results and a published wide-range correlation for nitrogen [33] lie between 0.6 and 4.5 percent. Reference [33] serves as the source of the equation of state for nitrogen.

Run 5 was measured at the same nominal pressure, about 16.3 MPa, with experimental temperatures varying from 297 to 309 K. For easy comparison these results are referred to a common temperature, 300.65 K, as indicated above. However, they are further adjusted to a common density of 6.3 mol/L using eq (8). The values so adjusted are shown in the last column of table 3, and are plotted in figure 12 versus the power applied, q. The first 15 points, shown as circles in figure 12, are repetitive measurements to establish the base of comparison. The mean of these 15 points is the straight line in the center of figure 12 while the lines above and below represent changes of one percent.

We indicated previously that the time increment can be varied. A series of such measurements was made on nitrogen gas with time delays of 5 and 10 ms. The runs are shown in table 3 as points 5016—5028. The actual time increment between voltage measurements is 9.02 ms for runs 5016—5020 and 14.02 ms for runs 5021—5028 compared to a normal time increment of 3.02 ms. A plot of point 5027 is given in figure 9b, where the straight line segment indicates the range of times, $t_1 = 154.22$ ms and $t_2 = 757.08$ ms, used to evaluate the result given in table 3. If proper times t_1 and t_2 are selected, then runs of this type can yield valid results. However, the associated regression statistics deteriorate because a smaller number of points is available to the least squares analysis.

A second test involves larger than normal powers. The idea is to compare measurements made at one reference temperature with a very large power to measurements made at a higher reference temperature with a much smaller applied power, an overlapping of isotherms so to speak. For example a run at $T_{ref}=295$ K and a power level to produce ΔT's of around 15 K or a T_{exp} of 310 K could be compared to a second run of $T_{ref} = 307$ K and a power level to produce ΔT's $\sim$ 4 K with a T_{ref} also of 310 K. The measurements taken are shown in table 3 as points 5031—5035. The test fails because we can see a slight dependence on power level for the high powers in figure 12. The reason the test fails is because the plot of ΔT versus $\ell n(t)$ instead of being a straight line is curved at the very large ΔT's involved, as shown in figure 9f for point 5035. The test might become valid in the future, provided a reanalysis of the corrections to the experimental ΔT_w is made which allows for sufficiently large ΔT.

A final experimental test involves the gradient along the high pressure cell. The cell is fitted with a thermocouple that measures the temperature difference from the top to the bottom of the cell. Nearly all runs were measured with the top of the cell slightly warmer than the bottom, about 10 to 15 mk. Test runs with the cell top hotter by 47 mk are shown as points 5036—5040 while similar measurements with the cell top colder by about 35 mk are given by points 5041—5045. The results show that the thermal conductivities measured under these conditions vary by roughly 0.2 percent, which in view of the other uncertainties is negligible.

6.2. Helium Results

The rare gas selected initially was helium. Results obtained subsequently on argon have already been published [30]. For helium a single pseudo isotherm was measured at a nominal temperature of 307 K with pressures up to 68 MPa.

Table 3. Thermal Conductivity of Nitrogen Near 300 K.

Run Pt.	Pressure MPa	Temperature K	Density mol/L	Power W/m	Thermal Conductivity W/m•K	STAT	Adjusted Thermal Conductivity with T = 300.65 K W/m•K	Adjusted Thermal Conductivity with T = 300.65 K and ρ = 6.3 mol/L W/m•K
4001	69.123	297.004	17.5101	.14023	.06868	.034	.06891	
4002	69.124	297.439	17.4916	.20067	.06880	.021	.06900	
4003	69.124	298.096	17.4635	.27180	.06821	.013	.06837	
4004	69.123	298.759	17.4351	.35381	.06829	.009	.06841	
4005	69.125	299.583	17.4003	.44662	.06845	.007	.06852	
4006	69.125	300.322	17.3691	.55006	.06831	.004	.06833	
4007	61.132	298.146	16.4493	.27174	.06344	.012	.06360	
4008	61.133	298.905	16.4166	.35371	.06379	.009	.06390	
4009	61.128	299.709	16.3813	.44650	.06333	.006	.06339	
4010	61.131	300.741	16.3376	.54992	.06347	.005	.06346	
4011	54.586	298.026	15.5156	.23468	.05971	.014	.05988	
4012	54.588	298.703	15.4863	.31117	.05962	.009	.05974	
4013	54.588	299.475	15.4528	.39862	.05980	.007	.05987	
4014	54.588	300.334	15.4156	.49695	.05977	.006	.05979	
4015	47.903	300.778	14.3096	.49683	.05555	.004	.05554	
4016	47.903	299.771	14.3531	.39857	.05551	.006	.05557	
4017	47.905	298.863	14.3927	.31119	.05570	.009	.05581	
4018	47.905	298.042	14.4285	.23469	.05555	.014	.05571	
4019	40.607	297.907	13.0618	.20044	.05049	.016	.05066	
4020	40.608	298.705	13.0277	.27163	.05078	.010	.05090	
4021	40.609	299.584	12.9903	.35361	.05092	.007	.05099	
4022	40.609	300.704	12.9427	.44624	.05104	.005	.05104	
4023	33.596	298.229	11.4980	.20061	.04616	.015	.04631	
4024	33.596	299.023	11.4655	.27208	.04600	.010	.04610	
4025	33.596	300.028	11.4247	.35423	.04636	.007	.04640	
4026	33.596	301.176	11.3782	.44717	.04633	.005	.04630	
4027	26.643	297.741	9.7001	.14033	.04128	.023	.04146	
4028	26.642	298.530	9.6705	.20078	.04135	.013	.04148	
4029	26.643	299.522	9.6340	.27210	.04199	.009	.04206	
4030	26.642	300.611	9.5939	.35421	.04154	.006	.04154	
4031	19.700	300.643	7.4708	.31180	.03707	.006	.03707	
4032	19.700	299.992	7.4902	.27212	.03693	.008	.03697	
4033	19.700	298.934	7.5221	.20073	.03695	.012	.03706	
4034	19.700	297.950	7.5521	.14029	.03678	.019	.03695	
4035	19.700	297.532	7.5651	.11414	.03676	.026	.03696	
4036	12.708	297.418	5.0731	.09066	.03223	.035	.03243	
4037	12.708	298.319	5.0546	.14029	.03212	.017	.03227	
4038	12.708	299.457	5.0314	.20079	.03216	.011	.03224	
4039	12.708	300.749	5.0054	.27209	.03238	.008	.03237	
4040	5.681	301.332	2.2732	.23508	.02837	.010	.02833	
4041	5.681	300.556	2.2798	.20076	.02830	.013	.02831	
4042	5.681	299.102	2.2923	.14028	.02816	.021	.02826	
4043	5.681	297.843	2.3032	.09064	.02813	.042	.02831	
4044	5.681	299.714	2.2870	.16920	.02821	.016	.02827	
4045	5.681	298.464	2.2975	.11412	.02807	.030	.02821	
4046	1.430	299.675	.5751	.14031	.02605	.024	.02611	
4047	1.430	298.299	.5779	.09064	.02582	.041	.02597	
4048	1.429	297.129	.5799	.05179	.02618	.097	.02640	
4049	1.429	297.703	.5788	.06983	.02581	.064	.02600	
4050	1.429	298.984	.5761	.11411	.02608	.030	.02618	
5001	16.327	297.649	6.3985	.09069	.03439	.032	.03458	.03440
5002	16.327	298.523	6.3757	.14036	.03453	.019	.03466	.03452
5003	16.327	299.492	6.3507	.20084	.03484	.011	.03491	.03482
5004	16.327	300.657	6.3209	.27209	.03489	.007	.03489	.03485
5005	16.327	301.440	6.3010	.31171	.03508	.006	.03503	.03503
5006	16.328	301.373	6.3030	.31172	.03485	.006	.03480	.03479
5007	16.328	300.632	6.3218	.27203	.03495	.006	.03495	.03491
5008	16.329	299.496	6.3511	.20069	.03467	.011	.03474	.03465
5009	16.329	298.426	6.3787	.14025	.03471	.018	.03485	.03471
5010	16.329	297.614	6.3999	.09061	.03459	.035	.03478	.03460
5011	16.329	297.512	6.4028	.09071	.03447	.032	.03467	.03448
5012	16.329	298.293	6.3824	.14037	.03453	.018	.03468	.03453
5013	16.329	299.270	6.3571	.20090	.03463	.011	.03472	.03462
5014	16.329	300.472	6.3263	.27222	.03468	.007	.03469	.03464
5015	16.329	301.184	6.3083	.31195	.03482	.006	.03479	.03477

Table 3. (Continued)

Run Pt.	Pressure MPa	Temperature K	Density mol/L	Power W/m	Thermal Conductivity W/m·K	STAT	Adjusted Thermal Conductivity with T = 300.65 K W/m·K	Adjusted Thermal Conductivity with T = 300.65 K and ρ = 6.3 mol/L W/m·K
5016	16.330	297.460	6.4043	.09069	.03505	.060	.03525	.03506
5017	16.330	298.264	6.3834	.14035	.03459	.033	.03474	.03459
5018	16.330	299.300	6.3566	.20085	.03481	.019	.03490	.03480
5019	16.330	300.512	6.3255	.27213	.03476	.012	.03477	.03472
5020	16.330	301.228	6.3074	.31179	.03470	.009	.03466	.03465
5021	16.329	296.862	6.4199	.05183	.03397	.186	.03421	.03399
5022	16.329	297.554	6.4017	.09073	.03459	.081	.03479	.03460
5023	16.329	298.358	6.3807	.14043	.03436	.041	.03450	.03435
5024	16.329	299.454	6.3524	.20091	.03447	.024	.03455	.03445
5025	16.329	300.573	6.3235	.27225	.03468	.014	.03468	.03464
5026	16.329	302.013	6.2871	.35420	.03497	.011	.03488	.03490
5027	16.329	303.570	6.2483	.44706	.03505	.009	.03487	.03496
5028	16.329	305.150	6.2095	.55073	.03486	.010	.03458	.03474
5031	16.328	301.848	6.2910	.35473	.03465	.008	.03457	.03459
5032	16.328	303.341	6.2537	.44782	.03481	.006	.03464	.03472
5033	16.328	305.077	6.2109	.55174	.03514	.005	.03486	.03502
5034	16.328	306.934	6.1660	.66648	.03509	.004	.03469	.03493
5035	16.327	308.967	6.1175	.79195	.03528	.003	.03476	.03509
5036	16.333	297.573	6.4025	.09074	.03478	.037	.03497	.03478
5037	16.333	298.377	6.3815	.14047	.03471	.019	.03485	.03470
5038	16.333	299.450	6.3537	.20096	.03479	.011	.03487	.03477
5039	16.333	300.685	6.3222	.27231	.03488	.007	.03488	.03484
5040	16.333	301.270	6.3073	.31209	.03483	.006	.03479	.03478
5041	16.337	297.448	6.4073	.09066	.03435	.034	.03455	.03435
5042	16.337	298.207	6.3874	.14029	.03464	.019	.03479	.03463
5043	16.337	299.265	6.3600	.20074	.03469	.011	.03478	.03467
5044	16.338	300.475	6.3293	.27202	.03477	.007	.03478	.03473
5045	16.338	301.173	6.3115	.31171	.03483	.006	.03480	.03478

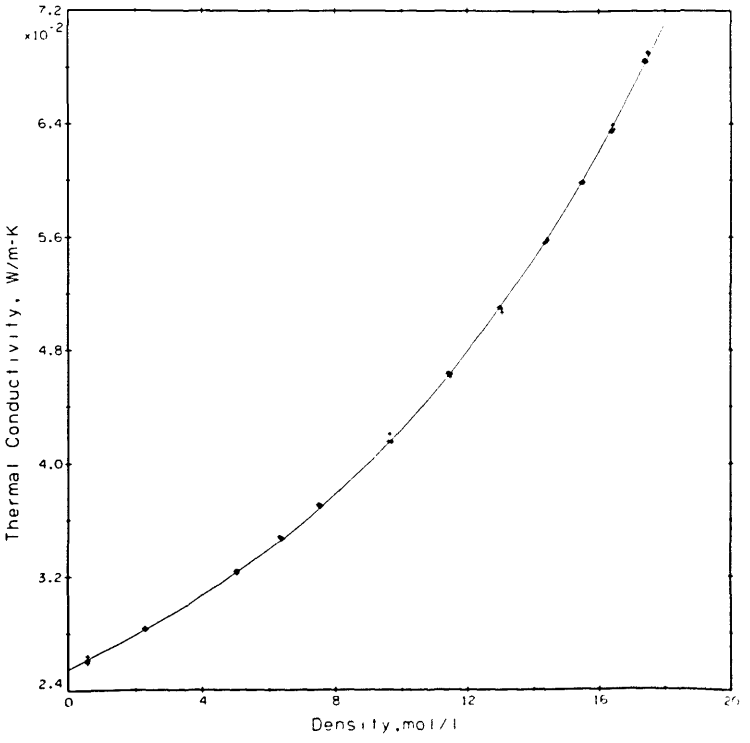

FIGURE 10. Nitrogen measurements shifted to 300.65 K with curve fit, eq (8).

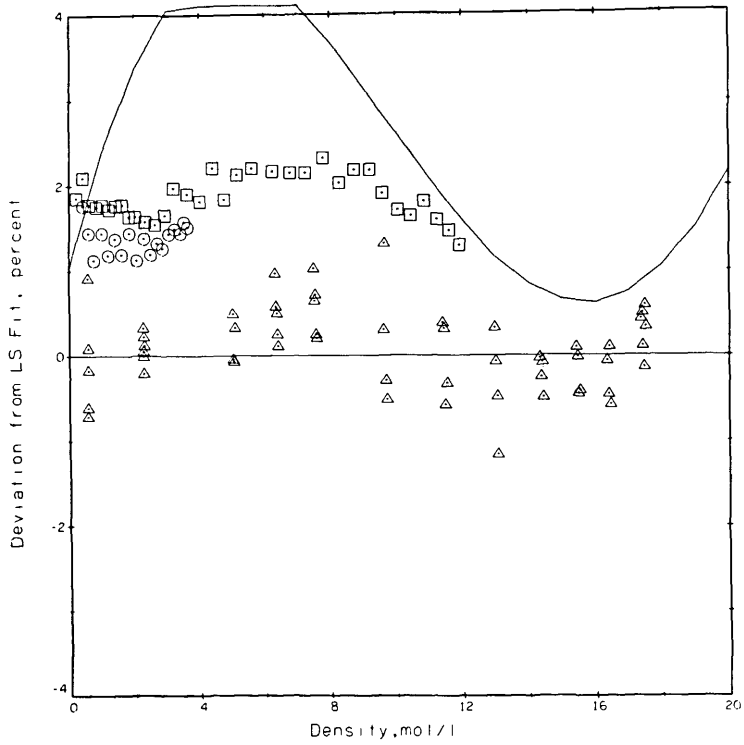

FIGURE 11. Comparison of the present results with those of others for nitrogen at 300.65 K. Base line eq (8), △ this paper, □ Clifford, et al. [31], ○ Assael, et al. [32], —— Hanley, et al. [33] correlation.

At each pressure (density) level two different power settings were used, while at three selected densities a larger range of power was covered. The results, a total of 77 points at varying temperatures are shown in table 4. For easy comparison with the results of others and using a fixed $d\lambda/dT$ of 0.00035 W/m•K² the results were shifted at the experimental densities to a temperature of 300.65 K as shown in the last column of table 4. The results so adjusted are represented with a curve fit of the same type as used on argon earlier.

$$\lambda = A + B\varrho + C\{e^{0.13\rho} - 1.0\} \qquad (9)$$

The coefficients were determined as $A = 0.153099$, $B = 0.108257 \times 10^{-2}$, and $C = 0.613662 \times 10^{-3}$ with λ in W/m•K and ϱ in mol/L. The standard deviation for the fit is 0.00049 W/m•K which translates to roughly 0.6 percent at the 95 percent confidence level or 0.9 percent at the 99 percent confidence level. In other words, of the 77 measurements 71 lie within ± 0.5 percent of the fitted curve. The experimental measurements as adjusted to 300.65 K and the curve fit are shown in figure 13. The densities at which a larger variety of power settings was measured are easily noted in figure 13 as 5.7, 11.5, and 19.6 mol/L. Taking the curve fit of eq (9) as the base, the present results and those of others [7,34,35,36,37] are compared in figure 14. These results span a range of ±2 percent. The deviations between the present results and those of Le Neindre, et al. [34], Johannin, et al. [35], and Ho and Leidenfrost [36] are a nominal 1 percent or less. The differences between the present results and those of Kestin, et al. [7], who also use a transient hot wire system, range between 1.3 and 1.9 percent, while the differences between the present results and a published wide-range correlation for helium [37] also lie between 1 and 2 percent. Differences between the present results and the most recent ones of Assael, et al. [10], who also use a transient hot wire system, range from 1.0 to 1.7 percent. The source used as equation of state for obtaining the densities of helium is [37].

Finally, we apply a test that has not been applied extensively to other transient hot wire systems. In analogy to a flat plate steady state thermal conductivity apparatus [38] we insist that the measured thermal conductivity in the present apparatus should be independent of the applied power. Figure 15 shows the measurements for helium gas at 19.6, 11.5, and 5.7 mol/L plotted as a function of the applied

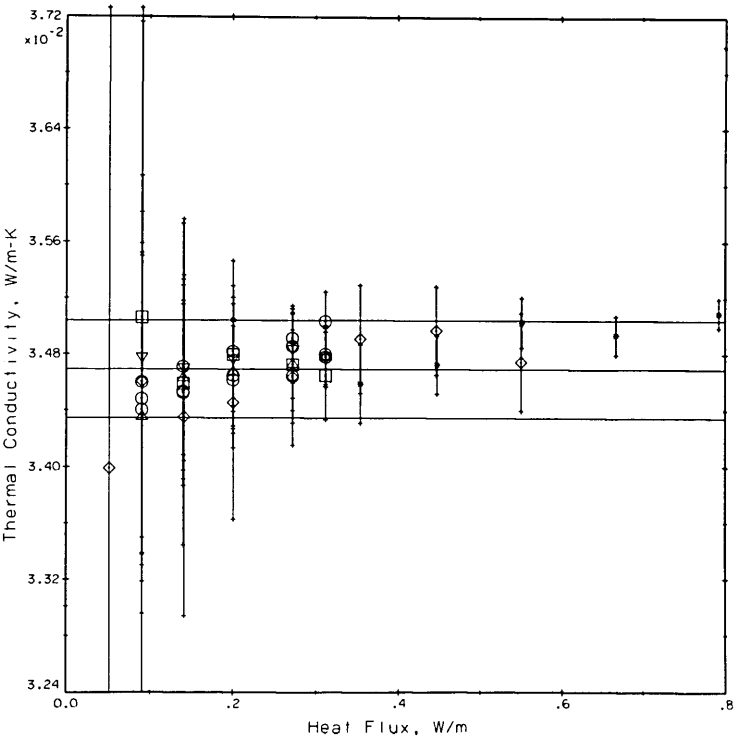

FIGURE 12. Measured thermal conductivity as a function of the applied power. Apparatus tests with nitrogen gas.
○ normal measurements, △ cell top cold, ∇ cell top hot
□ 5 ms delay, time increment 9.02 ms
◇ 10 ms delay, time increment 14.02 ms
* larger than normal powers.

power. Whereas q changes by a factor of nearly five no dependence of the measured conductivity on power level is discernible. For reference, the values of the curve fit (eq (9)) plus or minus 0.5 percent are shown as three straight lines for each density in figure 15. The error bars for each point are those originating from the regression straight line fit for each point, see column STAT in table 4.

6.3. Cell Alinement

During the construction of the apparatus we sought to keep the cell in vertical alinement to insure that convection in the cell would be delayed as long as possible. Later we sought to verify the alinement by a series of experimental measurements, some 162 points with oxygen gas as a sample at a pressure near 10 MPa and a temperature of around 240 K. The position of each cell alinement screw was varied in turn by a measured amount. For each setting of the screws a series of seven to nine measurements were taken varying the applied power, q. If the cell is out of alinement the measured thermal conductivity increases. The increase is more pronounced at the higher power levels. The proper setting for the alinement screws occurs when the measured results are most nearly independent of q as illustrated in figure 15. The final settings chosen were nearly identical to those first achieved during construction of the apparatus. In fact, the measurements on helium, Run No. 9, were taken four months before the series on alinement, Run No. 19.

6.4. Other Tests

Tests were run on nitrogen gas at room temperature with only a single hot wire in the bridge. The circuit was rewired so that either R_4 or R_3, see figure 2, were replaced by yet another 100 Ω standard resistor. The data reduction program had to be modified accordingly. The results were evaluated only on the minicomputer, and are relative to similar

Table 4. Thermal Conductivity of Helium Near 300 K.

Run Pt.	Pressure MPa	Temperature K	Density mol/L	Power W/m	Thermal Conductivity W/m•K	STAT	Adjusted Thermal Conductivity with T = 300.65 K W/m•K
9001	63.980	306.154	19.6780	.36457	.18386	.022	.18193
9002	63.978	306.459	19.6629	.46029	.18445	.014	.18242
9003	63.978	306.788	19.6469	.56726	.18336	.011	.18121
9004	63.979	307.287	19.6229	.68489	.18479	.009	.18247
9005	63.979	307.741	19.6010	.81392	.18424	.006	.18176
9006	63.979	308.241	19.5769	.95386	.18427	.005	.18161
9007	61.905	306.849	19.1335	.56688	.18268	.010	.18051
9008	61.905	308.397	19.0601	.95337	.18285	.005	.18014
9009	59.692	306.827	18.5826	.56708	.18132	.010	.17916
9010	59.693	307.794	18.5380	.81386	.18250	.007	.18000
9011	57.621	306.382	18.0798	.46038	.17957	.014	.17756
9012	57.622	307.822	18.0144	.81384	.18141	.006	.17890
9013	55.588	306.292	17.5633	.46046	.17811	.015	.17614
9014	55.588	307.767	17.4977	.81391	.17947	.006	.17698
9015	53.338	306.324	16.9781	.46030	.17822	.015	.17623
9016	53.338	307.769	16.9154	.81397	.17892	.007	.17643
9017	51.292	306.429	16.4358	.46023	.17730	.015	.17528
9018	51.293	307.763	16.3793	.81388	.17749	.006	.17500
9019	49.069	306.377	15.8453	.46028	.17662	.014	.17462
9020	49.070	307.784	15.7876	.81385	.17682	.006	.17432
9021	46.963	306.311	15.2786	.46031	.17652	.015	.17454
9022	46.964	307.749	15.2211	.81389	.17577	.006	.17329
9023	44.676	306.361	14.6495	.46023	.17437	.013	.17237
9024	44.678	307.731	14.5966	.81401	.17554	.006	.17306
9025	42.449	306.396	14.0279	.46025	.17243	.013	.17042
9026	42.449	307.874	13.9726	.81371	.17387	.006	.17134
9027	40.222	306.328	13.4010	.46013	.17191	.014	.16992
9028	40.222	307.816	13.3472	.81378	.17336	.006	.17085
9029	38.053	306.321	12.7787	.46027	.17121	.013	.16923
9030	38.053	307.861	12.7251	.81376	.17216	.006	.16964
9031	35.850	306.292	12.1378	.46029	.17026	.014	.16829
9032	35.851	307.886	12.0847	.81381	.17134	.006	.16881
9033	33.592	305.206	11.5040	.20675	.16850	.042	.16691
9034	33.592	305.508	11.4943	.28015	.16954	.029	.16784
9035	33.592	305.853	11.4833	.36455	.16908	.020	.16726
9036	33.592	306.306	11.4688	.46028	.16863	.014	.16665
9037	33.593	306.741	11.4552	.56704	.17039	.010	.16826
9038	33.594	307.256	11.4389	.68485	.16933	.008	.16702
9039	33.594	307.857	11.4198	.81389	.17057	.006	.16805
9040	33.594	305.799	11.4856	.36407	.16952	.020	.16772
9041	33.594	306.338	11.4684	.45965	.16955	.013	.16756
9042	33.595	306.824	11.4531	.56620	.16952	.011	.16736
9043	33.595	307.313	11.4375	.68391	.16982	.008	.16749
9044	33.595	307.790	11.4223	.81285	.17030	.006	.16780
9045	33.595	308.438	11.4018	.95255	.17128	.005	.16855
9045	31.497	306.173	10.8425	.46033	.16840	.013	.16647
9046	31.497	307.807	10.7931	.81402	.16980	.006	.16730
9047	28.968	306.381	10.0629	.46036	.16811	.013	.16610
9048	28.968	307.941	10.0184	.81396	.16769	.006	.16514
9049	26.634	306.344	9.3369	.46035	.16695	.014	.16496
9050	26.634	307.965	9.2936	.81397	.16735	.005	.16479
9051	24.532	306.354	8.6709	.46038	.16588	.014	.16388
9052	24.532	307.963	8.6306	.81417	.16621	.006	.16365
9053	22.396	306.379	7.9829	.46046	.16482	.013	.16281
9054	22.395	308.019	7.9445	.81418	.16552	.006	.16294
9055	20.255	306.511	7.2793	.46102	.16399	.013	.16194
9056	20.255	308.186	7.2434	.81536	.16490	.006	.16226
9057	17.991	306.347	6.5288	.46009	.16298	.014	.16099
9058	17.913	308.066	6.4692	.81378	.16397	.006	.16137
9059	15.627	305.967	5.7333	.36458	.16262	.018	.16076
9060	15.627	306.425	5.7254	.46017	.16148	.012	.15946
9061	15.626	306.897	5.7170	.56700	.16220	.010	.16001
9062	15.626	307.578	5.7052	.68465	.16218	.008	.15976
9063	15.626	308.170	5.6951	.81363	.16305	.006	.16042
9064	13.436	305.988	4.9748	.36453	.16032	.019	.15841
9065	13.436	307.519	4.9516	.68483	.16199	.007	.15959

Table 4. (Continued)

Run Pt.	Pressure MPa	Temperature K	Density mol/L	Power W/m	Thermal Conductivity W/m•K	STAT	Adjusted Thermal Conductivity with T = 300.65 K W/m•K
9066	11.253	305.990	4.2056	.36453	.16059	.019	.15872
9067	11.253	307.633	4.1844	.68454	.16030	.008	.15786
9068	9.013	305.969	3.4013	.36451	.15889	.019	.15703
9069	9.013	307.727	3.3827	.68445	.15957	.007	.15709
9070	6.648	305.860	2.5362	.36460	.15773	.012	.15591
9071	6.648	307.452	2.5232	.68476	.15851	.006	.15613
9072	4.466	305.982	1.7199	.36440	.15684	.016	.15497
9073	4.466	307.438	1.7119	.68485	.15705	.008	.15467
9074	2.419	306.028	.9401	.36441	.15672	.023	.15484
9075	2.418	307.670	.9349	.68458	.15595	.012	.15349
9076	.415	306.143	.1627	.36423	.15477	.222	.15285

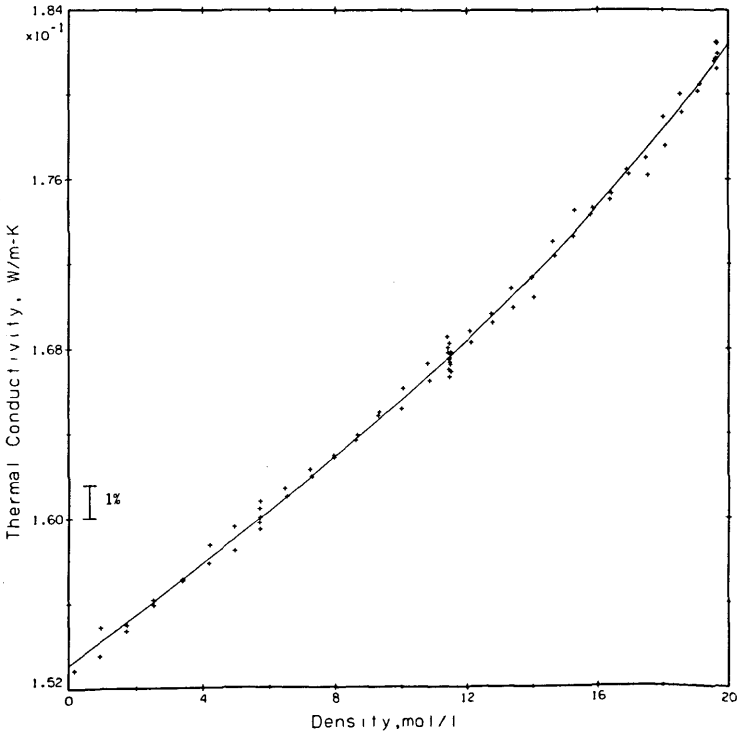

FIGURE 13. Helium measurements shifted to 300.65 K with curve fit, eq (9).

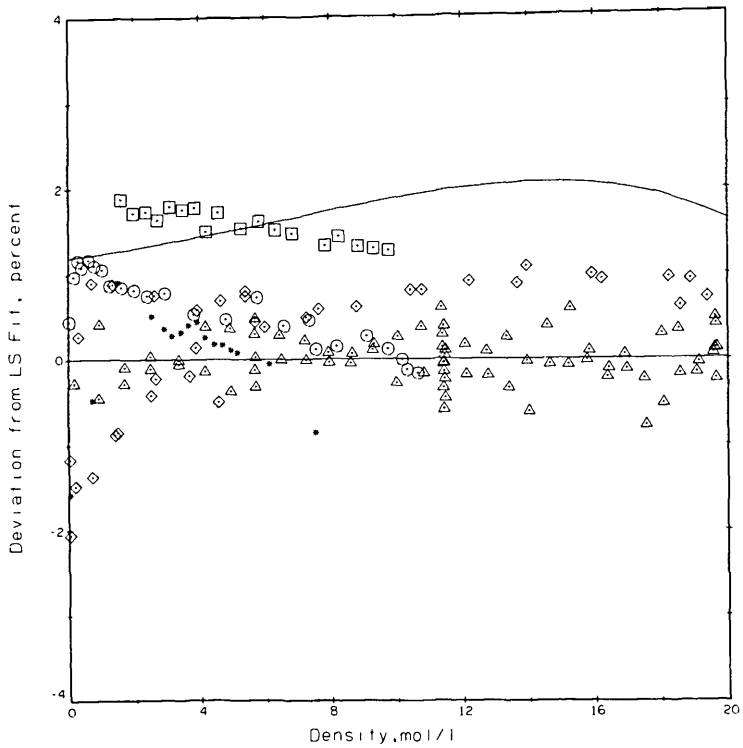

FIGURE 14. Comparison of the present results with those of others for helium at 300.65 K. Base line eq (9), △ this paper, □ Kestin, et al. [7], ◇ Le Neindre, et al. [34], * Johannin, et al. [35], ○ Ho and Leidenfront [36], —— McCarty [37] correlation.

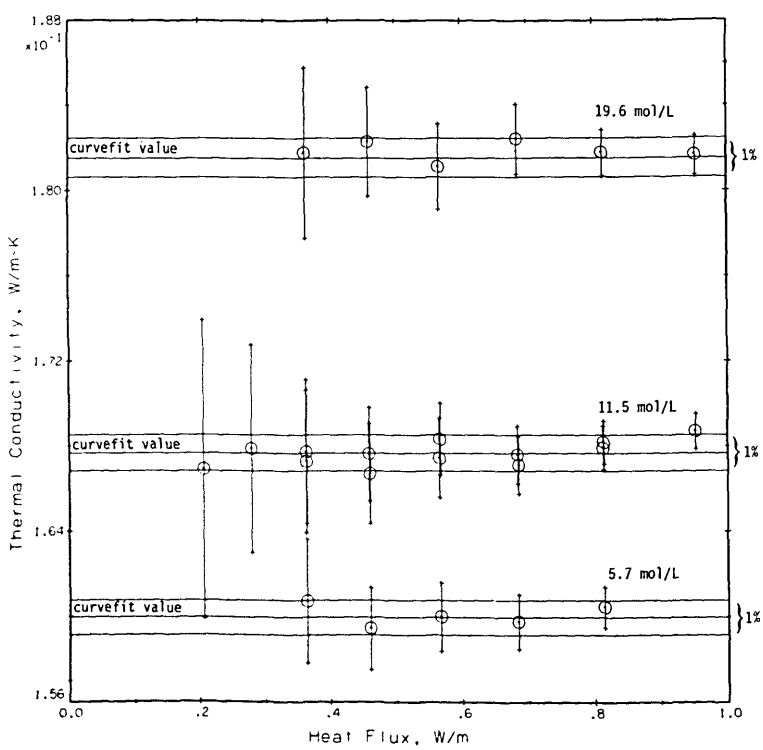

FIGURE 15. Measured thermal conductivity as a function of the applied power. Apparatus test with helium gas.

measurements made the same day with the full bridge. The apparent conductivities for the single wires increase above those of the full bridge as follows

full bridge	1.000
long hot wire only	1.048
short hot wire only	1.083.

Measurements of this type show the relative effect of the end corrections which would be required for the single wire, but which are presumed to be off setting in the bridge circuit.

7. Errors

Precision, reproducibility, internal consistency, and accuracy are discussed here.

Precision. The measurement variation in the voltages across the Wheatstone bridge is $\pm 28\ \mu V$ which corresponds to about 25 mK. The effective errors in the experimental ΔT values are 6 percent for the very small power levels, i.e., a final ΔT of about 0.5 K, to 0.4 percent for a final ΔT of about 6 K. An example of the distribution of the experimental ΔT's about the calculated straight line was shown in figure 8b. The regression program accounts for the spread in measurements by assigning a variance to the coefficients of the calculated straight line. The value STAT as printed in tables 3 and 4 is the fractional error in the slope of the straight line obtained from the variance in the slope (2σ) divided by by the slope itself. The value STAT is the primary measure of the experimental precision because other contributions such as an error in q are quite negligible. For final ΔT values of 3.5 K or more which includes about 70 percent of all measurements made to date the nominal precision (2σ) is 0.6 percent or slightly less.

Reproducibility was tested by measuring (a) repeatedly the same point at the same fluid conditions on a given day, (b) by measuring similar points at different power levels, and (c) by repeating different isotherms at different times some months apart. Examples of (a) are found in table 3, examples of (b) are given in the sections on nitrogen and helium. For (c), isotherms at 160 K, 200 K, and 240 K were repeated during the measurements on oxygen [26].

Internal consistency. When measurements are made over a large portion of the thermal conductivity surface, and if an analytical function is used to represent the surface, then it becomes possible to check the internal consistency of the set of measurements by intercomparing the deviations and deviation patterns for the various isotherms. Such checks are possible for both propane [27] and oxygen [26]. In propane seven different liquid isotherms can be represented with an overall deviation of 1.2 percent (2σ). For oxygen, 13 isotherms from the surface which includes gas, liquid, subcritical vapor and the near critical region for an average deviation of 1.6 percent.

Accuracy. The accuracy of the measurement can in principle be established from the measurements and certain theoretical considerations, i.e., for the rare gases the Eucken factor [7]. For argon [30] the 0.3 percent obtained in the low density extrapolation was considered a fortunate coincidence and an overall accuracy of ± 1 percent was claimed. For the results on helium in table 4 the low density extrapolation yields a result which is 1.8 percent low. Accuracy can also be estimated by comparison to the results of others. For the present apparatus these intercomparisons cover a wide range of fluids, and a wide range of pressures, densities and temperatures. Summarized these comparisons are:

Nitrogen: this apparatus is 1.3 to 2.3 percent lower than other authors [31,32,33].

Helium: this apparatus is 1. to 1.8 percent lower than other authors [7,34,35,36,37].

Argon: this apparatus is 1. percent lower than other authors [30].

Oxygen: this apparatus is 1–2 percent lower than other authors [26].

Propane: this apparatus is higher at some densities, lower at other densities when compared to other authors [27].

Hydrogen: this apparatus is 1.5 percent lower than other authors [39].

8. Summary

A new transient hot wire thermal conductivity apparatus for fluids has been developed. It differs from some of the other transient hot wire systems in that it uses compensating wires in a Wheatstone bridge arrangement. It differs from those transient hot wire systems that use a bridge in that the voltages developed across the bridge are measured directly. The apparatus is a very rapid measuring device. Sixty points, a full pseudo-isotherm, are possible in a day. The system is capable of measuring a wide range of fluid temperatures, densities, and pressures. Fluid states, such as dilute gas, dense gas, the near critical states, vapor at temperatures below critical, compressed liquid states, and metastable liquid states at densities below saturation, are accessible for many liquefied gases. A wide variety of simple fluids has been measured in the system so far. It appears that the precision of the new system is on the order of 0.6 percent while its accuracy is close to 1.5 percent.

9. References

[1] Pittman, J. F. T. Fluid thermal conductivity determination by the transient line source method. Thesis. University of London; London; 1968.

[2] Haarman, J. W. Thesis. Technische Hogeschool; Delft; 1969.

[3] Mani, N. Precise determination of the thermal conductivity of fluids using absolute transient hot-wire technique. Thesis. University of Calgary. Calgary, Alberta, Canada. 1971 August.

[4] de Groot, J. J.; Kestin, J.; Sookiazian, H. Instrument to measure the thermal conductivity of gases. Physica. **75**: 454–482; 1974.

[5] Healy, J. J.; de Groot, J. J.; Kestin, J. The theory of the transient hot-wire method for measuring thermal conductivity. Physica **82C**(2): 392-408; 1976 April.

[6] de Groot, J. J.; Kestin, J.; Sookiazian, H. The thermal conductivity of four monatomic gases as a function of density near room temperature. Physica. **92A**: 117-144; 1978.

[7] Kestin, J.; Paul, R.; Clifford, A. A.; Wakeham, W. A. Absolute determination of the thermal conductivity of the noble gases at room temperature up to 35 MPa. Physica **100A**(2): 349-369; 1980 February.

[8] Kestin, J.; Wakeham, W. A. A contribution to the theory of the transient hot-wire technique for thermal conductivity measurements. Physica. **92A**(1 and 2): 102-116; 1978 June.

[9] Clifford, A. A.; Kestin, J.; Wakeham, W. A. A further contribution to the theory of the transient hot-wire technique for thermal conductivity measurements. Physica. **100A**(2): 370-374; 1980 February.

[10] Assael, M. J.; Dix, M.; Lucas, A.; Wakeham, W. A. Absolute determination of the thermal conductivity of the noble gases and two of their binary mixtures. J. Chem. Soc., Faraday Trans. **77**(1): 439-464; 1981.

[11] Menashe, J.; Wakeham, W. A. Absolute measurements of the thermal conductivity of liquids of pressures up to 500 MPa. to be published, Physica.

[12] de Castro, C. A. Nieto; Calado, J. C. G.; Wakeham, W. A.; Dix, M. An apparatus to measure the thermal conductivity of liquids. Journal of Physics E: Scient. Inst. **9**: 1073-1080; 1976.

[13] de Castro, C. A. Nieto; Calado, J. C. G.; Wakeham, W. A. Absolute measurements of the thermal conductivity of liquids using a transient hot-wire technique. Cezarilyan, A. ed. Proceedings of the seventh symposium on thermophysical properties; 1977 May 10-12; Gaithersburg, Maryland; New York; ASME; 1977; 730-738.

[14] Carslaw, H. S.; Jaeger, J. C. *Conduction of heat in solids*. 2nd Ed. Oxford: University Press; 1959. 510 p.

[15] Riddle, J. L.; Furukawa, G. T.; Plumb, H. H. Platinum Resistance Thermometry. Nat. Bur. Stand. (U.S.) Monogr. 126; 1973 April. 129 p.

[16] Lyman, T., ed. Metals Handbook. 8th Ed. Vol **1**. Properties and Selection of Metals. American Society for Metals. Metals Park, Ohio; 1969 September. 1300 p.

[17] Younglove, B. A. Speed of sound in fluid parahydrogen. J. Acoust. Soc. Am. **38**(3): 433-438; 1965 September.

[18] Diller, D. E. Measurements of the viscosity of parahydrogen. J. Chem. Phys. **42**(6): 2089-2100; 1965 March 15.

[19] Weber, L. A. Density and compressibility of oxygen in the critical region. Phys. Rev. A **2**(6): 2379-2388; 1970 December.

[20] Haynes, W. M.; Hiza, M. J.; Frederick, N. V. Magnetic suspension densimeter for measurements on fluids of cryogenic interest. Rev Sci. Instrum. **47**(10): 1237-1250; 1976 October.

[21] Straty, G. C.; Younglove, B. A. A fluorine compatible low temperature electrical feed through. Rev. Sci. Instrum. **43**(1): 156-157; 1972 January.

[22] Key, C. F. Compatibility of materials with liquid oxygen, III. National Aeronautics and Space Administration, Marshall Space Flight Center, Huntsville, Ala; Tech. Memo X67-10596; 1966 November.

[23] Bankaitis, H.; Schueller, C. F. ASRDI Oxygen technology survey Volume II: cleaning requirements, procedures, and verification techniques. National Aeronautics and Space Administration Special Publication SP-3072; 1972. 76 p.

[24] Goodwin, R. D. Apparatus for determination of pressure-density-temperature relations and specific heats of hydrogen to 350 atmospheres at temperatures above 14 K. J. Res. Nat. Bur. Stand. (U.S.) **65C**(4): 231-243; 1961 October-December.

[25] Goodwin, R. D. *An improved DC power regulator*. Timmerhaus, K. D., ed. *Advances in Cryogenic Engineering*. Proceedings of the 1959 Cryogenic Engineering Conference. Plenum Press Inc., New York; 1960. 577-579.

[26] Roder, H. M. The thermal conductivity of oxygen. J. Res. Nat. Bur. Stand. (U.S.). to be published.

[27] Roder, H. M.; de Castro, C. A. N. Thermal conductivity of liquid propane. Submitted to J. Chem. Engr. Data.

[28] Hall, L. A. Survey of electrical resistivity measurements on 16 pure metals in the temperature range 0 to 273 K. Nat. Bur. Stand. (U.S.) Tech. Note 365; 1968 February. 111 p.

[29] de Castro, C. A. Nieto; Wakeham, W. A. Experimental aspects of the transient hot-wire technique for thermal conductivity measurements. Mirkovich, V. V. ed. *Thermal conductivity 15*. 1977 August 24-26; Ottawa, Ontario, Canada; New York; Plenum Publ. Corp.; 1978; 235-243.

[30] de Castro, C. A. N.; Roder, H. M. Absolute determination of the thermal conductivity of argon at room temperature and pressures up to 68 MPa. J. Res. Nat. Bur. Stand. (U.S.). 86(3): 293-307; 1981 May-June.

[31] Clifford, A. A.; Kestin, J.; Wakeham, W. A. Thermal conductivity of N_2, CH_4, and CO_2 at room temperature and at pressures up to 35 MPa. Physica. **97A**(2): 287-295; 1979 July.

[32] Assael, M. J.; Wakeham, W. A. Thermal conductivity of four polyatomic gases. J. Chem. Soc., Faraday Trans. **77**(1): 697-707; 1981.

[33] Hanley, H. J. M.; McCarty, R. D.; Haynes, W. M. The viscosity and thermal conductivity for dense gaseous and liquid argon, krypton, xenon, nitrogen and oxygen. J. Phys. Chem. Ref. Data **3**(4): 979-1017; 1974.

[34] Le Neindre, B.; Bury, P.; Tufeu, R.; Johannin, P.; Vodar, B. Recent developments at Bellevue on thermal conductivity measurements of compressed gases. Flynn, D. A.; Peavy, B. A., Jr. ed. Thermal conductivity; Proceedings of the seventh conference; 1967 November 13-16; Gaithersburg, Maryland. Nat. Bur. Stand. (U.S.) Spec. Publ. 302; 1968 September. 579-593.

[35] Johannin, P.; Wilson, M.; Vodar, B. Heat conductivity of helium at elevated temperatures. Masi, J. F.; Tsai, D. H. ed. *Progress in International Research on Thermodynamic and Transport Properties*. Academic Press, New York. 1962. 418-433.

[36] Ho, C. W.; Leidenfrost, W. Precise determination of the thermal conductivity of helium gas at high pressures and moderate temperatures. Grigull, U.; Hahnl, E. eds. *Progress in Heat and Mass Transfer*. Pergamon Press, Oxford; 1969. 55-98.

[37] McCarty, R. D. Thermophysical properties of helium-4 from 2 to 1500 K with pressures to 1000 atmospheres. Nat. Bur. Stand. (U.S.) Tech. Note 631; 1972 November. 161 p.

[38] Roder, H. M.; Diller, D. E. Thermal conductivity of gaseous and liquid hydrogen. J. Chem. Phys. **52**(11): 5928-5949; 1970 June 1.

[39] Roder, H. M. Thermal conductivity of normal hydrogen. Presented at the 17th International Thermal Conductivity Conference. Gaithersburg, Maryland; 1981 June 15-18.

```
10 REM  PROGRAM TEST, RESULTS ONTO TAPE, REVISED 20 DEC 79
20 DIM A[255],B[255]
30 LET I2=250
40 REM  WHEATSTONE BALANCE
50 REM  HOTWIRE SIDE ONLY
60 PRINT " DIAL IN VOLTS SHOULD BE 0.1"
70 PRINT "TOTAL R3","TOTAL R4","R3 POT SET","R4 POT SET"
75 CALL 9,3, 0
80 CALL 9,1,6
90 FOR J= 0 TO 7
100   LET V[J]= 0
105   CALL 5,1,128,J,J,4
110   FOR I=1 TO 250
120     CALL 6,A[I]
150     LET V[J]=V[J]+A[I]
160   NEXT I
170   LET V[J]=V[J]/250
180 NEXT J
190 CALL 9,1, 0
210 LET C=V[ 0]/100
220 FOR I=1 TO 7
230   LET R[I]=V[I]/C
240 NEXT I
250 LET R3=R[1]+R[2]+R[3]
260 LET R4=R[4]+R[5]+R[7]
300 PRINT R3,R4,R[2],R[5]
310 PRINT "GO AGAIN ?"
320 INPUT K1
330 IF K1= 0 GOTO  80
340 REM  FULL BRIDGE
350 LET V[6]= 0
360 CALL 9,3,6
370 CALL 9,1,6
380 CALL 5,1,1024,6,6,4
390 FOR I=1 TO 250
400   CALL 6,A[I]
410   LET V[6]=V[6]+A[I]
420 NEXT I
430 LET V[6]=V[6]/250
440 CALL 9,1, 0
450 CALL 9,3, 0
460 PRINT "WHEATSTONE BALANCE =",V[6]," GO AGAIN ? "
470 INPUT K1
480 IF K1= 0 GOTO  350
490 REM  INITIAL CONDITIONS
500 LET T1= 0
510 LET T2=296.06+(R[3]-90.58)/.33
520 LET A[ 0]=V[6]
530 PRINT
540 PRINT "TIME-Z","TEMP--Z","R3-Z","R4-Z","V OFFS-Z"
550 PRINT T1,T2,R[3],R[4],A[ 0]
```

```
560 PRINT
570 REM  DATA AQUISITION SECTION
580 PRINT " SET HP POWER"
590 INPUT V1
600 CALL 9,3,6
610 CALL 5,1,512,6,6,9
620 CALL 1, 0, 0
630 CALL 9,1,6
640 FOR I=1 TO I2
650   CALL 6,A[I]
660 NEXT I
670 CALL 2,A2,A3,A4,A5
680 FOR I=1 TO 100
690   CALL 7, 0,B[I]
700 NEXT I
710 LET V2= 0
720 FOR I=1 TO 100
730   LET V2=V2+B[I]
740 NEXT I
750 LET V2=V1-V2/100
760 CALL 9,1, 0
770 CALL 9,3, 0
780 LET A4=A4+A5/1000
790 LET A5=A4/I2
795 GOTO  900
800 PRINT
810 PRINT "TOTAL RUN TIME","TIME INCR."
820 PRINT A4,A5
821 PRINT
823 PRINT "DATE RUN/PT PRT - L PRESS BAR ?"
824 INPUT O1,O2,O3,O4,O5,O6
825 LET S4=R3-R[3]
826 LET S5=R4-R[4]
827 PRINT
828 CALL 22
829 PRINT O1;","O2;","O3;","O4;","O5;","O6;","
830 PRINT R[3];","S4;","R[4];","S5;","A5;","V2;","
840 FOR I=1 TO 49
850   LET N=(I-1)*5
860   PRINT A[N+1];","A[N+2];","A[N+3];","A[N+4];","A[N+5];","
870 NEXT I
871 PRINT A[246];","A[247];","A[248];","A[249];","A[250]
872 CALL 11
874 END
900 PRINT
910 PRINT A[246];","A[247];","A[248];","A[249];","A[250]
920 PRINT
930 PRINT "RECORD ON TAPE?"
940 INPUT K1
945 PRINT
950 IF K1= 0 GOTO  800
960 GOTO  874
```

800116, 9044, 57515.7, .7, 4710.1, 626.7,
93.3094, 6.65579, 46.7144, 53.4657, .00302, 6.07389,
-7.06954E-4, 5.15612E-4, 1.07951E-3, 1.40795E-3, 1.68155E-3,
1.84488E-3, 2.00463E-3, 2.1614E-3, 2.2985E-3, 2.43559E-3,
2.47911E-3, 2.55064E-3, 2.65734E-3, 2.74794E-3, 2.79682E-3,
2.86418E-3, 2.91842E-3, 2.96074E-3, 3.01201E-3, 3.07459E-3,
3.16818E-3, 3.16639E-3, 3.16878E-3, 3.23256E-3, 3.31303E-3,
3.32376E-3, 3.35952E-3, 3.38992E-3, 3.44953E-3, 3.45609E-3,
3.48649E-3, 3.55206E-3, 3.56219E-3, 3.55087E-3, 3.58603E-3,
3.64683E-3, 3.6671E-3, 3.6975E-3, 3.69869E-3, 3.73088E-3,
3.75174E-3, 3.77559E-3, 3.84712E-3, 3.82506E-3, 3.82149E-3,
3.84414E-3, 3.90017E-3, 3.90673E-3, 3.94309E-3, 3.94249E-3,
3.95084E-3, 3.96335E-3, 3.99375E-3, 4.04263E-3, 4.03667E-3,
4.01819E-3, 4.02296E-3, 4.09568E-3, 4.10284E-3, 4.12549E-3,
4.11595E-3, 4.13562E-3, 4.14874E-3, 4.1696E-3, 4.19344E-3,
4.22086E-3, 4.20119E-3, 4.19881E-3, 4.24292E-3, 4.26914E-3,
4.29835E-3, 4.27332E-3, 4.27391E-3, 4.29716E-3, 4.32518E-3,
4.32994E-3, 4.35677E-3, 4.34485E-3, 4.36571E-3, 4.37644E-3,
4.39194E-3, 4.42115E-3, 4.4128E-3, 4.40505E-3, 4.41161E-3,
4.44678E-3, 4.45691E-3, 4.48672E-3, 4.46406E-3, 4.47062E-3,
4.49268E-3, 4.51115E-3, 4.5499E-3, 4.51712E-3, 4.52248E-3,
4.52904E-3, 4.55586E-3, 4.55884E-3, 4.60414E-3, 4.58268E-3,
4.56361E-3, 4.5797E-3, 4.61964E-3, 4.64229E-3, 4.62203E-3,
4.6107E-3, 4.62262E-3, 4.66494E-3, 4.66316E-3, 4.69475E-3,
4.68461E-3, 4.67269E-3, 4.68163E-3, 4.72336E-3, 4.72813E-3,
4.72753E-3, 4.70727E-3, 4.71203E-3, 4.74601E-3, 4.75555E-3,
4.78476E-3, 4.76211E-3, 4.75078E-3, 4.76866E-3, 4.79847E-3,
4.79727E-3, 4.81277E-3, 4.80383E-3, 4.82589E-3, 4.82469E-3,
4.83006E-3, 4.8688E-3, 4.84973E-3, 4.82767E-3, 4.83125E-3,
4.87357E-3, 4.87834E-3, 4.89265E-3, 4.87476E-3, 4.88669E-3,
4.89622E-3, 4.90934E-3, 4.94451E-3, 4.91828E-3, 4.90993E-3,
4.90874E-3, 4.93378E-3, 4.94272E-3, 4.97729E-3, 4.9457E-3,
4.93199E-3, 4.95404E-3, 4.98444E-3, 4.99637E-3, 4.97789E-3,
4.97371E-3, 4.9761E-3, 5.0071E-3, 5.0071E-3, 5.03988E-3,
5.02379E-3, 5.00352E-3, 5.01604E-3, 5.05776E-3, 5.05538E-3,
5.0524E-3, 5.0369E-3, 5.03392E-3, 5.0673E-3, 5.07624E-3,
5.10724E-3, 5.07743E-3, 5.0673E-3, 5.08339E-3, 5.10903E-3,
5.09889E-3, 5.11618E-3, 5.10187E-3, 5.12333E-3, 5.1126E-3,
5.12452E-3, 5.16387E-3, 5.14062E-3, 5.11618E-3, 5.1275E-3,
5.17281E-3, 5.16565E-3, 5.17817E-3, 5.15016E-3, 5.16983E-3,
5.17221E-3, 5.17817E-3, 5.22169E-3, 5.19605E-3, .005174,
5.1734E-3, 5.20678E-3, 5.21632E-3, 5.23599E-3, 5.20976E-3,
5.19725E-3, 5.21871E-3, 5.23838E-3, 5.25685E-3, 5.23838E-3,
5.23063E-3, 5.22407E-3, 5.26222E-3, 5.25924E-3, 5.28725E-3,
5.26639E-3, 5.2503E-3, 5.25745E-3, 5.28368E-3, 5.29798E-3,
5.29321E-3, 5.26937E-3, 5.27176E-3, 5.31229E-3, 5.31229E-3,
5.33434E-3, 5.31169E-3, 5.30514E-3, 5.30514E-3, 5.32838E-3,
5.32242E-3, 5.34686E-3, 5.32361E-3, 5.3409E-3, 5.33673E-3,
.005357, 5.38263E-3, 5.35461E-3, 5.33375E-3, 5.34984E-3,
5.38084E-3, 5.37607E-3, 5.39097E-3, 5.37667E-3, 5.38322E-3,
5.3862E-3, 5.39157E-3, 5.43866E-3, 5.40766E-3, 5.38322E-3,
5.37965E-3, 5.41243E-3, 5.42137E-3, 5.43926E-3, 5.41005E-3

```
      PROGRAM HE(INPUT,OUTPUT,TAPE1)

C     HELIUM COND. DATA REDUCTION, FINAL DR/DT, REVISED 9 MAR 81
C     FOR LS ALONG THE DATA: CALL LS
C     FOR PLOT: CALL PLOT(G(1),G(2))

      DIMENSION DTR(250),DTC(250),TLOG(250),VOF(250)
      DIMENSION F(40),G(10)
      DIMENSION BFY(5),GNU(5),DT1(250),DT2(250),DT3(250),DT4(250),
     1 DT5(250),VOLT(250),QI(250)
      DIMENSION ITITLE(13),NAME(8)
      COMMON/DDC/LU,LUC,IFL
      COMMON/8/ IN,IK, P,T,DEN, E,H,S, CV,CP,CSAT, W,WK
      COMMON/LSS/DTR,DTC,TLOG,Q,PRTT
      COMMON /FITT/ F,Y,NFUN
      COMMON/DATATC/R1,R2,R3Z,R4Z,R3B,R4B,PRESS,TEMP,VOF,TINC
      DATA BFY/0.509927,-0.338935,0.271009,-0.232425,0.206431/
      DATA GNU/2.4048,5.5201,8.6537,11.7315,14.9309/
      DATA NAME/10HHANS RODER,10H X 3528   ,10H          ,
     110H          ,10H          ,10H          ,10H          ,
     210H          /

C     PT, HELIUM, 0.0005 INCH WIRE

C     INITIALIZE

      IFL=156
      CALL GRPH(0,0,8,NAME,0,0)
      R1=100.1299
      R2=100.1428
      RHOPT=21.37
      A=0.000635
      B=0.45
      PI=3.14159
      DENT=20.
      PRINT 1
    1 FORMAT(1H1/* RUNPT    PRT-T   WIRE-T    R3Z       R4Z      TINC
     1VOLTS   PRESS    DEN      T-EXP    TC-EXP    STAT  TC-TN      PCT
     2 POWER*/)

C     READ DATATC

      DO 200 K=1,78
      TTRIAL=1.0
      READ(1,*) IDATE,IRUNPT,PRT,PRT1,COUNTS,BAR
      IF(EOF(1)) 9999,100
  100 CONTINUE
      READ(1,*) R3Z,R3B,R4Z,R4B,TINC,VNOVA
      DO 11 I=1,50
      L=(I-1)*5
      READ(1,*) VOF(L+1),VOF(L+2),VOF(L+3),VOF(L+4),VOF(L+5)
      IF(EOF(1))9999,11
```

```
   11 CONTINUE
C
C     INITIAL CALC. AND CORRECTIONS
C
      DO 12 I=1,250
   12 VOF(I)=VOF(I)-0.000012
   30 R=PRT/2000.
      PRTT=TEMPP(R)
      TEMP=PRTT
      CPPT=0.129+0.004/80.*(TEMP-220.)
      TCPT=0.74-0.03/100.*(TEMP-300.)
      DIFPT=TCPT/RHOPT/CPPT
      PSIA=0.8728+1.0351740*COUNTS-0.183212E-6*COUNTS**2
      R3C=-0.319308E-1+0.637332E-3*TEMP+0.151192E-5*TEMP**2
     1 -0.262966E-8*TEMP**3
      R4C=-0.806515E-1+0.151734E-2*TEMP+0.582652E-5*TEMP**2
     1 -0.899257E-8*TEMP**3
      R3Z=R3Z-R3C
      R3B=R3B+R3C
      R4Z=R4Z-R4C
      R4B=R4B+R4C+0.0024
      PRESS=PSIA/14.696
      VOLT2=2.0*VNOVA
      VEST=0.5
      DO 4 I=1,50
      HPVOLT=VEST+0.1
      VMIN=HPVOLT*0.99
      VMAX=HPVOLT*1.01
      IF(VOLT2.GT.VMIN.AND.VOLT2.LT.VMAX) GO TO 5
    4 VEST=VEST+0.5
    5 CONTINUE
      R3=R3Z+R3B
      R4=R4Z+R4B
      RBRIDGE=1.0/(1.0/(R3+R4)+1.0/(R1+R2))
      RCIR=100.3288+RBRIDGE
      VOLTS=HPVOLT/RCIR*RBRIDGE

C     CALCULATE DELTA-T AND T-CORRECTIONS

      IST=51
      IF(IRUNPT.GE.9070) IST=15
      ISTOP=250
      IF(IRUNPT.EQ.9070) ISTOP=220
      IF(IRUNPT.EQ.9071) ISTOP=180
      IF(IRUNPT.EQ.9072) ISTOP=155
      IF(IRUNPT.EQ.9073) ISTOP=126
      IF(IRUNPT.EQ.9074) ISTOP=110
      IF(IRUNPT.EQ.9075) ISTOP= 82
      IF(IRUNPT.EQ.9076) ISTOP= 25
      IF(IRUNPT.EQ.9077) ISTOP= 25
      V250=VNOVA/1.00319
      V50=V250/1.00033
      CV2=(V250-V50)/(ALOG(TINC*250)-ALOG(TINC*50))
      CV1=V50-CV2*ALOG(TINC*50)
```

```
      DO 8 I=1,250
    8 VOLT(I)=CV1+CV2*ALOG(TINC*I)
      DTW=(FINDDT(VOLT(IST),VOF(IST),TTRIAL)+FINDDT(VOLT(ISTOP),
     1 VOF(ISTOP),TTRIAL))/2.
      TEM=DTW+TEMP
      RESW3=FIND1(TEM)
      RESW4=FIND2(TEM)
      RTOTAL=R3B+R4B+RESW3+RESW4
      IQ=(IST+ISTOP)/2+1
      Q=(VOLT(IQ)/RTOTAL)**2*(RESW3+RESW4)*100./15.596
      DEN=FNDDHE(PRESS,TEMP)
      RHOGAS=DEN*4.0026/1000.
      TC=THERHE(DEN,TEMP)/10.
      CPGAS=CPHE(DEN,TEMP)/4.0026
      CVGAS=CVHE(DEN,TEMP)
      DIFGAS=TC/100./RHOGAS/CPGAS
      QQ=Q/(4.*PI*TC)
      QQQ=Q*8.3143*10./(DEN*CPGAS*39.948*CVGAS*PI*B**2)
      QQQQ=8.*PI*A/100.*5.6697E-8*TEMP**3/Q
      TIME=0.
      DO 3 I=1,250
      TIME=TIME+TINC
      TLOG(I)=ALOG(TIME*1000.)
      DELT=QQ*ALOG(4.0*DIFGAS*TIME/A**2/1.781)
      DTR(I)=FINDDT(VOLT(I),VOF(I),TTRIAL)
      TTRIAL=DTR(I)
      DT1(I)=A**2*(RHOPT*CPPT-RHOGAS*CPGAS)/(2.*TC/100.*TIME)*DELT
     1 -QQ*A**2/(4.*DIFGAS*TIME)*(2.-DIFGAS/DIFPT)
      DT2(I)=0.
      BKT=B**2/(DIFGAS*TIME)
      IF(BKT.GT.5.78) GO TO 10
      BRAK=0.
      DO 9 J=1,5
    9 BRAK=BRAK+EXP(-GNU(J)**2*DIFGAS*TIME/B**2)*(PI*BFY(J))**2
      DT2(I)=QQ*(ALOG(4.0*DIFGAS*TIME/B**2/1.781)+BRAK)
   10 CONTINUE
      DT3(I)=-QQQ*TIME
      DT4(I)=0.
      DT5(I)=QQQQ*DELT**2
      DTC(I)=DTR(I)+DT1(I)+DT2(I)+DT3(I)+DT4(I)+DT5(I)
      TTT=TEMP+DTR(I)
      R3=FIND1(TTT)+R3B
      R4=FIND2(TTT)+R4B
      RBRIDGE=1.0/(1.0/(R3+R4)+1.0/(R1+R2))
      VOLT(I)=HPVOLT*RBRIDGE/(RBRIDGE+100.3288)
      RTOTAL=R3+R4
      RESW3=R3-R3B
      RESW4=R4-R4B
      QI(I)=(VOLT(I)/RTOTAL)**2*(RESW3+RESW4)*100./15.596
    3 CONTINUE
      DO 54 I=1,250
   54 DTC(I)=DTC(I)*QI(IQ)/QI(I)

C     LEAST SQUARE DELTA-T VS. LOG(TIMES)
```

```
C       CALL LS
        DO 7 I=1,2
      7 G(I)=0.0
        NFUN=2
        NF=2
        NO PTS=ISTOP-IST+1
        DO 17 L=IST,ISTOP
        F(1)=1.0
        F(2)=TLOG(L)
     16 Y=DTC(L)
     17 CALL FIT
        CALL COEFF
        DO 20 I=1,NF
     20 G(I)=F(I)
        DO 13 I=1,250
        DTR(I)=(DTC(I)-(G(1)+G(2)*TLOG(I)))/DTC(I)*100.
     13 CONTINUE
        CALL PLOT1(IRUNPT)
        CALL STAT
        TCSTAT=F(2)/G(2)

C       CALCULATE THERMAL CONDUCTIVITY

        DEN=FNDDHE(PRESS,TEM)
        DENT=DEN
        TC=THERHE(DEN,TEM)/10.
        TCEXP=Q/(4.*3.14159*G(2))
        PCT=(TCEXP-TC)/TCEXP*100.
        PRINT 50,IRUNPT,PRTT,TEMP,R3Z,R4Z,TINC,VOLTS,PRESS,DEN,
       1 TEM,TCEXP,TCSTAT,TC,PCT,Q
     50 FORMAT(I6,2F9.3,2F9.4,F9.5,F7.2,F9.3,F8.4,F9.3,F9.5,F8.3,
       1 F9.5,F8.2,F9.5)

C       PLOT RESULTS

        CALL PLOT(G(1),G(2),IRUNPT)
    200 CONTINUE
   9999 CONTINUE
        CALL ENDGRPH(0,0,0,0,0,0)
        CALL DDDF
        END
        FUNCTION OFFSV(EB,RR1,RR2)
C       CALCULATES OFFSET VOLTAGE WHEN RESISTANCES ARE KNOWN
        COMMON/DATATC/R1,R2,R3Z,R4Z,R3B,R4B,PRESS,TEMP,VOF,TINC
        DATA(RG=1.0E+07)
        R3=RR1+R3B
        R4=RR2+R4B
        DIV=R1*R2*R3+R2*R3*R4+R3*R4*R1+R4*R1*R2+RG*(R1+R2)*(R3+R4)
        GALVI=EB*(R2*R3-R1*R4)/DIV
        OFFSV=GALVI*RG
        RETURN
        END
        FUNCTION FIND1(TIN)
C       WIRE RESISTANCE AS A FUNCTION OF TEMPERATURE
```

```
      COMMON/DATATC/R1,R2,R3Z,R4Z,R3B,R4B,PRESS,TEMP,VOF,TINC
      P=PRESS*14.696
      IF(TIN.GT.150.) GO TO 2
      FIND1=-10.231206+0.3670809*TIN-0.9903371E-4*TIN**2-0.5375358E-5*P
      RETURN
    2 FIND1=-9.0654718+0.35344447*TIN-0.59234427E-4*TIN**2-0.966271E-5*P
      RETURN
      END
      FUNCTION FIND2(TIN)
C     WIRE RESISTANCE AS A FUNCTION OF TEMPERATURE
      COMMON/DATATC/R1,R2,R3Z,R4Z,R3B,R4B,PRESS,TEMP,VOF,TINC
      P=PRESS*14.696
      IF(TIN.GT.150.) GO TO 2
      FIND2=-5.057558+0.1823527*TIN-0.525728E-4*TIN**2-0.285743E-5*P
      RETURN
    2  FIND2=-4.346459+0.17402506*TIN-0.2831553E-4*TIN**2-0.452695E-5*P
      RETURN
      END
      FUNCTION FINDDT(V1,V2,T1)
C     AN APPROXIMATION, TO REPLACE WIRE-R
      COMMON/DATATC/R1,R2,R3Z,R4Z,R3B,R4B,PRESS,TEMP,VOF,TINC
      V=V2
      TT=T1+TEMP
      DO 10 I=1,10
      RE1=FIND1(TT)
      RE2=FIND2(TT)
      VOFF1 =OFFSV(V1,RE1,RE2)
      IF(ABS(V-VOFF1)-1.0E-6  ) 20,20,1
    1 T=TT+0.01
      RE1=FIND1(T )
      RE2=FIND2(T )
      VOFF2 =OFFSV(V1,RE1,RE2)
      DVDT=(VOFF2-VOFF1)/0.01
      CORR=(V-VOFF1)/DVDT
   10 TT=TT+CORR
   20 FINDDT=TT-TEMP
      RETURN
      END
      FUNCTION TEMPP(R)
C     ABBR. FOR 1776265 FROM 70 TO 310 K, CORR.12/19/80
      DIMENSION RR(241)
      DATA(RR(I),I=1,131)/3.99645, 4.10575, 4.21531, 4.32508, 4.43505,
     1  4.54520, 4.65550, 4.76594, 4.87649, 4.98714, 5.09788, 5.20868,
     2  5.31954, 5.43045, 5.54139, 5.65235, 5.76332, 5.87430, 5.98527,
     3  6.09622,          6.20716, 6.31807, 6.42895, 6.53979, 6.65058,
     4  6.76134, 6.87204, 6.98268, 7.09327, 7.20379,
     5                    7.31426, 7.42465, 7.53498, 7.64523, 7.75541,
     A  7.86552, 7.97555, 8.08550, 8.19538, 8.30517, 8.41489, 8.52453,
     B  8.63408, 8.74356, 8.85295, 8.96226, 9.07149, 9.18065, 9.28971,
     C  9.39870, 9.50761, 9.61644, 9.72519, 9.83386, 9.94245,10.05096,
     D 10.15939,10.26775,10.37603,10.48424,10.59237,10.70043,10.80841,
     E 10.91632,11.02416,11.13192,11.23962,11.34725,11.45480,11.56229,
     F 11.66971,11.77707,11.88435,11.99158,12.09873,12.20583,12.31286,
     G 12.41982,12.52673,12.63357,12.74036,12.84708,12.95375,13.06036,
```

```
     H 13.16690,13.27340,13.37983,13.48621,13.59254,13.69881,13.80502,
     I 13.91118,14.01729,14.12335,14.22935,14.33530,14.44121,14.54706,
     J 14.65286,14.75861,14.86431,14.96997,15.07557,15.18113,15.28664,
     K 15.39210,15.49752,15.60289,15.70822,15.81350,15.91873,16.02392,
     L 16.12907,16.23417,16.33923,16.44424,16.54922,16.65414,16.75903,
     M 16.86387,16.96868,17.07344,17.17816,17.28284,17.38747,17.49207,
     N 17.59663,17.70114,17.80562,17.91006,18.01445/
      DATA(RR(I),I=132,241)/      18.11881,18.22313,18.32741,18.43165,
     A 18.53586,18.64002,18.74415,18.84824,18.95229,19.05630,19.16028,
     B 19.26422,19.36812,19.47199,19.57582,19.67961,19.78337,19.88709,
     C 19.99078,20.09442,20.19804,20.30162,20.40516,20.50867,20.61214,
     D 20.71558,20.81898,20.92235,21.02568,21.12898,21.23225,21.33548,
     E 21.43867,21.54184,21.64497,21.74806,21.85112,21.95415,22.05715,
     F 22.16011,22.26304,22.36594,22.46880,22.57163,22.67443,22.77720,
     G 22.87993,22.98263,23.08530,23.18793,23.29054,23.39311,23.49565,
     H 23.59816,23.70063,23.80308,23.90549,24.00787,24.11022,24.21254,
     I 24.31483,24.41708,24.51931,24.62150,24.72366,24.82579,24.92789,
     J 25.02996,25.13199,25.23400,25.33597,25.43791,25.53982,25.64170,
     K 25.74355,25.84537,25.94715,26.04891,26.15063,26.25232,26.35398,
     L 26.45561,26.55721,26.65877,26.76031,26.86181,26.96329,27.06473,
     M 27.16614          ,27.26752,27.36887,27.47019,27.57147,27.67273,
     1 27.77395,27.87514,27.97631,28.07744,28.17854,28.27961,28.38065,
     2 28.48165,28.58263,28.68357,28.78449,28.88537,28.98622,29.08704,
     3 29.18783,29.28859/
      DO 3 I=1,241
      IF(R.LT.RR(I)) GO TO 4
   3  CONTINUE
   4  TEMPP=I
      TEMPP=TEMPP+68.+(R-RR(I-1))/(RR(I)-RR(I-1))
      RETURN
      END
      SUBROUTINE LS

C     LEAST SQUARE ALONG THE DATA

      DIMENSION DTR(250),DTC(250),TLOG(250),VOF(250)
      DIMENSION F(40),G(10)
      DIMENSION RES(20),ERR(20),IM(20),TM(20)
      COMMON/LSS/DTR,DTC,TLOG,Q,PRTT
      COMMON /FITT/ F,Y,NFUN

      IST=11
      DO 13 J=1,16
      ISTOP=IST+89
      IM(J)=(IST+ISTOP)/2
      TM(J)=PRTT+DTC(IM(J))
      NFUN=2
      NF=2
      NO PTS=ISTOP-IST+1
      DO 17 L=IST,ISTOP
      F(1)=1.0
      F(2)=TLOG(L)
  16  Y=DTC(L)
  17  CALL FIT
```

```
      CALL COEFF
      RES(J)=Q/(4.*3.14159*F(2))
      CALL STAT
      ERR(J)=RES(J)/(Q/(4.*3.14159*F(2)))
   13 IST=IST+10
      PRINT 15,((IM(J),TM(J)),J=1,10)
      PRINT 14,((RES(J),ERR(J)),J=1,10)
      PRINT 15,((IM(J),TM(J)),J=11,16)
      PRINT 14,((RES(J),ERR(J)),J=11,16)
   14 FORMAT(5X,20F6.4)
   15 FORMAT(5X,10(I4,F8.3))
      RETURN
      END
      SUBROUTINE PLOT(G1,G2,IDNO)
C     PLOTS RESULTS
      DIMENSION ITITLE(13),NAME(8),ICOMM(2)
      DIMENSION DTR(250),DTC(250),TLOG(250),VOF(250)
      COMMON/LSS/DTR,DTC,TLOG,Q,PRTT
      DATA ITITLE/10H          ,10H HELIUM  T,10HHERMAL CON,
     110HDUCTIVITY ,10H          ,10H          ,10HLN(T) T IN,
     210H MILLISEC ,10H          ,10H          ,10HDELTA T,  ,
     310HT IN K    ,10H          /
      DATA ICOMM(1)/10H    RUNPT /
      ENCODE(10,1,ICOMM(2))IDNO
    1 FORMAT(I10)
      NO PTS=240
      DO 51 I=11,250
      L=I-10
      TLOG(L)=TLOG(I)
   51 DTC(L)=DTC(I)
      CALL PGRPH(TLOG,DTC,NO PTS,ITITLE,0,6)
      DTC(1)=G1+G2*TLOG(1)
      DTC(2)=G1+G2*TLOG(NO PTS)
      TLOG(2)=TLOG(NO PTS)
      CALL CLGRPH(TLOG,DTC,2,0,0,0)
      ABFRACT=0.05
      ORDFR=0.9
      CALL COMGRPH(ABFRACT,ORDFR,2,ICOMM)
      RETURN
      END
      SUBROUTINE PLOT1(IDNO)
C     PLOTS DEV. FROM LS LINES
      DIMENSION ITITLE(13),NAME(8),TT(250),ICOMM(2)
      DIMENSION DTR(250),DTC(250),TLOG(250),VOF(250)
      COMMON/LSS/DTR,DTC,TLOG,Q,PRTT
      DATA ITITLE/10H          ,10H HELIUM  T,10HHERMAL CON,
     110HDUCTIVITY ,10H          ,10H          ,10HLN(T), T I,
     210HN MILLISEC,10H          ,10H          ,10HDEV. FROM ,
     310HLS FIT    ,10H          /
      DATA ICOMM(1)/10H    RUNPT /
      ENCODE(10,1,ICOMM(2))IDNO
    1 FORMAT(I10)
      NO PTS=240
      DO 51 I=11,250
```

```
      L=I-10
      TT(L)=TLOG(I)
   51 DTR(L)=DTR(I)
      CALL PGRPH(TT,DTR,NO PTS,ITITLE,0,6)
      ABFRACT=0.05
      ORDFR=0.9
      CALL COMGRPH(ABFRACT,ORDFR,2,ICOMM)
      RETURN
      END
      SUBROUTINE FITTER
C     CHANGED 13 SEPT., 1973   OLDER VERSION OF FITTER
C     COMMON STATEMENT ADDED TO MATCH CALLING SEQUENCE OF NEWER VERSION
C     SPECIAL, TO GET RESS IN F(10)
      DIMENSION F(40),A(40,41)
      COMMON /FITT/ F,Y,NFUN
      DOUBLE PRECISION A,SY,SYY,RES,DET
      EQUIVALENCE(NC,FNC)
      DATA (NTR=-1)            $ DATA(NDIM=40)
      ENTRY FIT
      IF(NTR) 1,3,3
    1 NP=0
      NF=NFUN
      IF(NF.GT.NDIM) GO TO 44
      NC=0
      SY=0.
      SYY=0.
      NY=NF+1
      DO 2 I=1,NY
      DO 2 J=1,NF
    2 A(J,I)=0.
      IF(NTR.EQ.0) GO TO 11
      NTR=0
    3 SY=SY+Y
      SYY=SYY+Y*Y
      DO 4 J=1,NF
      A(J,NY)=A(J,NY)+Y*F(J)
      DO 4 I=1,NF
    4 A(I,J)=A(I,J)+F(I)*F(J)
      NP=NP+1
      RETURN
      ENTRY CONSTR
      IF(NTR) 10,11,11
   10 NTR=0
      GO TO 1
   11 N=NY-1
      IF(NY+NC+2.GT.NDIM) GO TO 44
      DO 12 I=1,N
      A(I,NY+1)=A(I,NY)
   12 A(I,NY)=A(NY,I)=A(NDIM-NC,I)=F(I)
      NC=NC+1
      DO 13 I=NF,N
   13 A(I+1,NY)=A(NY,I+1)=0.
      NY=NY+1
      A(NY-1,NY)=Y
```

```
      RETURN
      ENTRY COEFF
      N=NY-1
      DO 20 I=1,NF
   20 F(I)=A(I,NY)
      IF(N.EQ.1)GO TO 23
      DO 22 I=2,N
      DO 21 J=I,NY
   21 A(I-1,J)=A(I-1,J)/A(I-1,I-1)
      DO 22 J=I,N
      DO 22 K=I,NY
   22 A(J,K)=A(J,K)-A(J,I-1)*A(I-1,K)
   23 A(N,NY)=A(N,NY)/A(N,N)
      IF(N.EQ.1)GO TO 26
      DO 24 I=2,N
      L=N-I+2
      DO 24 J=L,N
   24 A(L-1,NY)=A(L-1,NY)-A(L-1,J)*A(J,NY)
   26 NTR=-1
      RES=SYY
      DO 25 I=1,NF
      RES=RES-F(I)*A(I,NY)
   25 F(I)=A(I,NY)
      NFUN=NP
      DF=NP-NF+NC
      Y=FNC
      FNP=NP
      RETURN
      ENTRY STAT
      IF(NC.LE.0)GO TO 28
      DO 27 I=1,NC
      DO 27 J=1,NF
   27 RES=RES-A(NDIM-I+1,J)*A(J,NY)*A(NF+I,NY)
   28 TOT=SYY-SY*SY/FNP
      REG=TOT-RES
      SYY=RES/DF
      ST=1.96+2.72/DF+8.04/DF**3
      DET=1.0D+0
      DO 30 I=1,NF
      DET=DET*A(I,I)
   30 A(I,I)=1.0D+0/A(I,I)
      IF(NF.EQ.1)GO TO 322
      DO 32 I=2,NF
      DO 32 J=2,I
      SY=0.
      DO 31 K=J,I
   31 SY=SY-A(I,K-1)*A(K-1,J-1)
   32 A(I,J-1)=SY*A(I,I)
  322 CONTINUE
      DO 36 I=1,NF
      L=NF-I
      DO 33 J=1,L
      K=NF-J
      DO 33 M=1,J
```

```
      N=NF-M+1
   33 A(K,I)=A(K,I)-A(K,N)*A(N,I)
      IF(I.EQ.1)GO TO 344
      DO 34 J=2,I
   34 A(J-1,I)=A(I,J-1)*SYY
  344 CONTINUE
      DO 35 J=1,I
   35 A(I,J)=A(I,J)*SYY
      IF(A(I,I).LE.0.0)A(I,I)=-A(I,I)
   36 F(I)=ST*DSQRT(A(I,I))
C     PRINT 37,(A(I,NY),F(I),I=1,NF)
   37 FORMAT(*1THE COEFFICIENTS AND THEIR ESTIMATED ERRORS ARE:*/
     1(* *E18.10,* +OR-*E9.2))
      SYY=DSQRT(SYY)
C     PRINT 38,RES,REG,TOT,SYY,DET
      F(10)=RES
   38 FORMAT(         * ESTIMATED RESIDUAL SUM OF SQUARES =*E17.9/
     1               * ESTIMATED REGRESSION SUM OF SQUARES =*E17.9/
     2                    * ESTIMATED TOTAL SUM OF SQUARES =*E17.9/
     3* STANDARD DEVIATION =*E17.9/* DETERMINANT OF THE MATRIX =*E17.9/
     4        * DISPERSION MATRIX*     )
      DO 39 J=1,NF
C  39 PRINT 40,(A(I,J),I=1,NF)
   39 CONTINUE
   40 FORMAT(7E19.9)
C     PRINT 46
   46 FORMAT(1H )
      RESSS=RES
      Y=SQRT(RESSS/DF)
      NFUN=DF
   43 RETURN
   44 PRINT 45
   45 FORMAT(*1THE ARRAYS IN THE FITTING PROGRAM ARE TOO SMALL TO HOLD T
     1HE NUMBER OF CONSTRAINTS AND FUNCTIONS ASKED FOR IN THE CALLING PR
     2OGRAM*)
      STOP
      END
```

JOURNAL OF RESEARCH of the National Bureau of Standards
Vol. 86, No. 5, September–October 1981

The Graphite Calorimeter as a Standard of Absorbed Dose for Cobalt-60 Gamma Radiation

John S. Pruitt,* Steve R. Domen,* and Robert Loevinger*

National Bureau of Standards, Washington, DC 20234

May 6, 1981

Absorbed dose to water in a cobalt-60 gamma-ray beam has been determined using a thick-walled graphite ionization chamber. The chamber was calibrated in a graphite phantom against a graphite calorimeter, and the graphite calibration factor was converted to a water calibration factor using published energy absorption coefficient ratios and a measured replacement factor. Comparisons between the graphite and water measurements were made at pairs of points that were scaled in position according to the ratio of electron densities, so that the photon spectra were the same for the two points in a given pair. Measurements performed in graphite over a wide range of phantom depths, field sizes, and source distances, showed that the calibration factor varies slowly with the phantom depth and field size, and probably has a negligible dependence on source distance. By comparison with the thick-walled chamber in a cobalt-60 gamma-ray beam, a secondary ionization chamber can be calibrated in terms of absorbed dose to water with an estimated uncertainty of about ±1 percent.

Key words: absorbed dose standard; cobalt-60 gamma rays; electron density; ionization chamber; graphite calorimeter; *scaling theorem*; *water phantom*.

1. Introduction

It has long been recognized that calorimetry offers, in principle, the most direct method of determining absorbed dose. Practical calorimeter materials (e.g., graphite) were not, however, the media of interest (e.g., water). In 1969, it was proposed [1][1] that a thin-walled ionization chamber be calibrated in the calorimeter medium and this calibration be transferred to a water phantom with ionization-chamber measurements in water, using stopping-power ratios and perturbation factors. The basic limitations of this method are (1) the need for a chamber wall strong enough for practical use and thin enough to have a negligible influence on the chamber current, (2) the relatively large uncertainties in the stopping-power ratios (±2 percent), and (3) the difficulty in evaluating the perturbation factors.

Recent work has proceeded along three lines. One approach uses a small thimble-shaped graphite calorimeter for direct measurements of absorbed dose in a water phantom [2]. This technique avoids the need for a transfer ionization chamber between two different media, and consequently avoids the use of stopping-power ratios, but the perturbation factors remain.

Another approach is exemplified by a proposal from the National Physical Laboratory [3] that the transfer instrument used between the calorimeter medium and water be a thick-walled ionization chamber. This technique avoids the need to know stopping-power ratios if it is known that photon fluence spectral distributions are similar in the two media. This proposal suggests the use of a tungsten ion chamber that would be thick-walled for photon energies up to about 10 MeV.

The third approach uses a calorimeter of water, which avoids all three of the limitations mentioned above. A water calorimeter for determination of absorbed dose has been constructed and tested at the National Bureau of Standards [4], but, at the time of this writing, results are still preliminary.

The present work was performed to establish an NBS standard for absorbed dose to water in a cobalt-60 gamma-ray beam, traceable to a graphite calorimeter. The work was done with a graphite ion chamber [5], shown in cross section in figure 1, which is thick-walled for photons with energies up to about 1 MeV. Since the work was performed with colbalt-60 radiation, the transfer technique used is similar to that proposed by NPL, with no need for stopping-power ratios and only a small error (less than 0.15 percent) for contributions to the chamber current from electrons originating outside the chamber.

*Center for Radiation Research, National Measurement Laboratory.

[1] Figures in brackets indicate literature references at the end of this paper.

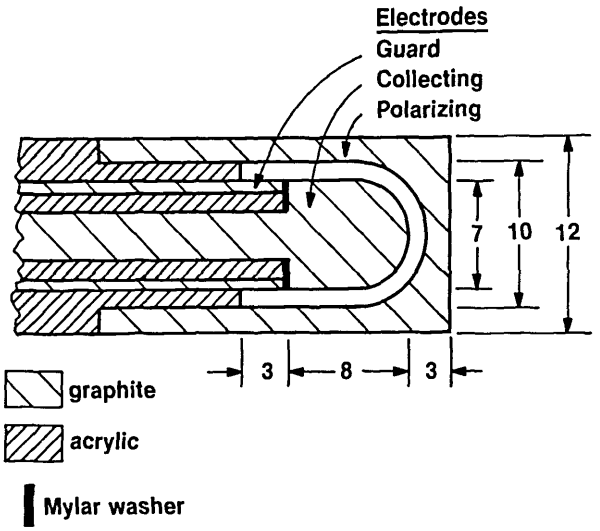

FIGURE 1. Schematic cross section of type PL1 graphite ionization chamber. Dimensions are in millimeters. From [5].

The absorbed-dose calibration factor for an ionization chamber in an absorbing medium is the quotient of the absorbed-dose rate at the position of the reference point of the chamber in the undisturbed medium (i.e., with the chamber replaced by the medium), and the current from the chamber when it is irradiated in the medium. In the work reported here, an absorbed-dose calibration factor in graphite was obtained using a graphite calorimeter; from the graphite factor, an absorbed-dose calibration factor in water was calculated; and from that calibration factor, absorbed-dose rate to water was obtained by multiplication by the chamber current. Use was made of a photon-fluence scaling theorem [6] which assures that the spectra of primary and scattered photons have the same energy and angle distributions in the graphite and the water phantoms. The perturbation factor is evaluated by an extrapolated replacement technique in which the effect of replacing graphite by water is measured experimentally.

2. The Calibrations in Graphite

Calibration measurements were made in two graphite phantoms, one containing a graphite calorimeter and the other the graphite ionization chamber. These phantoms were irradiated separately by a beam of cobalt-60 gamma rays in the geometry shown schematically in figure 2. For a given set of calibrations, the source-detector distance z was held constant while the field size f (the field was square) and the phantom depth x were varied. Both phantoms consisted of cylindrical blocks, 30 cm in diameter and about 17 cm thick. In each case the center of the detector was about 1 cm below the front surface of the block and the phantom depth

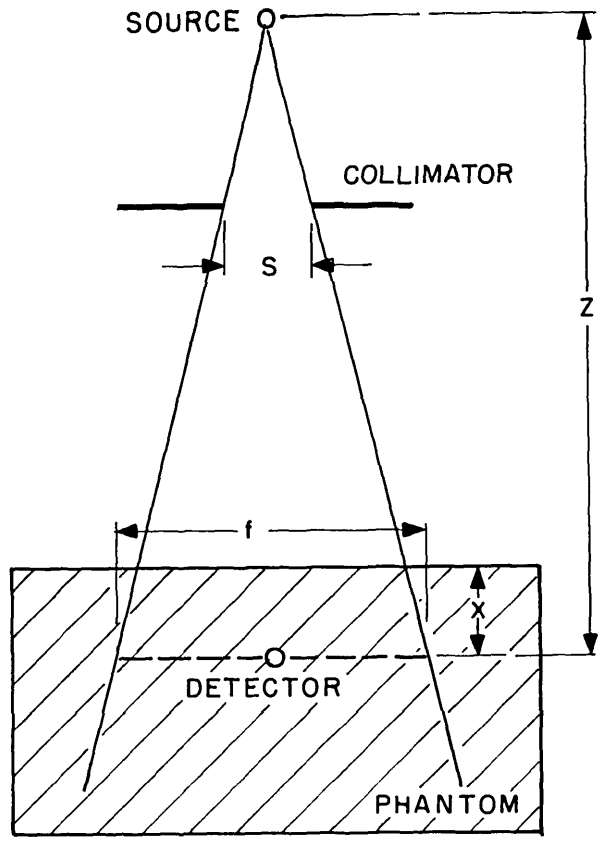

FIGURE 2. Schematic diagram showing experimental parameters used in the text.

was varied by the addition of extra graphite plates, with densities between 1.65 and 1.72 g/cm^3.

Most of the calibration measurements were made with a 10-kCi cobalt-60 source in our laboratory. In this case, the two phantoms were moved alternately into the beam and the same extra plates added in the same order to each in turn. The earliest calibrations were made with a 0.5-kCi source in our laboratory, and an intermediate set of calibrations was made with a 5-kCi source at the National Institutes of Health. All these earlier calorimeter measurements preceded the ion-chamber measurements by weeks or months, and were corrected for decay using a half-life of 5.271 years [7].

Field sizes and source-detector distances were varied only with the 10-kCi source, where field sizes were reproduced accurately by setting the collimator jaws with metal jigs. The relation between collimator size and field size for the 10-kCi source was determined from ionization-chamber profile measurements in air, using only one collimator size and one source distance, and assuming direct proportionality between field size f and the product of collimator size s and source distance z.

Dose rates were measured with the NBS portable graphite calorimeter [8], and ion-chamber currents were measured with a commercial high-gain electrometer and a digital voltmeter. The mode of calorimeter operation differed slightly from that of the ionization chamber because of the need to determine beam-off drift rates before and after each calorimeter run. Calorimeter irradiation times were determined by the beam shutter system. These times required a small correction to agree with ionization-chamber integration times, which were determined electronically without turning off the beam. The correction was never larger than 0.1 percent for the NBS sources and 0.5 percent for the NIH source.

Table 1 is a list of field sizes for all the combinations of source distance and collimator size for which calibrations were made. The chamber calibration factors are listed in table 2. In both tables, the collimator sizes listed for the 0.5-kCi source and for the 5-kCi source are synthetic numbers. They represent what the collimator size would have been for the 10-kCi source to produce the field sizes measured for these two sources.

TABLE 1. *Field sizes in graphite f* (mm).

Source Distance	Nominal source activity (kCi)						
	10	10	10	5	10	0.5	10
z	Collimator size *s* (mm)						
(m)	24.0	28.0	33.4	34.1	40.5	43.0	50.8
0.654		52	62		75		95
0.800			76				
0.900			86				
1.000		80	95	97	115	123	145
1.100			105				
1.200			114				
1.250	86	100	119		144		181

For the 10-kCi source, field sizes were calculated from $f = 2.85\ s\ z$. For the other sources, field sizes were measured.

TABLE 2. *Calibration factor of chamber PL1-11* (mGy/nC at 22 °C and 1 standard atmosphere).

Source Distance	*Graphite Depth*	Nominal source activity (kCi)						
		10	10	10	5	10	0.5	10
z	*ρx*	Collimator size *s* (mm)						
(m)	(g/cm²)	24.0	28.0	33.4	34.1	40.5	43.0	50.8
0.654	1.65		101.4	101.5		101.6		101.7
	3.18		101.0	101.2		101.3		101.5
	5.84		100.4	100.7				
	5.87					101.0		101.2
	8.37		100.4	100.6		100.7		100.9
	11.42		100.1					
	11.59			100.5		100.5		100.7
0.800	5.08			101.1				
0.900	"			101.2				
1.000	0.86						101.7	
	1.65		101.6	101.8	101.7	101.8		102.0
	3.18		101.3	101.4	101.4	101.8		101.6
	4.06					101.7	102.4	
	5.08			101.2		101.4	101.7	
	5.84			101.1				
	5.87		101.0	101.2	101.1	101.4		101.4
	6.08						101.9	
	8.16				101.0			
	8.37		100.7	101.0		101.4		101.4
	9.05						101.5	
	11.59		100.6	101.1	100.7	101.2		101.3
1.100	5.08			101.3				
1.200	"			101.4				
1.250	1.65	101.6	102.1	101.8		101.8		101.8
	3.18	101.5	101.5	101.4		101.7		101.6
	5.84	101.0	101.0	101.1		101.2		101.4
	6.38		101.3					
	8.37	101.0	100.9	101.0		101.4		101.5
	11.42	100.7	100.8	101.0		101.1		101.4

The calibration factors of table 2 at each source distance z have been fitted to an equation of the type:

$$N_{graph} = N^{ref}_{graph}\,[1 + k_x\,(1 - e^{-\gamma_x(\rho x - \rho x_r)}) + k_f\,(1 - e^{-\gamma_f(f - f_r)})] \quad (1)$$

where ϱ is the mass density of the phantom, N_{graph} is the calibration factor in absorbed dose per unit charge at depth x and field size f, and N^{ref}_{graph} is the calibration factor at reference depth x_r and reference field size f_r. Exponential representation was chosen arbitrarily on the assumption that the calibration factor approaches a limiting value for either large fields or large depths.

The values of the parameters and the coefficients obtained from the curve-fitting procedure are listed in table 3, along with the coefficient of variation V of each fit. As can be seen from the latter, eq (1) is a satisfactory description of the dependence of N_{graph} on phantom depth and field size for the NBS 10-kCi and the NIH sources. The larger coefficient of variation for the 0.5-kCi NBS source is caused by larger scatter in the relatively small calorimeter signals, rather than failure of eq (1). The three values at $z = 1$ m have been combined to form a weighted mean of N^{ref}_{graph} (1 m) = 101.27 mGy/nC at 22 °C and one standard atmosphere, with a coefficient of variation of 0.08 percent.

Figure 3 shows the dependence of the calibration factor on distance, depth, and field size, as predicted by eq (1), varying one parameter while holding the others at their reference values ($z_r = 1$ m, $x_r = 5$ g/cm², $f_r = 100$ mm). The ordinate is the change from the reference calibration factor N^{ref}_{graph}. The three points in figure 3 are the predictions of eq (1) at 0.654, 1.000, and 1.250 m, showing that variation with

TABLE 3. *Curve-fitting parameters and coefficients, and coefficients of variation for eq (1), at* 22° C and one standard atmosphere. $\gamma_x = 0.25$ cm²/g and $\gamma_f = 0.025$ mm⁻¹.

Source location and nominal activity	Distance z (m)	N^{ref}_{graph} (mGy/nC)	ϱx_r (g/cm²)	f_r (mm)	k_x	k_f	V (%)
NBS, 10 kCi	0.654	100.8	5.56	65.4	−0.00443	0.00569	0.1
"	1.000	101.3	5.00	100.0	−0.00363	0.00384	0.1
NBS, 0.5 kCi	"	101.6	5.00	100.0	−0.00363	0.00384	0.5
NIH, 5 kCi	"	101.2	5.00	100.0	−0.00363	0.00384	0.1
NBS, 10 kCi	1.250	101.2	5.00	100.0	−0.00356	0.00269	0.2

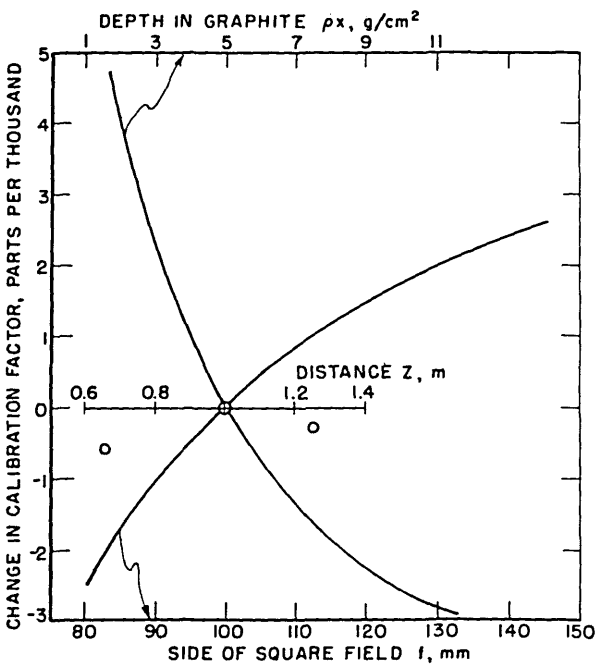

FIGURE 3. Variation of PL1-11 graphite calibration factor with phantom depth, field size, and source distance, as predicted by eq (1).

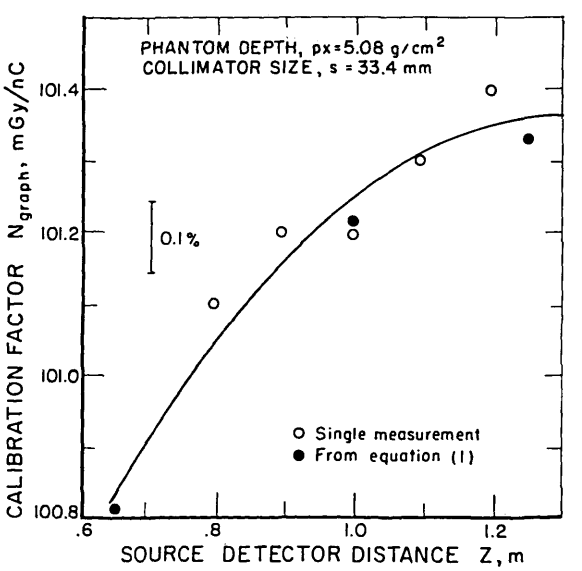

FIGURE 4. Comparison of the graphite calibration factor as predicted by eq (1) with measured calibration factors at phantom depth 5.08 g/cm² and collimator size 33.4 mm x 33.4 mm. The line is a parabolic least squares fit to all eight points.

distance alone is small, and is within the uncertainty of measurement. Plots similar to figure 3 at 0.654 and 1.250 m look quite similar.

Finally, the calibration factors at $\varrho x = 5.08$ g/cm² and $s = 33.4$ mm are compared with the prediction of eq (1) at 0.654, 1.000, and 1.250 m in figure 4. The agreement is within 0.1 percent.

3. Calibration Transfer Theory

Consider an ionization chamber in a absorbing and scattering medium irradiated by a cobalt-60 gamma-ray beam. The chamber is assumed to be thick-walled, i.e., all electrons reaching the cavity arise in the chamber walls, and is further assumed to be made of a single, but unspecified, wall material. An expression for the absorbed dose to the undisturbed medium at the position of the reference point of the chamber, i.e., in the absence of the chamber, can be obtained from eqs (23) and (24) of reference [9]. Omitting terms that relate only to the properties of the wall and the cavity gas, we obtain

$$D_{med} \propto J_{gas}\,(\beta)^{med}_{wall}\,(\bar{\mu}_{en}/\varrho)^{med}_{wall}\;{}_{chamb}\,(\Psi)^{med}_{wall} \qquad (2)$$

In eq (2) J_{gas} is the charge per unit mass of cavity gas corresponding to D_{med}. β is the quotient of absorbed dose and the collision part of kerma, and $(\beta)^{med}_{wall}$ is the ratio β_{med}/β_{wall}. $(\bar{\mu}_{en}/\varrho)^{med}_{wall}$ is the ratio of the mean mass energy-absorption coefficient of the medium to that of the wall material. Ψ is the photon energy fluence at the chamber center, and ${}_{chamb}(\Psi)^{med}_{wall}$ is a factor that corrects for the replacement of the medium by wall material in the volume of the entire chamber, wall plus cavity.

The calibration factor for the chamber in the medium is proportional to D_{med}/J_{gas}. Assume that the chamber has been calibrated in a cobalt-60 gamma-ray beam in graphite, and is user in water at a point where the photon spectral energy fluence is the same as in the graphite. Then expressions for N_{graph} and N_{water} can be obtained from eq (2), and the ratio of these expressions gives

$$N_{water} = N_{graph}\,(\beta)^{water}_{graph}\,(\bar{\mu}_{en}/\varrho)^{water}_{graph}\;{}_{chamb}(\Psi)^{water}_{graph} \qquad (3)$$

Equation (3) provides the required relationship between the calibration factor N_{graph} determined in graphite using the graphite calorimeter, and the desired calibration factor N_{water} that applies in undisturbed water. The energy-absorbtion coefficients are averaged over the spectral energy fluence in the undisturbed medium, at the point of measurement. The replacement factor corrects for the replacement of water by graphite in the volume of the entire chamber. More explicitly, the replacement factor is

$${}_{chamb}(\Psi)^{water}_{graph} = \Psi_{water}/\Psi_{graph} \qquad (4)$$

where Ψ_{water} is the photon energy fluence at the position of the chamber center in undisturbed water, i.e., in water in the absence of the chamber; and Ψ_{graph} is the photon energy fluence in water at the same position inside a piece of graphite that has the same outer dimensions as the ionization chamber.

The derivation of eq (3) required that the spectral energy fluence be the same in water and in graphite, at the measurement points. It has been shown [6] that this can be achieved by scaling all dimensions in the inverse ratio of the electron densities in order to define corresponding points in the two media, and then comparing measurements only at pairs of corresponding points.

Equation (3) is independent of the wall material of the ionization chamber. This is the basis of the proposal [3] to use a high-density material for the ionization chamber, so as either to reduce the size of the chamber (which in turn causes the replacement factor to be closer to unity), or to increase the energy range within which the chamber can be considered thick-walled, or both. The designation "graph" in eqs (3) and (4) refers to the graphite of the phantom, not to the graphite of which the chamber was constructed.

4. Experimental Realization of Calibration Transfer

Values of β for cobalt-60 gamma radiation calculated for polystyrene, carbon, and air, assuming secondary electron equilibrium, do not differ by more than 0.1 percent [9, app. B]. Therefore it is assumed that the ratio $(\beta)^{water}_{graph}$ in eq (3) can be taken as unity, with an uncertainty of about 0.1 percent.

The mean mass energy-absorption coefficient at a point in a scattering medium is a function of the photon spectral energy fluence at that point. The spectral energy distribution varies with both field size and depth in the medium, as then does the mean mass energy-absorption coefficient. The ratio of coefficients at corresponding scaled points in two media varies with field size and depth much more slowly than do the coefficients themselves. This ratio was evaluated as a function of depth using the cobalt-60 spectra in graphite of Seltzer, Hubbell, and Berger (an example of which is shown in figure 26 of reference [10]), and the graphite and the water mass energy-absorption coefficients of Hubbell [11]. The variation with field size was deduced using the cobalt-60 spectra in water of Bruce and Johns [12], normalized to graphite for one field size. Figure 5 shows the result: variation of the ratio is almost negligible over the range of depths and field sizes of interest here.

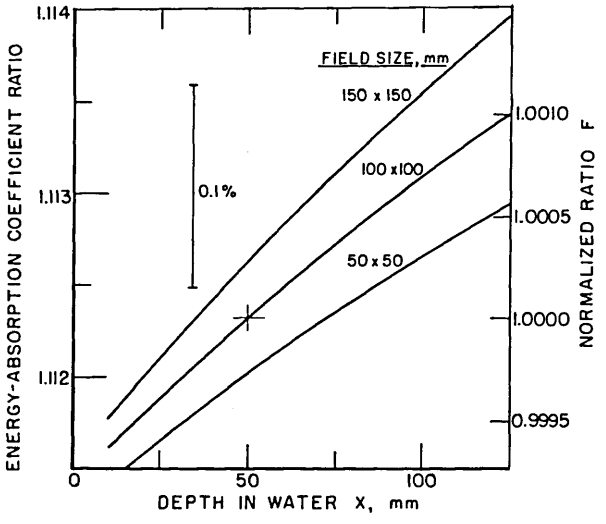

FIGURE 5. Ratio of the mean mass energy-absorption coefficients of water and of graphite, as a function of field size and depth in a water phantom.

The replacement factor in eq (3) was evaluated experimentally, using the graphite ionization chamber in a water phantom. The outer diameter of the chamber was increased by addition of cylindrical graphite sleeves, replacing water by graphite outside the chamber. It was found that the chamber current decreased at the rate of 0.068 percent per millimeter increase in diameter.[2] Assuming that the same rate of change of current can be extrapolated to the chamber center, the replacement factor is then calculated from the 12.5-mm chamber diameter as 1.0085. From figure 5, the energy-absorption coefficient ratio for a square field 100 mm on a side, at a depth of 50 mm in water, is 1.1123. Then eq (3) can be written in the form

$$N_{water}(z,x,f) = 1.122\ F(x,f)\ N_{graph}(z',x',f') \qquad (5)$$

for the NBS graphite chamber designated PL1. In eq (5), $F(x,f)$ is the energy-absorption coefficient ratio at a depth x and a field size f in water, divided by the ratio at a depth of 50 mm and a field size of 100 mm. $F(x,f)$ is shown on the right-hand scale of ordinates in figure 5, and is assumed to be independent of source distance z. $N_{graph}(z',x',f')$ is to be evaluated from eq (1) for the values z',x',f' that correspond to z,x,f, according to the scaling rule used here.

The scaling rule [6] requires that all distances be scaled inversely as the number of electrons per unit volume. The mass densities of water and the graphite used in the phantom were taken to be 1.00 g/cm³ and 1.70 g/cm³, respectively. The number of electrons per unit volume are then 0.555 N_A and 0.849 N_A, where N_A is Avogadro's number, and the scaling factor is 1.530. Then $z' = z/1.530$, and similarly for x' and f'.

[2] This number contains corrections for the difference between the average graphite phantom density, 1.70 g/cm³, and the graphite sleeve density 1.77 g/cm³.

The reference conditions at NBS for an absorbed-dose calibration in water are source distance $z = 1$ m, depth in water $x = 50$ mm, and field size $f = 100$ mm. The corresponding scaled distances in graphite are in the first line of table 3. An expression for the calibration factor as a function of depth in water and field size is then obtained from eqs (1) and (5) in the form

$$N_{water}(1,x,f) = N^{ref}_{water}\ F(x,f)\,[1 + k_x(1 - e^{-\xi_x(x\,-\,50)}) + k_f(1 - e^{-\xi_f(f\,-\,100)})] \qquad (6)$$

where $N^{ref}_{water} = N_{water}(1,50,100) = 113.1$ mGy/nC at 22 °C and 1 standard atmosphere. The coefficients in eq (6) are $k_x = -0.00443$, $k_f = 0.00569$, $\xi_x = 0.028$ mm^{-1}, and $\xi_f = 0.016$ mm^{-1}.

5. Calibration Accuracy

The absorbed-dose calibration of chamber PL1-11 can be transferred to another (secondary) ionization chamber by substitution in a water phantom in the cobalt-60 gamma-ray beam. The component uncertainties that enter into the absorbed-dose rate to water and into the calibration of the secondary chamber are given in table 4. The "statistical" uncertainties s_i are values of the coefficient of variation (the standard deviation in percent), estimated from repeated measurements. These include the uncertainties that are conventionally identified as random. The "other" uncertainties w_i are estimated values of the upper bound (expressed in percent) of all possible errors that have been identified but cannot be assigned a coefficient of variation. These include the uncertainties that are conventionally identified as systematic, but may include some that are conventionally identified as random.

The dominant systematic uncertainty in table 4 is that for the energy-absorption coefficient ratios. The uncertainty quoted is based on Hubbell's estimate [11] of an uncertainty of ±0.3 percent for monoenergetic photons in the cobalt-60 energy range, increased to ±0.5 percent because of the presence of low-energy photons, for which the ratio of the coefficients is much less accurately known.

For some purposes, it is convenient to combine the statistical and the other uncertainties into an estimated overall uncertainty. In the absence of a rigorous theory to guide formation of an overall uncertainty, several approaches are presented here, and the results compared. According to conventional statistical theory, the combined variance of a distribution is obtained by adding the variances of the component distributions. Then the component coefficients of variation are combined in quadrature to obtain an overall coefficient of variation:

$$s = \sqrt{\Sigma s_i^2} \qquad (7)$$

TABLE 4. *Uncertainty analysis.*

Component uncertainty	Estimated uncertainly (%)	
	statistical s_i	other w_i
1. Calorimeter [13]		
Impurities during calibration		0.1
Impurities during irradiation		0.02
Measurement of calibration power	0.04	0.03
2. PL1-11 chamber in graphite		
Calibration factor	0.15	0.1
Position uncertainty, chamber *vs* calorimeter		0.1
Lack of full wall buildup [6]		0.15
3. Dose-rate conversion, graphite to water		
Absorption coefficient ratio [11]		0.5
β ratio		0.1
Replacement factor		0.2
4. Calibration of secondary chamber in water		
Measurement of current	0.1	0.1
Chamber shape, possible airgaps, etc.		0.1
Position uncertainty, secondary *vs* PL1 chamber		0.03
Absorbed-dose rate to water (1 to 3)		
Linear combination, eq (8)	1.8	
Quadratic combination, eq (10)	0.8 (1.1)	
Calibration of secondary chamber (1 to 4)		
Linear combination, eq (8)	2.1	
Quadratic combination, eq (10)	0.8 (1.2)	

Suppose now that a factor k_1 is chosen so that the confidence level of the individual products $k_1 s_i$ is approximately the same as that believed to be associated with the individual estimated w_i. Then the component uncertainties can be combined linearly to give an overall uncertainty in the form

$$U = k_1 s + \Sigma w_i \tag{8}$$

An expression for the overall uncertainty is sometimes obtained by combination of the component uncertainties in quadrature, based on a direct analogy with eq (8), in the form

$$U = \sqrt{(k_1 s)^2 + \Sigma w_i^2} = k_1 \sqrt{s^2 + \Sigma (w_i/k_1)^2} \tag{9}$$

Equation (9) is essentially a combination in quadrature of confidence limits, which has no theoretical justification.

It has recently been suggested [14] that each w_i be adjusted by a suitable factor k_2 so that it becomes plausible to treat the terms $(k_2 w_i)^2$ as if they were variances. Then the overall uncertainty takes the form

$$U = k_1 \sqrt{s^2 + \Sigma (k_2 w_i)^2} \tag{10}$$

The value of k_2 depends on the form assumed for the population underlying the w_i, which is usually not known. If it is assumed that the distribution of possible errors is normal, $k_2 = k_1^{-1}$ and eq (10) becomes identical to eq (9).

The "other" uncertainties w_i have been estimated here as realistic upper bounds of the possible errors, so it is reasonable to assume that the w_i correspond very roughly to 99 percent confidence limits. Therefore we choose $k_2 = 1/3$ and $k_1 = 3$. Then from eqs (8), and (9) or (10), we obtain the overall uncertainties shown in table 4. It is sometimes argued that a single large uncertainty should be combined linearly with the remaining uncertainties combined in quadrature. When this is done with the uncertainty in the absorption-coefficient ratio, we obtain the values shown in parentheses in table 4.

Combination of uncertainties in quadrature is chosen over linear combination, since it is considered to be very unlikely that all errors would occur in the same sense. Since the component uncertainties are at best rough estimates and may have been underestimated, and noting the considerable variations in values of the overall uncertainty obtained using different methods of calculation, secondary chamber calibrations based on this work will be stated to have an overall uncertainty of about ± 1 percent. It does not appear to be justified to specify the overall uncertainty to two significant figures.

We are grateful to the physics staff of the Radiation Oncology Department of the National Cancer Institute of the National Institutes of Health for making their cobalt-60 source available for these studies. We are also grateful to Ronald Collé for many helpful discussions on statements of uncertainty.

6. References

[1] Radiation dosimetry: x-rays and gamma rays with maximum photon energies between 0.6 and 50 MeV. Int. Comm. on Rad. Units and Meas. (Wash., D.C.) Report 14; 1969 September. 30 p.

[2] Sundara Rao, I. S.; Naik, S. B. Graphite calorimeter in water phantom and calibration of ionization chambers in dose to water for ^{60}Co gamma radiation. Med. Phys. 7(3): 196-201; 1980 May-June.

[3] Burns, J. E. Conversion of calibrations from absorbed dose to carbon into absorbed dose to water for high energy x radiation. Nat. Phys. Lab. (Teddington, U.K.) Report RS 50; 1980 August.

[4] Domen, Steve R. Absorbed dose water calorimeter. Med. Phys. 7(2): 157-159; 1980 March-April.

[5] Pruitt, J. S.; Loevinger, R. Ionization chamber for absorbed-dose calibration. Proceedings of Symposium on Measurements for the Safe Use of Radiation; 1976 March 1-4; Gaithersburg, Md. Nat. Bur. Stand. (U.S.) Spec. Publ. 456: 37-39; 1976 November.

[6] Pruitt, J. S.; Loevinger, R. The photon-fluence scaling theorem for Compton-scattered radiation. Submitted to Med. Phys.

[7] A handbook of radioactivity measurements procedures. Nat. Comm. on Rad. Protec. and Meas. (Wash., D.C.) Report 58; 1978 November. 506 p.

[8] Domen, Steve R.; Lamperti, Paul J. A heat-loss compensated calorimeter: theory, design, and performance. J. Res. Nat. Bur. Stand. (U.S.) **78A**(5): 595-610; 1974 September-October.

[9] Loevinger, Robert. A formalism for calculation of absorbed dose to a medium from photon and electron beams. Med. Phys. **8**(1): 1-12; 1981 January-February.

[10] Seltzer, S. M.; Hubbell, J. H.; Berger, M. J. Some theoretical aspects of electron and photon dosimetry. Proceedings of the International Atomic Energy Agency International Symposium on National and International Standardization of Radiation Dosimetry; 1977 December 5-9; Atlanta, Ga. Int. Atomic En. Agency (Vienna) 1978, 3-43.

[11] Hubbell, J. H. Photon mass attenuation and mass energy absorption coefficients for H, C, N, O, Ar, and seven mixtures from 0.1 keV to 20 MeV. Rad. Res. **70**(1): 58-81; 1977 April.

[12] Bruce, W. R.; Johns, H. E. The spectra of x-rays scattered in low atomic number materials. Brit. J. Rad. (London) Supplement 9; 1960. 57 p.

[13] Domen, S. R.; Lamperti, P. J. Comparisons of calorimetric and ionometric measurements in graphite irradiated with electrons from 15 to 50 MeV. Med. Phys. **3**(5): 294-301; 1976 September-October.

[14] Collé, Ronald. Personal communication concerning a meeting of a Working Group on the Statement of Uncertainties, Bureau International des Poids et Mesures (Sèvres) 1980 October.

JOURNAL OF RESEARCH of the National Bureau of Standards
Vol. 86, No. 5, September-October 1981

Upper Limits for the Number of Bound States Associated with the Yukawa Potential

Herbert S. Bennett*

National Bureau of Standards, Washington, DC 20234

July 23, 1980

The number of bound-state solutions of the Schrödinger equation for the screened Coulomb potential (Yukawa potential), $-(C/r)\exp(-\alpha r)$, occurs frequently in theoretical discussions concerning, for example, gas discharges, nuclear physics, and semiconductor physics. The number of bound states is a function of (C/α). Three upper limits for the number of bound states associated with the Yukawa potential are evaluated and compared. These three limits are those given by Bargmann, Schwinger, and Lieb. In addition, the Sobolev inequality states that whenever $(C/\alpha) < 1.65$ no bound state occurs. This agrees to within a few percent of the numerical calculations of Bonch-Bruevich and Glasko. The Bargmann and Lieb limits and the Sobolev inequality are substantially easier to evaluate than the Schwinger limit. Among the three limits, the Schwinger limit gives the most restrictive limit for the existence of only one bound state and, therefore, is the best one to use for the approach to no binding, i.e., $1.65 < (C/\alpha) \leq 1.98$. The Lieb limit is the best among the three when $(C/\alpha) > 1.98$. The Bargmann limit is the least restrictive.

Key words: Bargmann limits; bound-state estimates; Lieb limits; number of bound states; Schwinger limits; screened Coulomb potential; Sobolev's inequality; Yukawa potential.

1. Introduction

Many theoretical topics in such areas as plasma, nuclear, solid state, and semiconductor physics [1-6][1] require knowledge about the number of bound-state solutions of the Schrodinger equation for two particles that interact according to the Yukawa or screened Coulomb potential. For example, as semiconductor devices become smaller, required dopant ion densities and their spatial gradients increase. The density of states for such highly doped materials is needed to predict device performance and degradation mechanisms. The density of states involves summation over bound states and integration over continuum states. The disappearance of bound-impurity levels in semiconductors due to free-carrier screening of the Coulomb field of impurity ions is thereby fundamental in understanding the behavior of electronic devices. [7]

During the course of research on the effect of donor impurities on the continuum electronic states in semiconductors, the author has used the Bargmann limit [8], the Schwinger limit [9], and the Lieb limit [10] to evaluate upper limits for the number of bound states associated with the screened Coulomb potential. The analytic methods used here to calculate these limits are more general and may be applied to other fields such as those mentioned above.

We shall show that 1) when the Yukawa potential permits only one bound state to exist, Schwinger's extension of Bargmann's limit gives a more restrictive limit for the number of bound states than do the Bargmann and Lieb limits; 2) when many bound states exist, the Schwinger and Bargmann limits agree to within a few percent and are not as restrictive as the Lieb limit; and 3) the Sobolev inequality [10,11] predicts no binding when $(C/\alpha) < 1.65$. The limit 1.65 from the Sobolev inequality agrees to within a few percent of the limit 1.68 from the numerical work of Bonch-Bruevich and Glasko. [5]

*Center for Electronics and Electrical Engineering, National Engineering Laboratory.

[1] Figures in brackets indicate literature references at the end of this paper.

2. Yukawa Potential and Schrödinger Equation

The Schrödinger equation for two particles that interact according to the Yukawa potential is

$$[\nabla^2 + \frac{2m}{\hbar^2}\{E - V(r)\}]\,\psi(r) = 0, \tag{1}$$

where E is the energy of the two-particle system, m is the reduced or effective mass, $\mathbf{r}$ is the relative coordinate vector between the two particles, and $r = |\mathbf{r}|$ is its magnitude. The spherically symmetric potential energy $V(r)$ is assumed to have the Yukawa form:

$$V(r) = -Cr^{-1}\exp(-\alpha r). \tag{2}$$

For many applications, the Yukawa potential is an idealized one which gives a reasonable description of the physical phenomena under study. Expressions for the parameters C and α in terms of physical quantities then depend upon the application. For donors such as phosphorus or arsenic in silicon, the quantities C and α become, respectively, $C = (e^2/\epsilon)$ and $\alpha = 1/r_s$. The charge of the electron is e, the dielectric constant is ϵ, and the screening length is r_s. The last depends in part upon the temperature and the dopant density. It gives the extent to which free carriers screen the Coulomb field of the donor ion.

The radial wave equation obtained from the Schrödinger equation, eq. (1), for the spherically symmetric potential $V(r)$ is

$$\frac{d^2}{dr^2}\phi_\ell(r) + [\frac{2m}{\hbar^2}\{E - V(r)\} - \frac{\ell(\ell+1)}{r^2}]\,\phi_\ell(r) = 0, \tag{3}$$

where

$$\underset{\sim}{\psi(r)} = \Sigma\, a_{\ell m}\,\phi_\ell(r)\,Y_{\ell m}(\theta,\phi).$$

The quantities, $\Sigma_{\ell m}$, are constants. The normalization and orthogonality conditions for the spherical harmonics $Y_{\ell m}(\Theta,\phi)$ are

$$\int_0^{2\pi} d\phi \int_0^{\pi} d\theta \sin Y_{\ell_1 m_1}(\theta,\phi)\,Y_{\ell_2 m_2}(\theta,\phi) = \delta_{\ell_1 \ell_2}\delta_{m_1 m_2}. \tag{4}$$

In the following sections, we shall calculate upper limits for the total number of bound-state solutions N of the Schrödinger equation, equation (1), and the number of bound-state solutions n_ℓ of the radial wave equation, eq. (3), for a given ℓ. Counting multiplicity, we perform the following summation to obtain the total number of bound states for a given spherically symmetric potential V.

$$N[V] = \sum_{\ell=0}^{\ell_{max}} (2\ell+1)\,n_\ell[V], \tag{5}$$

where ℓ_{max} is the largest value of ℓ for which $n_\ell \neq 0$.

3. Bargmann Limits

When the integral,

$$I_B[V] = \int_0^\infty r|V(r)|\,dr, \tag{6}$$

is finite, the Bargmann formulation [8] gives the inequality that

$$(2\ell+1)\,n_\ell < I_B[V]. \tag{7}$$

Thus, for the Yukawa potential, eq. (2), we have

$$I_B[V] = (C/\alpha)\,. \tag{8}$$

From the inequality (7), we note that the maximum $\ell = \ell_{max}$ for which $n_\ell \neq 0$ in the sum of eq. (5) has the upper limit $1/2\ (I_B - 1)$. Thus, we have the following inequality [9] for spherically symmetric potentials; namely,

$$N < \frac{1}{2} I_B (I_B + 1)\,. \tag{9}$$

4. Schwinger Limits

Schwinger [9] extends the Bargmann derivation to treat angular and spin-independent potentials and to give the number of states that lie at or below some chosen energy. His result for the upper bound I_S to the total number of bound states N associated with a general spin-independent three-dimensional potential $V(\underline{r})$ is

$$N < I_S\,, \tag{10}$$

where

$$I_S = \frac{1}{(4\pi)^2} \int\int d^3r d^3r' \frac{|V(\mathbf{r})|\,|V(\mathbf{r}')|}{|\mathbf{r}-\mathbf{r}|^2}\,. \tag{11}$$

We shall now proceed to evaluate the double integral in eq (11) for the case of the Yukawa potential given by eq. (2). Because the Yukawa potential is spherically symmetric, we expand the denominator in terms of the spherical harmonics; namely,

$$\frac{1}{|\mathbf{r}-\mathbf{r}'|} = 4\pi \sum_{\ell=0}^{\infty} \sum_{m=-\ell}^{\ell} \frac{1}{(2\ell+1)} \frac{r_<^\ell}{r_>^{\ell+1}} Y_{\ell m}(\theta',\phi')\, Y_{\ell m}(\theta,\phi)\,, \tag{12}$$

where $r_<$ and $r_>$ are, respectively, the lesser and the greater values of $|\mathbf{r}|$ and $|\mathbf{r}'|$ and where

$$Y_{\ell m}(\theta,\phi) = \left\{\frac{(2\ell+1)\,(\ell-m)!}{4\pi(\ell+m)!}\right\}^{1/2} P_\ell^m(\cos\theta)\, e^{im\phi}\,.$$

The Legendre polynomials P_ℓ^m satisfy the relation

$$P_\ell^{-m}(x) = (-1)^m \frac{(\ell-m)!}{(\ell+m)!} P_\ell^m(x). \tag{14}$$

Substituting relation (12) into eq. (11) and using for the volume element in spherical coordinates $d^3r = r^2 \sin\theta d\theta d\phi dr$, we perform the integrations over θ, ϕ, θ', and ϕ' by frequent reference to eqs. (4), (13), and (14) and obtain the result that for spherically symmetric potentials $V_s(r)$

$$\begin{aligned} I_S[V_s] = {} & \int_0^\infty r^2\, dr \int_0^\infty r'^2\, dr'\, |V_S(r)|\,|V_S(r')| \\ & \times \sum_{\ell=0}^{\infty} \frac{1}{(2\ell+1)} \frac{r_<^{2\ell}}{r_>^{2\ell+2}}\,. \end{aligned} \tag{15}$$

Equation (15) becomes for the Yukawa potential (2)

$$\begin{aligned} I_S(\mathrm{Y}) = {} & (C/\alpha)^2 \sum_{\ell=0}^{\infty} \frac{1}{(2\ell+1)} \left[\int_0^\infty z \exp(-z)\, dz\right. \\ & \left. \times \left\{\int_0^1 \eta^{2\ell+1} \exp(-z\eta)\, d\eta + \int_1^\infty \eta^{-2\ell-1} \exp(-z\eta)\, d\eta\right\}\right], \end{aligned} \tag{16}$$

where we made the substitutions $z = \alpha r$, $y = \alpha r'$, and then $\eta = (y/z)$ to obtain equation (16) from equation (15).

Let us consider the first term in the curly brackets in eq. (16). Interchanging the order of integration, we obtain

$$d_1(\ell) = \int_0^1 \eta^{2\ell+1} \{\int_0^\infty z \exp(-z) \exp(-z\eta)\, dz\}\, d\eta$$

$$= \int_0^1 \eta^{2\ell+1} (1+\eta)^{-2}\, d\eta\ .$$

We now examine the second term in the curly brackets of equation (16), namely,

$$d_2(\ell) = \int_0^\infty z \exp(-z) (\int_1^\infty \eta^{-2\ell-1} \exp(-z\eta)\, d\eta)\, dz\ . \tag{18}$$

Interchanging the order of integration in equation (18), we write the second term

$$d_2(\ell) = \int_1^\infty \eta^{-2\ell-1} (1+\eta)^{-2}\, d\eta\ . \tag{19}$$

By making the substitution $\eta = (1/x)$, it follows that $d_2(\ell) = d_1(\ell)$.

From the above, we obtain the Schwinger upper limit for the total number of bound states associated with the Yukawa potential

$$I_S[V] = (C/\alpha)^2 \sum_{\ell=0}^{\infty} 2(2\ell+1)^{-1} d_1(\ell)\ . \tag{20}$$

Interchanging the order of integration and summation in eq. (20),

$$I_S[V] = (C/\alpha)^2 \int_0^1 (1-\eta)^{-2} \sum_{\ell=0}^{\infty} 2\eta^{2\ell+1} (2\ell+1)^{-1}$$

and observing that when $\eta < 1$,

$$ln\left(\frac{1+\eta}{1-\eta}\right) = \sum_{\ell=0}^{\infty} \frac{2\eta^{2\ell+1}}{(2\ell+1)}\ ,$$

we write eq. (20) in the form

$$I_S[V] = (C/\alpha)^2 \int_0^1 \frac{ln\{(1+\eta)/(1-\eta)\}}{(1+\eta)^2}\, d\eta\ . \tag{21}$$

We show in Appendix A that the integral in eq. (21) equals 1/2. Hence, our final result is

$$I_S[V] = \frac{1}{2} \{I_B[V]\}^2\ . \tag{22}$$

5. Lieb Limits and Sobolev Inequality

In three dimensions, Simon [10] gives a bound for large (C/α) due to Lieb of the form

$$N \leq a_3 \int |V(r)|^{3/2}\, d^3r \equiv I_L[V]\ , \tag{23}$$

where $a_3 \leq 0.116$. For the potential (2), the Lieb limit $I_L[V]$ becomes

$$I_L[V] = 0.116 \times 6.062\, \{I_B[V]\}^{3/2}\ . \tag{24}$$

When (C/α) is small enough, bound states do not occur. The Sobolev inequality [10,11] predicts that bound states do not occur whenever $I_{SI}[V] < 1$, or equivalently, whenever

$$1 > 0.078 \times 6.062 \{I_B[V]\}^{3/2} \equiv I_{SI}[V] .$$

That is, according to the Sobolev inequality, $N = 0$ whenever $(C/\alpha) < 1.65$

6. Conclusions

We have shown in sections 3, 4, and 5 that the upper limit for the total number N of bound states associated with the Yukawa potential is for the Bargmann limit, eq. (9),

$$N < \frac{1}{2} I_B[V] \{I_B[V] + 1\} = N_B ,$$

for the Schwinger limit,

$$N < \frac{1}{2} \{I_B[V]\}^2 = N_S ,$$

and for the Lieb limit

$$N < 0.7032 \{I_B[V]\}^{3/2} = N_L .$$

Because $0 < N_S[V] < N_B[V]$ for all $I_B[V] > 0$, we conclude that the Schwinger upper limit, $N_S[V]$, is a more restrictive limit than $N_B[V]$. However, for large enough values of $I_B[V]$, the fractional difference $[(N_B - N_S)/N_B]$, between the Schwinger and Bargmann upper bounds approaches zero as $\{1/I_B[V]\}$ approaches zero.

When $(C/\alpha) > 1.98$, $N_L < N_S$ and the Lieb limit is best for large (C/α) and for many bound states. When $(C/\alpha) < 1.98$, $N_S < N_L$ and the Schwinger limit is best for the existence of only one bound state and for the approach to no binding, i.e., $1.98 > (C/\alpha) > 1.65$, and finally, the Sobolev inequality gives $N = 0$ whenever $(C/\alpha) < 1.65$. This value of 1.65 agrees to within 2 percent of the value $(C/\alpha) < 1.68$ which Bonch-Bruevich and Glasko [5] determined numerically to give no bound state.

And finally, we observe from table 1 that even the Lieb limit is more than a factor of 3 greater than the numerically determined number of bound states given in reference 5 for values of $(C/\alpha) > 8.92$.[2]

TABLE 1. *Comparison of the Number of Bound States N Determined Numerically by Bonch-Bruevich and Glasko[a] and the Three Upper Limits of Bargmann [Eq. (9)], Schwinger [Eq. (22)], and Lieb [Eq. (24)]. The Sobolev inequality is given by Eq. (25). All quantities are dimensionless.*

(C/α)	N	Bargmann Limit	Schwinger Limit	Lieb Limit	Sobolev Inequality
1.65	1	2.19	1.36	1.49	1.00
1.68	1	2.25	1.41	1.53	
1.90	1	2.76	1.81	1.84	
1.98	1	2.95	1.96	1.96	
2.00	1	3.00	2.00	1.99	
6.00	1	21.00	18.00	10.33	
6.45	2	24.03	20.80	11.52	
7.00	2	28.00	24.50	13.02	
8.50	2	40.38	36.13	17.43	
8.92	5	44.24	39.78	18.73	

[a] Reference 5.

[2] The relative strengths of the Lieb, Schwinger, and Bargmann limits are dependent upon the potential $V(r)$. For example, the table analogous to table 1 for the attractive three-dimensional square well shows that the Bargmann limit is best in the range $2.47 < V_0a^2 < 10.74$ and the Lieb limit is best when $V_0a^2 > 10.74$, where V_0 is the depth of the well and a is the width of the well. The Sobolev limit states that bound states do not occur when $V_0a^2 < 2.11$ whereas the exact numerical result states that bound states do not occur when $V_0a^2 < 2.47$.

The author thanks Arnold Kahn and Jeremiah Lowney for their helpful discussions.

7. References

[1] Margenau, H; Lewis, M. Structure of spectral lines from plasmas, Rev. Mod. Phys. **31**, 569 (1959).
[2] Hulthen, L.; Laurikainen, K.V. Approximate eigensolutions of $(d^2\varnothing/dx^2) + [a + b\{\exp(-x)/x\}] = 0$, Rev. Mod. Phys. **23**, 1 (1951).
[3] Stoneham, A.H. *Theory of defects in solids* Chapter 9, (Oxford: Clarendon Press, 1975).
[4] Toyozawa, Y. et al. On the interaction of additive electrons with the polarization in ionic crystals, II, Prog. Theor. Phys. **10**, 57 (1953).
[5] Bonch-Bruevich, V.L.; Glasko, V.B. Energy levels in a Debye field, Opt. Spectrosc. **14**, 264 (1963).
[6] Mott, N.F.; Gurney, R.W. *Electronic processes in ionic crystals*, chapter 3, (Oxford: Clarendon Press, 1978).
[7] Lowney, J.; Kahn, A.K.; Blue, J.; Wilson, C., Disappearance of impurity levels in silicon and germanium due to screening, J. Appl. Phys. (to be published).
[8] Bargmann, V., On the number of bound states in a central field of force, Proc. Natl. Acad. Sci. USA, **47**, 122 (1961).
[9] Schwinger, J., On the bound states of a given potential, Proc. Natl. Acad. Sci. USA, **47**, 122 (1961).
[10] Simon, B. *Functional integration and quantum physics*, pp 88-97, (New York: Academic Press, 1979).
[11] Rosen, G., Minimum valve for c in the Sobolev inequality, SIAMJ Appl. Math. **21**, 30 (1971).

8. Appendix

In this appendix, we outline the evaluation of the integral that appears in eq. (21); namely,

$$I_{21} = \int_0^1 (1+\eta)^{-2} \ln\{(1+\eta)/(1-\eta)\}\, d\eta\,. \tag{A1}$$

We let $1 + \eta = w$ and write

$$I_{21} = \int_1^2 w^{-2}\{\ln(w) - \ln(2 - w)\}\, dw\,. \tag{A2}$$

Referring to integral tables, we find that

$$I_{21} = \frac{1}{2} + \lim_{w\to 2} \frac{(2-w)}{4} \ln(2 - w) = \frac{1}{2}\,. \tag{A3}$$

JOURNAL OF RESEARCH of the National Bureau of Standards
Vol. 86, No. 5, September–October 1981

A "Uniformity Principle" for Evacuation Route Allocation*

Richard L. Francis

**Department of Industrial and Systems Engineering, University of Florida
Gainsville, FL 32611**

April 1, 1981

This paper establishes what might be called a "uniformity principle" for building evacuation problems. The principle may be stated as follows: given a building for which each occupant has reasonable access to every evacuation route, if the building is evacuated in minimum time, then the allocation of evacuees to routes is such that the route evacuation times are all the same. That is, there is a uniformity of route evacuation times. Also, analytical expressions for the minimum time to evacuate a building, and for the corresponding allocation of evacuees to routes, are obtained.

Key Words: building evacuation; mathematical optimization; network flow.

1. Introduction

The main purpose of this paper is to establish analytically what might be called a "uniformity principle" for building evacuation problems. The principle may be stated as follows: given a building for which the occupants have reasonable access to all the evacuation routes, if the building is evacuated in minimum time then the allocation of the people in the building to the various building evacuation routes is such that there is a *uniformity* of route evacuation times, that is, all route evacuation times are the same. This principle is easy to motivate. If the evacuation time for some route j is greater than for all the other routes, then some people using route j could be evacuated by other routes instead, thus reducing the time to evacuate route j while not increasing the evacuation times for the other routes above the time to evacuate route j.

The uniformity principle appears to fall into the "folklore" category. People involved with building evacuation appear aware of the principle, and assume it is true, but only implicit references to the principle, such as the ones by Pauls and Jones [6],[1] appear in the literature. As a consequence of the means by which we establish the principle, we obtain analytical expressions for the minimum time to evacuate a building, and for the number of people to be allocated to each evacuation route so as to achieve the minimum building evacuation time. We remark that even if the minimum building evacuation time is not achieved in an actual evacuation, it may still be of interest in the sense that it provides a benchmark, or standard of comparison, which gives some measure of how "good" an actual building evacuation time might be.

As concerns other related literature, for a graphical approach to the problems we shall consider, see Francis [3]. For various generalizations of the approach we shall consider, see Chalmet, Francis and Saunders [2], and Francis and Saunders [4]. For a general discussion of the evacuation literature, see Stahl and Archea [7].

The organization of the paper is as follows. We first give an analytical problem statement. We then give a solution procedure, followed by examples. Finally we consider and solve the more general problem where each route can have a capacity, i.e., can have an upper bound on the total number of people who can use the route. We motivate the correctness of the solution procedures we give, but omit proofs of correctness, as such proofs are relatively direct.

*This research was supported in part by the Center for Fire Research, National Bureau of Standards, Grant No. N879NAD0021, and by the Operations Research Division, Center for Applied Mathematics, National Bureau of Standards.

[1] Figures in brackets indicate literature references at the end of this paper.

2. Analytical formulation

So as to state the evacuation problem of interest analytically, suppose a building has k people to be evacuated, and there are n different evacuation routes. For $j = 1, ..., n$ we assume we know that the time to evacuate x_j people via route j, denoted by $t_j(x_j)$, is well structured, in the sense that it is a strictly increasing and continuous function with $t_j(0) = 0$. We call the function $t_j(\ )$ the route j evacuation time function.

Since the building is not evacuated until all the routes are evacuated, the building evacuation time, say z, is the maximum, i.e., the longest, of the route evacuation times, that is,

$$z = \max[t_1(x_1), ..., t_n(x_n)] . \tag{1}$$

Since we want to evacuate k people, we require that

$$x_1 + ... + x_n = k, \tag{2}$$

that is, the total number of people evacuated via all the routes is equal to k. Since we cannot allow the number of people using any route to be negative, we also require

$$x_1 \geq 0, x_2 \geq 0, ..., x_n \geq 0. \tag{3}$$

The evacuation problem can now be stated analytically: minimize (1) while satisfying (2) and (3). That is, find the (nonnegative) number of people to be evacuated via each route so as to minimize the time to evacuate the building.

Note it is assumed that routes do not "interact." For example, if routes 1 and 2 "cross" at some point, the time to evacuate route 1 would depend not only on x_1, the number of people using route 1, but on x_2, the number of people using route 2, as well; the model cannot handle such a situation. However, particularly for buildings for which the routes are essentially staircases, this assumption of no interaction appears reasonable. Further, in modeling a specific problem there may be more than one means of defining specific routes, in which case an appropriate definition might guarantee that in fact the routes do not interact.

It is also assumed that each of the k persons can use any one of the n routes; this assumption is implicit in the condition (2).

We emphasize the fact that the problem statement does not require x_j to be an integer. Thus an implicit assumption is that solutions to the problem can be rounded to adjacent integers with an acceptable loss of accuracy. Particularly when the total number of people in the building is large in comparison to the number of routes, as is often the case, this assumption does not appear too restrictive. Further, if the integrality condition is imposed, then the uniformity principle may fail, although probably by only a little. For example, if a building contains 501 people, has two evacuation routes, and the two routes have the same route evacuation time functions, an optimum solution to the problem is to evacuate 250.5 people by each route, giving uniform evacuation times. In reality, the closest one would come to uniform evacuation times would be to evacuate 250 people via one route, and 251 via the other route, giving (slightly) different route evacuation times.

It is worth emphasizing that the route evacuation time functions need not actually be known in order for the uniformity principle to be true. It is only necessary to know that they are well structured. In particular, the route evacuation time functions need not be linear; nonlinearity makes the theory no more difficult. On the other hand, nonlinearity would certainly make the theory more difficult to implement computationally.

3. Solution procedure

We denote by $p_j(z)$ the number of people who can clear route j in a time of z. Since $t_j(x_j)$ is the time to evacuate x_j people via route j,

$$z = t_j(p_j(z)) \tag{4}$$

is the time to evacuate $p_j(z)$ people via route j, and so we obtain $p_j(z)$ by solving the equation (4) for $p_j(z)$. (Note we are just finding the inverse function of $t_j(\,)$ when we solve (4) for $p_j(z)$.) The expression (4) holds for z satisfying $0 \leq z \leq t_j(k)$. If $z > t_j(k)$ then the time z is greater than that needed to evacuate all k people via route j, and so in this case the number of people who can clear route j in a time of z is just k, i.e.,

$$p_j(z) = k \text{ for } t_j(k) < z\,. \tag{5}$$

Thus we determine $p_j(z)$ either from (4) or from (5), depending upon whether $0 \leq z \leq t_j(k)$ or $t_j(k) < z$.

Note we can interpret $p_j(z)$ as the *most* people who can clear route j in a time of z, for if x_j people clear route j, and $x_j > p_j(z)$, then, using (4) and the fact that $t_j(\,)$ is a strictly increasing function, we have $t_j(x_j) > t_j(p_j(z)) = z$, i.e., the time to clear more than $p_j(z)$ people exceeds z. Hence it follows, if we let

$$P(z) = p_1(z) + \ldots + p_n(z) \text{ for } 0 \leq z, \tag{6}$$

that $P(z)$ is the *most* people who can exit the building in a time of z. Since there are k people in the building, let us find the time z^* for which

$$k = P(z^*), \tag{7}$$

in which case k is the most people who can exit the building in a time of z^*. We can now conclude that in any time say z', with $z' < z^*$, not all k people can exit the building, and thus z^* *is the minimum time to evacuate all k people.*

Once we know z^*, we can allocate

$$x_j^* = p_j(z^*) \text{ people for each route } j \tag{8}$$

and be assured that

$$x_1^* + \ldots + x_n^* = p_1(z^*) + \ldots + p_n(z^*) = P(z^*) = k.$$

Thus the allocation (8) evacuates all k people. Further, the time to evacuate x_j^* people via route j is given by

$$t_j(x_j^*) = t_j(p_j(z^*)) = z^* \text{ for each route } j. \tag{9}$$

Thus every route clears at the same time, z^*. Therefore we obtain a *uniformity principle*, in the sense that *the route evacuation times are uniform when the building is evacuated in minimum time.*

At this point we summarize our procedure for allocating people to routes so as to evacuate the building in minimum time. First use (4) and (5) to determine each function $p_j(\,)$. Then use (6) to find the function $P(\,)$. Given k, next solve (7) to find the minimum building evacuation time z^*. Then use (8) to determine an optimum allocation of people to routes, and conclude from (9) that all routes clear at the same time. We remark, if we suppose we draw every function $p_j(\,)$, as well as the function $P(\,)$, on a single graph, then we can envision all the steps of the procedure of this paragraph as being carried out using only this one graph.

We comment that the foregoing procedure is somewhat related to procedures given by Brown [1], but the applications he considers are quite different. Also, Brown does not consider the case where routes have capacities, which we treat in section 5.

4. Examples

Let us consider some examples. As a simple initial example, suppose we can compute the time for x_j people to clear route j by dividing x_j by a known (positive) flow rate r_j, so that $t_j(x_j) = x_j/r_j$ for every route j. Solving $z = p_j(z)/r_j$ for $p_j(z)$ gives $p_j(z) = r_j z$, so that $P(z) = r_1 z + \ldots + r_n z = Rz$, where $R = r_1 + \ldots + r_n$. Thus solving $k = P(z^*)$ for z^* gives $z^* = k/R$, which can be interpreted as the time to evacuate all k people

via a single-hypothetical-route of flow rate R. Similarly, $x_j^* = p_j(z^*) = r_j z^* = (r_j/R)k$ for every route j, and so the number of people allocated to each route j is directly proportional to the flow rate of the route.

As a second example, consider a situation where a positive constant c is known, as well as a positive constant a_j, a "route parameter," for each route j, and a strictly increasing and continuous function $t(\ )$ with $t(0) = 0$, so that $t_j(x_j)$ is computed as follows:

$$t_j(x_j) = t(x_j/(ca_j)) \ , \ 0 \leq x_j \leq k \ .$$

By taking $t(y) = y$, $c = 1$, and $a_j = r_j$ we get the previous example. By taking $c = 1$ and $a_j = 1$ for every route j we get the situation where the time functions are the same for all routes. By taking $t(y) = y^{.73}$, $c = (.206)^{1/.73}$ and $a_j = w_j$ we get an empirically determined route time function of Pauls [5], where each route j represents a stairwell and w_j is the "effective width" in meters of stairwell j, obtained by subtracting 0.3 meters from the actual stairwell width. Thus this example represents a number of situations of interest. Let $p(\ )$ denote the function for which $z = t(p(z))$ and $y = p(t(y))$. By solving $z = t_j(p_j(z)) = t(p_j(z)/(ca_j))$ for $p_j(z)$ we get $p(z) = p_j(z)/(ca_j)$, so that $p_j(z) = ca_j p(z)$. Letting $A = a_1 + \ldots + a_n$ for convenience, we have $P(z) = p_1(z) + \ldots + p_n(z) = cA\,p(z)$. Thus solving $k = P(z^*) = cA\,p(z^*)$ for z^* gives $z^* = t(k/(cA))$, which can be interpreted as the time for all k people to clear a single-hypothetical-route having a route parameter A. The number of people allocated to each route j is given by $x_j^* = p_j(z^*) = ca_j p(z^*) = ca_j\,p(t(k/cA)) = ca_j(k/cA) = (a_j/A)\,k$. Thus the number of people allocated to each route j is directly proportional to its route parameter a_j. For the case where $t(y) = y$, $c = 1$, $a_j = r_j$, and $A = R$ we get the same solution as in the previous example. By taking $c = 1$ and every $a_j = 1$, we have $A = n$, giving $x_j^* = k/n$ for every route j, so that when the time functions are the same for all n routes the k people are allocated evenly among the routes. For the case representing Pauls' time equation, letting $a_j = w_j$ and $A = W$ we get $x_j^* = (w_j/W)k$ for each route j, so that the number of people allocated to each route j is directly proportional to the effective width of the route.

5. Including route capacities

We now consider briefly a capacitated problem, a generalization of the earlier (uncapacitated) problem defined by (1), (2), and (3). For each route j we assume we know a *capacity function* $c_j(\ )$, where $c_j(z)$ is an upper bound on the *total* number of people who can be evacuated via route j in a time of z. For each j we assume $c_j(\ )$ is a continuous and nondecreasing function, with $c_j(0) \geq 0$. We obtain the capacitated problem by imposing the following capacity constraints upon the uncapacitated problem:

$$x_1 \leq c_1(z), \ldots, x_n \leq c_n(z) \ , \ 0 \leq z. \tag{10}$$

Note that if we take each $c_j(z) = k$ in (10) that (10) becomes redundant, so that the capacitated problem includes the uncapacitated problem as a special case.

There are a number of reasons for considering capacity constraints. For example, a solution to the uncapacitated problem might allocate unrealistically large numbers of peoples to certain routes, which could be remedied by giving capacities to the routes in question. Alternatively, letting $c_j(z)$ be some constant c_j might represent a situation where route j becomes blocked after c_j people exit the route. Further, the capacity functions permit the representation of situations where no extra people use the route in certain time intervals, e.g., if $c_j(30) = 60 = c_j(90)$ then the capacity of route j is 60 at every point in time between $z = 30$ and $z = 90$, and if 60 people have cleared the route by the time $z = 30$ then no extra people can clear the route until $z > 90$: such a situation might represent a temporary route blockage.

It turns out that the uniformity principle may fail for the capacitated problem, but the solution procedure remains much the same. For each route j, let $q_j(z)$ now denote the most people who can clear (capacitated) route j in a time of z. Continuing to let $p_j(\ )$ denote the function defined by (4) and (5), we have $q_j(z) = p_j(z)$ provided $p_j(z) \leq c_j(z)$, while $q_j(z) = c_j(z)$ if $c_j(z) < p_j(z)$, as the route capacity cannot be exceeded. Hence for each route j we conclude

$$q_j(z) = \text{minimum of } p_j(z) \text{ and } c_j(z) \ , \ 0 \leq z. \tag{11}$$

With the definition (11) we can state the following procedure to solve the capacitated problem. First use (4) and (5) to determine each function $p_j(\,)$, and then use (11) to determine each function $q_j(\,)$. Next construct the function $Q(\,)$ defined by $Q(z) = q_1(z) + \ldots + q_n(z)$ for $0 \leq z$. If $k > Q(z)$ for all nonnegative z then the capacity functions make it impossible to solve the problem as formulated, as all k people can never be evacuated. Otherwise, given k, solve the equation

$$k = Q(z) \tag{12}$$

and take the minimum building evacuation time z^* to be the *smallest* z satisfying (12). (In case (12) has a unique solution take z^* to be the unique solution.) Then determine an optimum allocation of people to routes by letting $x_j^* = q_j(z^*)$ for each route j. As with the procedure for the uncapacitated problem, if we suppose we draw every function $q_j(\,)$, as well as the function $Q(\,)$, on a single graph, then we can envision the steps of the procedure of this paragraph as being carried out using only this graph.

While the uniformity principle may fail, it can be shown that *the principle still holds for routes that are not saturated.* That is, every route j for which $x_j^* < c_j(z^*)$ is cleared in a time of z^*.

Acknowledgement: The author would like to thank Dr. Alan J. Goldman for his many constructive suggestions.

6. References

[1] Brown, J. R. The knapsack sharing problem. Operations Research 27(2): 340-355; 1979 March-April.

[2] Chalmet, L. G.; Francis, R. L.; Saunders, P. B. Network models for building evacuation. Gainesville, FL: University of Florida, Department of Industrial and Systems Engineering; 1980 April; Research report 80-8. 41 p. (to appear in Management Science).

[3] Francis, R. L. A simple graphical procedure to estimate the minimum time to evacuate a building. Boston, MA: Society of Fire Prevention Engineers, 60 Batterymarch St.; 1979; SFPE technology report 79-5. 14 p.

[4] Francis, R. L.; Saunders, P. B. EVACNET: prototype network optimization models for building evacuation. Nat. Bur. Stand. (U.S.) NBSIR 79-1593, 1979 October. 107 p.

[5] Pauls, J. L. Management and movement of building occupants in emergencies. Ottawa, Canada: National Research Council of Canada, Division of Building Research; 1977 September. NRCC 16845, DDR Paper No. 788.

[6] Pauls, J. L.; Jones, B. K. Case studies of building evacuations (and) Building evacuation findings and recommendations, chapters in *Behavior in Fires*, D. Canter, ed. New York, NY: John Wiley & Sons; 1978.

[7] Stahl, F.; Archea, J. An assessment of the technical literature on emergency egress from buildings. Nat. Bur. Stand. (U.S.) NBSIR 77-1313, 1977 October. 57 p.